Environmentally-benign Electroless Nickel-Phosphorus Plating on Thermoplastic Polymers using Co-polymer Based Hydrophilic Modification and Supercritical Carbon Dioxide Pd-complex Infusion

Siwach Tengsuwan

2014

Contents

Chapter I

General Introduction

Chapter II

Electroless Nickel Plating on Polypropylene via Hydrophilic Modification and Supercritical Carbon Dioxide Pd-complex Infusion

Chapter III

Supercritical Carbon Dioxide-assisted Electroless Nickel Plating on Polypropylene —The effect of Copolymer Blend Morphology on Metal-Polymer Adhesion—

Chapter IV

Environmentally Benign Electroless Nickel Plating using Supercritical Carbon-Dioxide on Hydrophilically Modified Acrylonitrile-Butadiene-Styrene

Chapter V

Chapter I

General introduction

1.1. Metallization of plastic

Metallization of plastic parts has been conducted for various industrial applications ranging from the fabrication of printed circuits in microelectronics to decorative coatings in general manufacturing. The plastic parts can be metalized for decorative or functional purposes. A thin metal coating can provide plastic parts a glossy appearance, reflectivity, abrasion resistance or high electrical conductivity or to provide electromagnetic shielding. Metalized plastic parts possess several advantages over comparable plated metal parts, such as low weight, corrosion resistance, greater design-ability, and low costs [1-3].

Metallization can be carried out by several techniques, like vacuum vapor deposition [4-6], arc and flame spraying [7, 8] and electroless coating/plating [9-12]. The vacuum vapor deposition technique uses a vacuum or partially vacuum chamber for depositing the metal to the plastic surface. In the vacuum chamber, a metal is evaporated and the vapor is condensed onto the surface of plastic substrate, leaving a thin layer of metal coating. This deposition process is also called physical vapor deposition (PVD). In flame spraying technique, a layer of metallic coating is sprayed onto the plastic substrate. The primary driving force of deposition in the flame spraying is a combustion flame, driven by oxygen and gas. Metallic powder is heated and melted. The combustion flame accelerates the mixture of gas and metal powder and releases it as spray. This process has a high deposition rate and creates very thick layers, but the coatings tend to be porous and somewhat rough.

Plating techniques can be classified into two categories, electroless and electro plating. In electroless plating, electric current is not used. On the other hand, it is used in electroplating technique. Generally speaking, both plating techniques are more effective than vacuum metallization technique in terms of strong adhesiveness between metal and plastic. The electroless plating has several other advantages, which

are the higher quality of the deposition in terms of the physical and mechanical properties, the possibility of a partial coating, flexibility in the plating volume and thickness, automatic monitoring of chemical replenishment and controllability of surface brightness [10, 13]. Therefore, the electroless plating has been the most widely used plastic metallization technique. It is used especially for metalizing the printed circuit boards (PCBs), automobile plastic parts, air craft and aerospace parts and the electric devise such as magnetic interference shielding materials [14, 15].

1.2. Electroless plating

1.2.1. Electroless plating reaction

Electroless plating is an autocatalytic chemical reaction technique to deposit the nickel or cupper to the surface of plastics where metallic ions are reduced with a reducing agent, for example, hydrated sodium hypophosphite ($NaPO_2H_2 \cdot H_2O$) and deposited to the plastic surface [10, 13, 14, 16]. The reaction process is carried out without externally passing any electric current through the solution to form a deposit.

The electroless plating was first noted by Wurtz as a chemical accident [17]. He accidentally deposited the metallic nickel from aqueous solution in the presence of hypophosphite in 1844. In 1911, the second electroless plating experiment was reported by Roux. He reported that metal was precipitated in the power form. Unfortunately, their works were not advanced to practical applications until 1946. In 1946, Brenner and Riddell developed a process for plating the inner walls of tubes with nickel-tungsten alloy. They were credited with this success of development of the electroless deposition process [18]. Nowadays, Wurtz and Roux are given more of the discovery credit.

The electroless plating is a sort of chemical deposition of metals onto the plastic surfaces and it is carried out in the aqueous solution. The ingredients in an electroless plating solution are a source of metal (usually a salt), a reducer, a complexing agent to hold the metal in solution. Figure 1.1 illustrates the schematic of the autocatalytic reaction occurring in the aqueous solution. The autocatalytic chemical reaction is initiated when hydrogen is released and oxidized by a reduction agent R. A negative charge (electron) is then produced and delivered to a surface of

plastic parts. Then, a metal ion is reduced by receiving electron and the metal is deposited on the surface. The most common electroless plating scheme is electroless nickel plating although the silver, gold and copper can be also deposited in the same manner.

Beside the electroless plating with autocatalytic chemical reaction [19], the electroless plating can be conducted with two other schemes, immersion deposit plating and decomposition of metal carbonyl, for example, nickel carbonyl, $Ni(CO)_4$. The immersion deposit plating process is similar to the electroless plating process with autocatalytic reaction because it uses a chemical reaction to deposit metal coating. The major difference is the reaction mechanism. Because the reaction is caused by the metal substrate in the electroless plating while in immersion deposit plating process it is caused by mixing two chemicals in the plating bath. In decomposition of nickel carbonyl process, the gas is introduced to a reactor where the plastic is placed. The gas is decomposed to nickel and carbon monoxide and the plastic is coated by the nickel [20]. However, the immersion deposit plating provides poorly adherent and non-protective metal layers and gas decomposition expensive and hazardous. Thus, only electroless nickel plating has gained wide acceptance because the metal can be coated with uniformity in composition and thickness [13, 20].

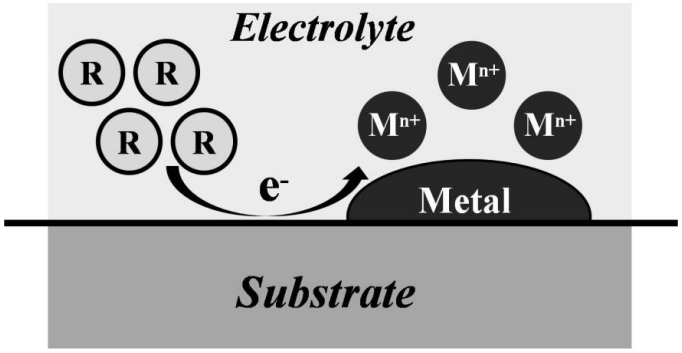

Figure 1.1. Schematic of electroless deposition process with reducing agent R as the resource of electrons

The electroless plating process can be considered as a particular process, where metal particles are continuously precipitated and agglomerated on a substrate by simply immersing the plastics in a suitable solution. Several autocatalytic reaction mechanisms have been as illustrated in Table 1.1. The electroless plating reaction starts after a chemical reducing supplies the electrons to convert the metal ion (M^{2+}) to metal form (M^0) [21],

$$M^{2+} + 2e \text{ (supplied by reducing agent)} \xrightarrow{\text{Catalytic Surface}} M^0 \qquad (1.1)$$

Table 1.1. Existing reaction mechanisms in reduced electroless plating solutions [21]

(i) The 'pure electrochemical' mechanism

Anodic : $H_2PO_2^- + H_2O \rightarrow H_2PO_3^- + 2H^+ + 2e^-$

Cathodic: $M^{n+} + ne \rightarrow M\downarrow$

$2H^+ + 2e \rightarrow H_2\uparrow$

(ii) The 'hydride ion' mechanism

$2RH + 2OH^- \rightarrow 2ROH + 2H^-$

$M^{2+} + 2H^- \rightarrow [M + 2H] \rightarrow M\downarrow + H_2\uparrow$

$2H_2O + 2H^- \rightarrow 2H_2\uparrow + 2OH^-$

(RH is formaldehyde or hypophosphite)

(iii) The 'atomic hydrogen' mechanism

Anodic: $RH + OH^- \rightarrow ROH + H + e^-$

Cathodic: $M^{n+} + ne \rightarrow M\downarrow$

$H^+ + e \rightarrow H\uparrow$

Recombination: $H + H \rightarrow H_2\uparrow$

(RH is formaldehyde, hypophosphite or borohydride)

Meerakker [21] proposed a universal electrochemical mechanism as described below. Each process can be made up of a series of elementary anodic and cathodic reactions. The first anodic reaction is the dehydrogenation of the reductant, as described in equation (1.2). The anodic reactions are given by four reactions of alkaline media:

(i) Dehydrogenation: $RH \rightarrow R + H$ (1.2)

(ii) Oxidation: $R + OH^- \rightarrow ROH + e$ (1.3)

(iii) Recombination: $H + H \rightarrow H_2 \uparrow$ (1.4)

(iv) Oxidation: $H + OH^- \rightarrow H_2O + e^-$ (1.5)

The cathodic reactions are given by four reactions of alkaline media:

(v) Metal deposition: $M^{+n} + ne \rightarrow M^0 \downarrow$ (1.6)

(vi) Hydrogen evolution: $2H_2O + 2e^- \rightarrow H_2 \uparrow + 2OH^-$ (1.7)

The reactions (iv) and (vi) can be differently expressed by

(iv´) Oxidation: $H \rightarrow H^+ + e^-$ (1.8)

(vi´) Hydrogen evolution: $2H^+ + 2e^- \rightarrow H_2 \uparrow$ (1.9)

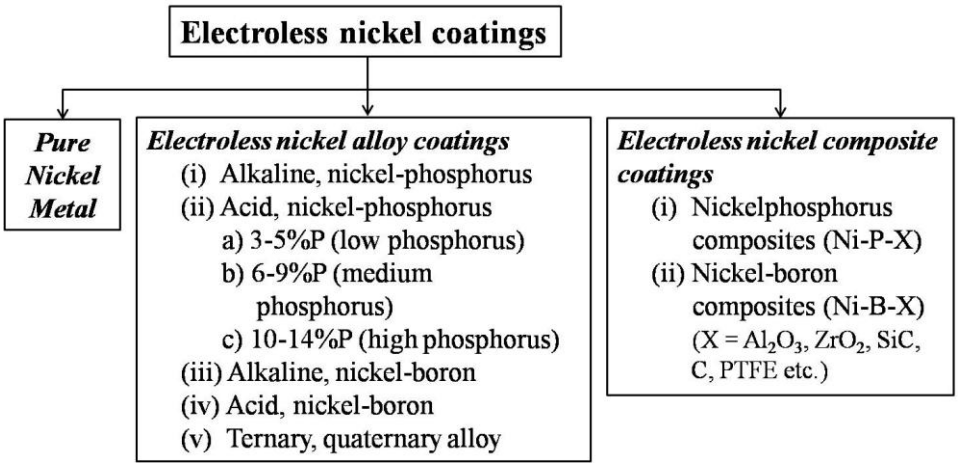

Figure 1.2. General categories of electroless nickel deposition [13, 27]

The electroless nickel plating can be classified into three primary processes: (i) alloy coatings, (ii) composite coatings and (iii) pure metallic coatings [14], as shown in Figure 1.2. In alloy coating, binary and ternary components are deposited to form an alloy layer. This includes the nickel–phosphorous (Ni-P) [18, 22], nickel–boron (Ni-B) [23], nickel–tungsten–phosphorous (Ni-W-P) [24] and nickel–cobalt–phosphorous (Ni-Co-P) [25] coating. The coated alloys could provide the superior physical and mechanical properties. Among them, nickel–phosphorous (Ni-P) alloy is

the most used alloy to produce the excellent wear resistance, corrosion resistance, solderability, polishability and magnetic property [14, 26, 27].

In general, the electroless plating bath contains a source of metal ions, reducing agent, complexing agent, stabilizer, buffering agent, wetting agent (surfactant), and its parameters include controlled temperature and pH. Their role is briefly summarized in Table 1.2 [13, 28].

Table 1.2. Components and parameters of electroless deposition bath (electrolytic) and their functions

Component/parameters	Function/Typical components
(i) Metal ions	Source of metal; nickel acetate, nickel sulfate, nickel chloride
(ii) Reducing agents	Supply electrons to reduce the metal ions; hydrazine, sodium hypophosphite, sodium borohydride, dimethylamine (DMAB)
(iii) Complexants	Prevent excess of free metal ions concentration; EDTA (tetrasodium salt), glycolic acid, citric, lactic, glycolic, proprionic acids, sodium citrate, succinic acid
(iv) Accelerators	Accelerate the reducing agent and increase the deposition; succinic acid
(v) Stabilizers	Stabilize the bath from decomposition by shielding catalytically active deposition; thiourea, lead acetate, heavy metal salts, thioorganic
(vi) Buffers	Sustain the pH for long time
(vii) pH regulators	pH adjustment; sodium hydroxide, sulfuric acid, ammonium hydroxide
(viii) Temperature	Energy for deposition

1.2.1.1. Reducing agents

Several reducing agents have been used in electroless alloys coating. Four types of reducing agent have been used for the electroless nickel bath including

sodium hypophosphite, amineboranes, sodium borohydride ($NaBH_4$), and hydrazine ($N_2H_4 \cdot H_2O$). In sodium hypophosphite plating bath, more than 70% electroless nickel is deposited from solutions. The main advantage of these solutions over those reduced by borohydride or hydrazine includes lower costs and greater ease of process control. The electroless plating in hypophosphite bath is described by the following phenomena:

i) Diffusion of reactants (Ni^{+2}, $H_2PO_2^-$) to the surface

ii) Adsorption of reactants at the surface

iii) Chemical reaction on the surface

iv) Desorption of products (HPO_3^-, H_2, H^+) from the surface

v) Diffusion of products away from the surface.

Several chemical mechanisms have been proposed for the hypophosphite reduced electroless nickel plating. Most widely accepted chemical reaction mechanisms are illustrated by [20]:

(i) Electrochemical mechanism [19], where the catalytic oxidation of the hypophosphite produces electrons at the catalytic surface, which in turn reduces the nickel and the hydrogen ions as illustrated below:

Anodic reaction occurs between water and hypophosphite, where electrons are formed by the reaction;

$$H_2PO_2^- + H_2O \rightarrow H_2PO_3^- + 2H^+ + 2e^-, \qquad E^0=0.50V \qquad (1.10)$$

Cathodic reaction utilizes the electrons generated anodic reaction, i.e., equation (1.10):

$$Ni^{2+} + 2e^- \rightarrow Ni^0, \qquad E^0 = -0.25V \qquad (1.11)$$

$$2H^+ + 2e^- \rightarrow H_2, \qquad E^0 = 0.00V \qquad (1.12)$$

$$H_2PO_2^- + 2H^+ + e^- \rightarrow P + 2H_2O, \qquad E^0 = 0.50V \qquad (1.13)$$

(ii) Atomic hydrogen mechanism [20], where the actual nickel reductant is atomic hydrogen, which acts with heterogeneous catalysis on the catalytic nickel surface. The atomic hydrogen is generated by the reaction of water with hypophosphite, and it is adsorbed at the catalytic surface:

$$H_2PO_2^- + H_2O \rightarrow HPO_3^{2-} + H^+ + 2H_{ads}, \quad (1.14)$$

The absorbed atomic hydrogen reduces nickel ions at the catalytic surface:

$$2H_{ads} + Ni^{2+} \rightarrow (Ni + 2H^+ + 2e) \rightarrow Ni^0 + 2H^+, \quad (1.15)$$

Gutzeit [20] attributed the formation of atomic hydrogen to the dehydrogenation of hypophosphite ion during formation of the metaphosphite ion:

$$H_2PO_2^- \xrightarrow{\text{catalyst}} PO_2^- + 2H, \quad (1.16)$$

Followed by the formation of orthophosphite molecule and an hydrogen ion according to:

$$PO_2^- + H_2O \rightarrow HPO_3^{2-} + H^+, \quad (1.17)$$

Secondary reaction between hypophosphite and atomic hydrogen results in the formation of phosphorus:

$$H_2PO_2^- + H_{ads} \rightarrow H_2O + OH^- + P. \quad (1.18)$$

1.2.1.2. Energy

An amount of energy or temperature of electroless nickel solutions is one of the important factors of affecting the rate of deposition. The rate of deposition is low at temperatures below 65 ºC, and increases with the increase of temperature. This is true for almost all the systems. Generally, when the operating temperature is set at 90 ºC or higher, the bath tends to be unstable [29].

1.2.2. Electroless plating of plastics

In general, before the electroless deposition of metal is carried out on the non-conductive surfaces such as plastics, glass even ceramics, the deposition requires one

or more of the following steps (as shown in Figure 1.3): (i) cleaning, (ii) surface modification, (iii) sensitization, (iv) catalyzing or (iii´) catalyzing and (iv´) activation (acceleration). Rinsing is required between the steps. [10, 12, 13, 16]

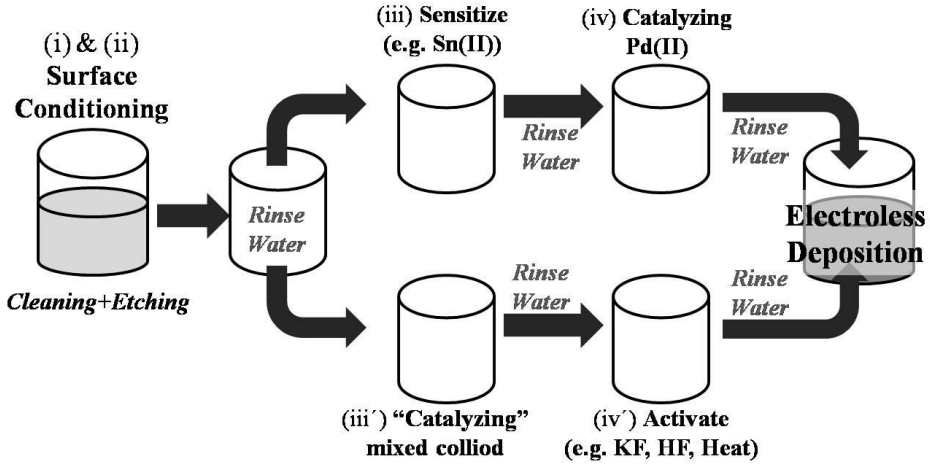

Figure 1.3. Schematic of the conventional electroless deposition process

1.2.2.1. Etching or surface conditioning

Etching, the initial processing step, is necessary to give strong metal-to-plastic adhesion. Etchants for plastic parts usually are strong oxidizing solutions that can remove away the plastic surface to vary the roughness of surface and to accomplish other two aims which are needed for adhesiveness between the plastic and the metal. First, the surface area of plastic parts is greatly increased, and the etching also made the surface of plastic parts turn from a hydrophobic (water-hating) to a hydrophilic (water-loving) material. Second, the microscopic or microcavity holes will be remained on the surface of the plastic parts after the etching, and these holes could provide the bonding sites for the deposited metal. The most common etching solution for plastics is a hot aqueous balanced mixture of chromic and sulfuric acid. More details of the etching process are described by section 1.4.1.

1.2.2.2. Sensitization and catalyzing

A catalyst is necessary to initiate the electroless metal deposition reaction on non-conductive surfaces. As mentioned in section 1.2.1, all electroless metal

reductions are dehydrogenations, however, it could be claimed that the most efficient dehydrogenation catalyst is palladium (Pd) metal. The first catalysts were only palladium chloride acid solutions and these solutions unfortunately did not absorb ions particularly well. Thus, the palladium chloride solutions usually had to be treated with a reducing agent to form the catalytic palladium metal [9]. It was discovered that stannous chloride/hydrochloric acid solution was an excellent reducing agent for the palladium chloride solutions. As shown in Figure 1.3, the sensitizing step was the stannous chloride/hydrochloric acid solution in which the stannous ion (Sn^{2+}) was adsorbed onto the surface. Then, the part was rinsed as well before the catalyzing step. In the catalyzing step, the part with the stannous ion was immersed in a palladium chloride/hydrochloric acid solution, which caused the palladium ion (Pd^{2+}) to be reduced to palladium metal (Pd^0) according to the reaction in equation (1.19) [10, 16]. However, there are other frequently used sensitizing agents which include, silver nitrate ($AgNO_3$), gold(III) chloride ($AuCl_3$) and metallic sodium (in naphthalene solution) [16].

$$Pd^{2+} + Sn^{2+} \rightarrow Sn^{4+} + Pd^0, \qquad E^0 = -0.873V \tag{1.19}$$

Moreover, as illustrated in Figure 1.3, the alternative method of catalyzing and activating is the usage of a mixed colloidal catalyst bath. In the other word, the palladium chloride, stannous chloride and hydrochloric acid are in one solution. A palladium-stannous hydrosol is one of the most common usages, which is a solution of complex ions and colloidal particles whose activity and stability depend on the chloride and stannous ion concentrations. In case of the using colloidal catalyst bath, the activation (acceleration) step is an essential step as the removal of the layer which was formed by the stabilizing agent by using potassium fluoride (KF), hydrogen fluoride (HF) or other chemicals such as hydrochloric acid or sodium hydroxide [10, 16].

1.3. Adhesion between metal and polymer

Whatever the intended propose of metallization might be, the adhesion of metal deposited onto polymer substrate must be one of the most considering issues of the finishing metalized polymer. In general, adhesion is a complex phenomena relating to the physical effects and chemical reactions at the interface [30-33]. Kinloch [30] proposed that the term adhesion is used when referring to the attraction

between the substances. Mittal [34] defines adhesion in three different forms: (i) fundamental adhesion, (ii) thermodynamic adhesion, and (iii) practical adhesion. Fundamental adhesion is defined as the summation of all interfacial intermolecular interactions between the contacting materials. The thermodynamic adhesion signifies the change in free energy when an interface is formed (or separated). The practical adhesion signifies the force or the work required to remove or detach a film or coating from the substrate irrespective of the locus of failure.

However, the recent adhesion literature contains studies of many adhesion mechanisms which include mechanical interlocking/coupling [35], molecular bonding [36, 37], thermodynamic adhesion [30], chemical bonding [38], electrical [39, 40], rheological [41, 42] and weak boundary layer (WBL) adhesion [43, 44] mechanisms. In the case of electrolytic metallization, there are several theories which have been used to explain the adhesion between electroless deposited metal and polymer substrate, and they are the mechanical interlocking, the chemical bonding, and the removal of the week boundary layer theories [9, 33, 45].

1.3.1. Thermodynamics of adhesion

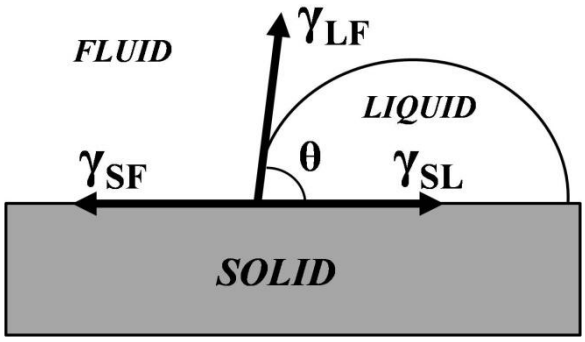

Figure 1.4. Sessile drop on a surface indicating the contact angle and the balance of interfacial forces at a fluid-solid contact

This adhesion model is introduced as the thermodynamic adsorption model or wetting model. The intimate contact between substrate and coating must be obtained as a first condition that required for this adhesion model [45]. Any trapped air, solvent or impurities must be removed from the interface of two surfaces before close

molecular contact between the materials is accomplished. Wetting equilibrium can be defined from the schematic of sessile drop on a flat solid surface. When a droplet of a liquid, L, with its fluid, F, is at rest on a solid surface, S, it takes a configuration which minimizes the energy of the system. Young [46] proposed for this equilibrium state, the vectorail representation indicated in Figure 1.4 and the equilibrium condition is written by the equation:

$$\gamma_{SF} = \gamma_{SL} + \gamma_{LF}\cos\theta \tag{1.20}$$

where θ is the contact angle measured between the solid-liquid interface. A combination of two of these subscripts represents the interfacial free energy or interfacial tension between the corresponding phases. Qualitatively, the rule holds true that the higher the surface energy of the solid is relative to the surface energy of a liquid, the better is the wettability of the solid and the smaller is the contact angle. When $\theta = 0$, the liquid totally wets the solid and spreads over the surface. Thus, the condition for spontaneous wetting to occur is:

$$\gamma_{SF} \geq \gamma_{SL} + \gamma_{LF} \tag{1.21}$$

After wetting and spreading of the liquid, physical adhesion must take place before any other bonding process can occur. According to Young equation, the thermodynamic work of adhesion W_A is given by:

$$W_A = \gamma_{SF} - \gamma_{SL} + \gamma_{LF} \tag{1.22}$$

Dupré also defined work of adhesion (W_A) leading to equation:

$$W_A = \gamma_{LF}(1 + \cos\theta) \tag{1.23}$$

Equation (1.23) may be derived from equations (1.20) and (1.22) by substitution, and it often referred to as the Young-Dupré equation [47]. Equation (1.23) provides a simple formula for W_A in terms of the measurable contact angle and the known surface tension of the test liquid.

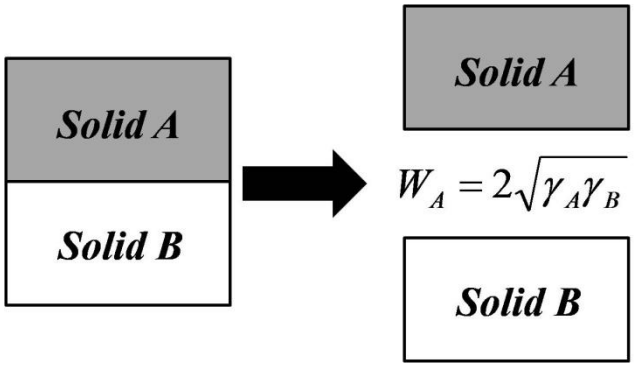

Figure 1.5. Work of adhesion at interface between two solids

However, when the thermodynamic adhesion model is used to consider the adhesion between two solids in contact as the result of interfacial interactions of physical nature occurring between the substrates and describes the energy of adhesion in terms of surface energies of materials as shown in Figure 1.5, where W_A is the work required to separate solid A and solid B creating a unit of surface area solid A and B at the expense of a unit area of solid A-B interface. In Figure 1.5, the reversible work of adhesion (W_A) is based on geometric mean theory which is proposed by Fowkes [48]. Thus, when the failure energy of an assembly of a few hundred $N \cdot m^{-1}$ is considerably higher than the reversible energy of adhesion (W_A) which is about 0.1 $N \cdot m^{-1}$ [45]. It could be said that the adhesion at polymer-metal interfaces may dominate by other adhesion mechanism.

1.3.2. Mechanical interlocking

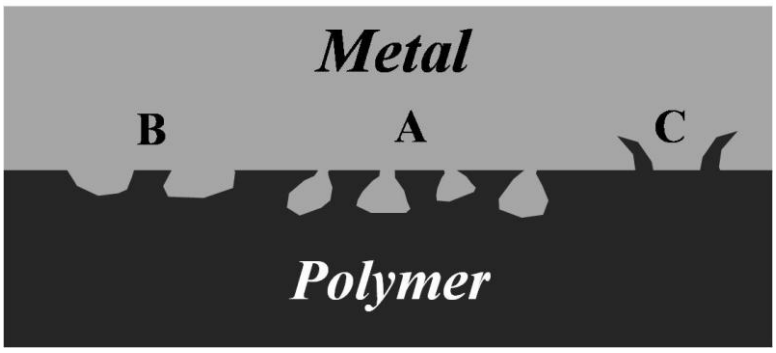

Figure 1.6. Illustration of mechanical interlocking between metal layer and polymer substrate

As the oldest adhesion theory, the mechanical interlocking theory was proposed by McBain [35]. Here the macroscopic substrate roughness provides a mechanical locking of the deposited metal film and a larger surface area of bonding. Three types of irregularities can be distinguished, as shown in Figure 1.6, of which only type A may be lead to mechanical interlocking. In case of surface irregularities of type B, a mechanical hooking is involved and the magnitude of the adhesive strength will depend on the direction of the applied force in case of type C irregularities. However, in most of the cases of enhanced adhesion due to surface irregularities this can be attributed to the increase of interfacial area. Moreover, it is possible to establish good adhesion between perfectly smooth surfaces, thus this theory cannot be considered as the universal theory and it should be considered as a possible factor in the total joint strength [30, 49]. Nevertheless, the significance of this mechanism has been rediscovered for surface irregularities of several orders of smaller magnitude. For example of interlocking on a microscopic scale, that the coating can penetrate into the pores of a substrate surface, which leads to the formation of a composite-like interphase between surface and coating layer [50, 51]. By the way, if there is no intimate contact between the metal film and the substrate, the increasing of roughness can lead to decreased adhesion by producing uncoated areas of voids or vacancies in the film, as illustrated in Figure 1.7.

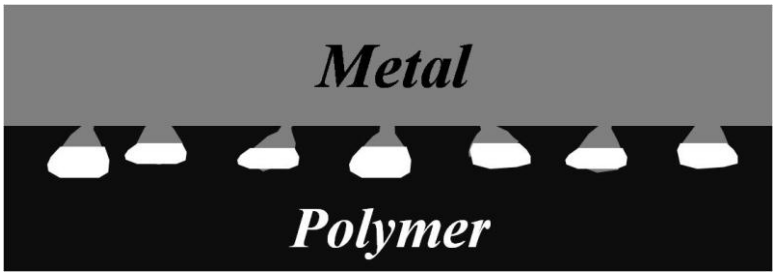

Figure 1.7. Diminished contact area between rough polymer substrate and metal layer due to poor wettability of the substrate surface

In the electroless deposition, many research groups have found that increasing of surface roughness of polymeric substrates could enhance the adhesion of electrolessly deposited metals onto polymer substrates [12, 52]. Because polymer

surfaces are usually treated with some etchants which serve to create an extensive network of fine shallow pits on the surface of the polymer and/or to create deep interlocking channels inside the polymer substrate. These pits and fissures provide anchoring points for the deposited metals. Moreover, these etchants also serve to chemically alter the polymer surface so as to render the hydrophilic property on polymer surface; thus unless the chemical nature of the polymer does not change, it is not possible to attribute changes in adhesion to differing roughness.

1.3.3. Chemical bonding

According to this theory, it proposes that when sufficiently intimate molecular contact is achieved at the interface between two materials, both materials will adhere because of the interatomic and intermolecular forces which are established between the atoms and/or molecules at the surface of adherent and substrate [30, 53]. In other word, a chemical bonds are formed between two materials coming into contact, and these chemical bonds are responsible for adhesion [30]. In general, the adhesion due to the formation of chemical bonds at the interface could obviously be strong after the surfaces are treated by employing proper surface treatments or by using various coupling agents. Similarly, in the case of deposition of metals on polymers, there are many examples in the literature where the role of chemical bonding mechanism of adhesion has been shown or suggested. Rantell studied the adhesion of polystyrene (PS) with electroless copper [54]. In Rantell's results demonstrated that different surface chemical groups were generated by different chemical treatments. The results of metal-polymer adhesion in Rantell's report are shown below:

Sample	*Peel strength ($N \cdot cm^{-1}$)*
Unmodified PS	0.7
Carboxylic acid group	3.5
Amino group	10.5
Diazo group	8.2
Hydroxy-azo group	9.8

Vilenskii et al. [54] studied metallic coating on polytetrafluoroethylene (PTFE) by vacuum sputtering of aluminum (Al). The adhesion was measured by a direct pull-off

method at room temperature. Their studies clearly show the relationship between the adhesive strength of the coating and the concentration of free peroxide radicals. Table 1.3 shows the dependence of adhesive strength of the bond on the prior treatments of PTFE surfaces. From their results of the surface of PTFE after removal of the aluminum film, they concluded that the peroxide radicals from RCOO-Al-type chemical bonds leading to high adhesive strength, and when these peroxide radicals are converted into hydroperoxide groups, the adhesion is considerably lower.

Table 1.3. Dependence of the adhesive strength of the bond of an aluminum coating to PTFE on the prior treatment of the PTFE surface

Treatment of the polymer before metallization	Functional group on the surface of the polymer	Water contact angle (º)	Uniform direct pull strength (kg_f/cm^2)
Without treatment	----	92	1-3
Glow discharge	ROO	45	197
Glow discharge + hydroquinone (1% solution in alcohol)	ROOH	70	110
Glow discharge + heat treatment at 200 ºC	─C═O─	47	150-160
Glow discharge + heat treatment at 300 ºC	─C═O─ (conjug.)	70	70-80

Moreover, there are several research groups that claimed about when the chemical bonds are formed at the metal-polymer interface, usually as a result of a charge transfer from the metal to the polymer. For example, in the case of sputter-deposition of aluminum onto polyimide, Pireaux et al. [55] have evidenced a C-O-Al complex followed by the formation of Al-O and Al-C bonds. Ho [56] proposes further that the existence of C-O-Metal complexes by charge transfer from the metal to the polymer has been observed on several other metals (Cr, Cu, Co, Ti, Ag, Au, and Pd) and seems to be a general characteristic of this type of interface. In addition, it is expected that, when the hydrophilic groups on the polymer surface make contact with the metal layer, electrons are transferred from the metal to hydrophilic groups on

polymer. Furthermore, Boiziau and Lecayon [38] have emphasized the role played by a local electrical field in the activation and improvement of interfacial reactions. The grafting on a metal (Ni, Al, Pt) of a polymerizable organic molecule, such as acrylonitrile, operates in various manners, depending on the polarization of the metallic surface.

1.3.4. Weak boundary layer (WBL)

This theory is proposed by Bikerman [44], the author showed that in the separation of an assembly, the propagation of the failure is very unlikely to take place exactly at the interface. The fracture is cohesively propagated in either solid in contact. Thus, whatever the mechanism is governing the formation of assembly, the adhesive strength of the assembly only depends on the bulk properties of the adherents. Nevertheless, Bikerman indicates that another failure mechanism can occur when the fracture moves forward in a weak interfacial layer located between the two materials. Thus, the existence of such a weak boundary layer is generally not suspected, and the removal of the weak boundary layer has been shown to improve the interfacial bonding strength. Several classes of weak boundary layers that lead to failure in adhesion are considered. They consist of one of the following four possibilities:

- Air, when the substrate is poorly wetted by the polymer

- Contaminates (impurities, additives, pollutants), or compounds of low molecular weight, moving toward the interface, and present in either the coatings or the substrates

- Products of reactions between air and substrates or between substrates.

- Unfavorable surface topography of the substrate, which acts as a rupture center.

The Bikerman's model is simple, thus it was criticized in the past. By the way, this model is recently admitted that many cases of poor adhesive strength can be attributed to these weak interfacial layers [45].

1.4. Surface treatment or conditioning of polymer surfaces

Polymers are inherently hydrophobic and low surface free energy materials, thus the metal-polymer adhesion is generally poor according to their surfaces properties [57]. Therefore, the adhesion enhancements with a variety of functional mechanisms have been introduced in industry and academia to provide solutions for poor adhesion of deposited metal on polymer. The approach to enhance the adhesion has been usually through either a dry process, i.e., plasma treatment, corona discharge, flame treatment, ion-assisted laser treatment, or a wet-chemical treatment. All treatments alter the surface region in one or many ways, for example, changing the chemical nature of the surface or the surface topography or by removing a weak boundary layer. Proper surface modifications can offer significant benefits by allowing the surface properties to be tailored to improve adhesion while leaving the bulk polymer unaffected [32, 58].

1.4.1. Wet-chemical treatment

Wet-chemical treatment or etching is essentially process that produces very roughened polymer surface which will increase surface areas, microcavities and bonding sites on polymer surfaces. As mentioned in section 1.3.2, these microcavities could provide the mechanical interlocking sites which are responsible for the enhancement of the adhesion between the deposited metals and the polymers. However, an aggressive treatment can affect the bulk polymer properties and cause fractures at the modified surface/virgin polymer interface, thereby degrading adhesion, thus this is one of the disadvantages of the chemical treatment.

Furthermore, in the early stage of treatment before the etching stage, the chemical treatments of polymer surfaces also aim to create to create new chemical/functional groups at the interface of the two materials undergoing adhesion. Thus, the surface treatment of polymers by chemical modification with reagents such as acids and oxidizers has been extensively investigated and it has been shown that the treatments increase the surface polarity. The increase in surface polarity causes an increase in molecular forces between substrates and hence the increase in adhesive strength [59]. According to the metal-polymer adhesion issue based on the surface properties of treated polymers, various types of chemicals such as potassium

permanganate and potassium dichromate/sulfuric acid can be used to modify the polymer surfaces, depending on the chemical nature of polymers. Because the chemical etching will cause specific chemical changes to the polymer surface allowing greater chemical and physical interactions to adhesives or coatings [9, 60]. As shown in some literatures, the wet-chemical etching process with dichromate/sulfuric acid solution ($K_2Cr_2O_7$-H_2SO_4-H_2O) is commonly used to improve the adhesion of electroless nickel deposition onto various polymers such as polypropylene (PP), polyethylene (PE) and acrylonitrile-butadiene-styrene (ABS) [61-63].

However, the main disadvantage of this method is the need for hazardous chemicals that sustain high costs in their safe use and the proper disposal of waste chemical solutions [32, 53]. Therefore, because the presence of chromic acid in the conventional etching imposes serious operating problems of an environmental nature, many researchers also proposed several of alternative surface-modifier solution to avoid using of chromium, Cr(VI), solutions. Teixeira et al. [64] introduced the pretreatment process for ABS substrate with non-polluting solutions of hydrogen peroxide (H_2O_2), nitric acid (HNO_3) and sulfuric acid (H_2SO_4) as an alternative to the chromic-sulfuric acid solutions. Wang et al. [65-67] also proposed an environment-friendly surface treatment of ABS resin system which is consisting of the manganese dioxide-phosphoric acid-sulfuric acid (MnO_2-H_3PO_4-H_2SO_4) colloid.

1.4.2. Plasma treatment

Plasma treatments are a very effective way of increasing the inherently poor surface properties of polymers, and only short plasma treatment times are required to increase the bond strength between two substrates. This form of surface treatment allows for modification or tailoring of surface properties without changing the overall bulk properties of the polymer and is generally environmentally friendly. Plasma treatment of surfaces often induces the formation of oxygen-containing functional groups such as hydroxyl (OH) groups, resulting in increased surface wetting and improved adhesion through the mechanism of molecules bonding [68-70] as described in section 1.3.3. For example, in case of polypropylene (PP) surface, the functional groups on polymer which include carbonyl (C=O), in particular, but also C–O,

carboxylate (COO), hydroxyl (OH) and carboxyl (–OOH), they are reported to aid adhesion at the surface of polymers [71]. There are many plasma treatment methods and techniques that have been investigated to enhance polymer surface adhesion [68, 72], thus, the plasma treatment of polymer surfaces also was introduced as the pre-treatment method before the metallization by many research groups [73-76]. However, according to environmental contaminants, re-orientation of surface groups and further chemical reaction at the surface with time, in many situations, result in an "ageing" effect, which also mean as the surface hydrophobicity is recovered with time. This is a very serious issue or disadvantage point of using plasma treatment in industry where surface treated films may be stored prior to further coating.

1.4.3. Flame treatment and corona discharge

Flame treatment and corona discharge [77-79], the effect on the polymer surface is almost the same for these pre-treatment methods. Because the polymer surface is oxidized which leads to the introduction of polar functional groups like hydroxyl, carboxylic and carboxylic groups. In flame treatment the polymer surface is passed through a flame generated by the combustion of an air-hydrocarbon gas mixture. It is usually applied to thick polyolefin objects such as blow-moulded bottles and thermo-formed tubs. The most important variables in the process are air/gas ratio, the air/gas flow rate, the distance between surface and burner, and exposure time. The high temperature involved (the adiabatic flame temperature is ≈ 2000 ºC) is the weak point of the flame treatment method. The corona discharge treatment is especially suitable for the continuous treatment of plastic films. The polymer surface is exposed to a discharge between grounded and powered electrodes at high voltage. However, the corona is a shower of arcs or sparks and each discharge point may cause localized damage and it is difficult to apply on three-dimensional components. Moreover, the effect of corona treatment is reported to be short-lived for many materials [53].

1.4.4. Other treatments

A variety of surface treatment techniques for improving adhesion other than chemical, plasma and flame/corona treatments have been introduced. For example, another method to increase the number of oxygen containing functional groups at the

polymer surface is to pre-treat it with UV/ozone. The ozone is generated from the oxygen of the air and the polymer surface is simultaneously bombarded with photons radiation. The process is mainly used for polypropylene and polyester parts and has shown rapid uptake of oxygen functional groups [80]. However, on a smaller scale many other techniques are used or developed. For example, fluorination [81], CO2 laser radiation [82], excimer laser treatment [83], electron beam irradiation in air [84, 85], photo grafting [86], and high-intensity ultrasound [87], but they are neither as efficient as wet-chemical treatment for reaching sufficient adhesion, nor available on the industrial scale [88].

1.5. Developed and environmental-friendly metallization

As mentioned in previous section, the surface conditioning of plastic surfaces prior to metallization is generally conducted with the harsh and/or toxic solutions namely sulfuric/chromic acid solutions. In addition, the etching, neutralization, catalyzing and activation of catalyst also are needed before the electroless plating on polymers, and they always come along with the generation of a huge amount of the waste water. Thus, the electroless metal deposition technique that does not require chemical etching and/or conventional catalyzing is desired as an environmentally benign production process.

Numerous chromium-free etching in solution and dried treatment techniques have developed for applying with the electroless deposition method. Garcia et al. [89] proposed an efficient palladium- and chromium-free process for the electroless plating on acrylonitrile-butadiene-styrene (ABS) polymers, which is based on the ion-exchange properties of poly(acrylic acid) (PAA) chemically grafted onto ABS, and then using copper seeding step before the nickel or copper metallization. Kimura et al. [90] introduce a simple route to depositing nickel layer patterns using photocross-linked polymer thin films containing palladium catalysts, which can be used as adhesive interlayers for fabrication of nickel patterns on glass and plastic substrates. Kim et al. [91] and Magallón-Cacho et al. [92] reported the surface modification of the ABS by the photocatalytic reaction in titanium dioxide (TiO_2) solution for the substitution of the etching stage in the electroless plating process.

1.5.1. Supercritical fluid-assisted metallization

Recently, supercritical fluid deposition (SCFD) has attracted attention as an environmentally benign technique for creating metal-polymer and metal composite materials. The SCFD involves two main steps as shown in Figure 1.8, namely: (i) first step is the dissolution of a metallic precursor into the supercritical fluid (SCF) and the exposure of a substrate to the SCF solution so as to incorporate the metallic precursor on the substrate surface. (ii) Then, the metallic precursor is reduced to metal by some methods, such as chemical reduction with a reducing agent, thermal reduction and decomposition by heating, and consequently metal films or nanoparticles are formulated on the surfaces [93, 94].

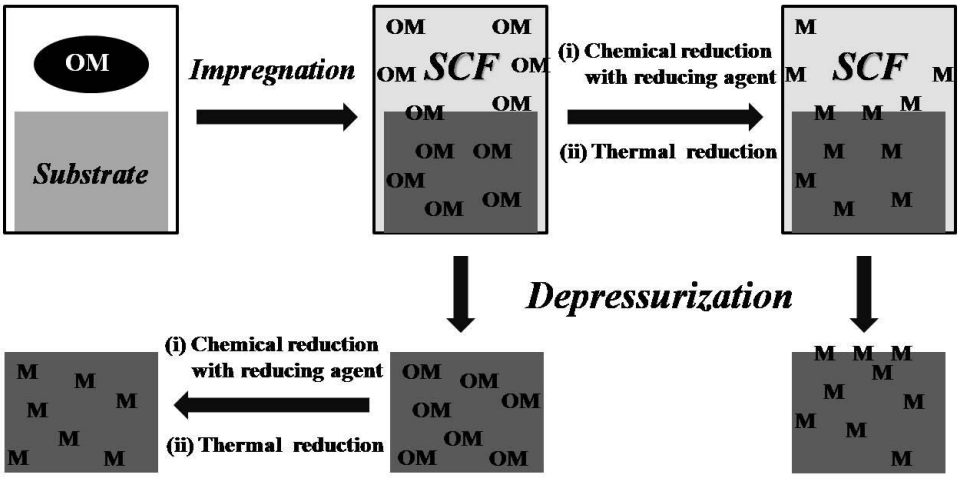

Figure 1.8. Schematic of using supercritical fluid (SCF) as a solvent to synthesize metal nanoparticles via deposition or impregnation (OM: metal complex, M: metal nanoparticles) [94]

Using SCF as the processing medium for deposition of metal nanoparticles or layer has many advantages which are related to properties of the SCF. The properties of the SCF are different from those of liquids and gases and are tunable simply by changing the pressure and temperature of fluids. In particular, density and viscosity of fluids change dramatically at conditions close to the critical point of the fluids. Since fluid densities can approach or even exceed those of liquids, various supercritical fluids (SCFs) are good solvents for a wide range of organic and organometallic

compounds. Compared with conventional liquid solvents, high diffusivities in the SCFs combined with their low viscosities result in enhanced mass transfer characteristics. The low surface tension of the SCFs not only permit better penetration and wetting of pores than liquid solvents do, but also avoid the pore collapse which can occur on certain structures such as in the aerogels with using of the liquid solvents [95]. Among the SCFs, a supercritical carbon dioxide ($scCO_2$), readily accessible with a T_c of 31 ºC and a P_c of 7.38 MPa, is attractive since it is abundant, inexpensive, non-flammable, non-toxic and environmentally benign. Besides the environmental benefits, the $scCO_2$ has high permeation rate in virtually all polymers and the exposure to the $scCO_2$ results in various extents of swelling and enhanced chain mobility of the polymer, which makes it possible to incorporate metallic precursors into various polymers [96, 97]. Moreover, the degree of polymer swelling, diffusion rates within the substrate, and the partitioning of precursors between the SCF and the swollen polymers can be controlled by density mediated adjustments of solvent strength via changes in temperature and pressure of fluids [97].

According to the benefits of using $scCO_2$, many researchers have attempted to apply $scCO_2$ in the electrodeposition methods for several substrates. Sone et al. [98] developed a new electroplating technology for metallic substrates. They combined the conventional electroplating technique with $scCO_2$-assisted deposition where an electroplating solution was emulsified with a non-ionic surfactant, i.e., dense CO_2 and hexane. They consecutively studied the effects of dense CO_2 on the Ni film and found that low viscosity of dense CO_2 and its miscibility with hydrogen made the surface of the plated nickel metal film surface uniform and smooth [99]. Sone's research group also advanced their $scCO_2$-emulsification technique to an electroless plating technique for coating a polyimide (PI) substrate with nickel-phosphorus metal film [100-102]. They reported that the catalyzation in $scCO_2$ with palladium(Pd)-bis(acetylacetonate) influenced the electroless plating mechanism on the PI substrate. Zhao et al. [103] proposed a $scCO_2$-assisted electroless plating method for polymeric substrates, especially polymeric fibers, where Pd(II) hexafluoroacetylacetonate, $Pd(hfa)_2$, was infused into Kevlar® fibers with $scCO_2$ and simultaneously activated by over-heating to use the palladium metal as a catalyst of the plating reaction. The Kevlar fibers was then immersed in an electroless copper plating solution to coat the Kevlar with a copper metal layer. They extended their plating technique to several polymeric fibers

and studied the effect of a thermal treatment on the adhesive strength of the metal layer to poly-(p-phenylene terephthalamide) (PPTA), i.e., aramid fibers [104]. Adachi et al. [105] proposed a novel process of electroless nickel–phosphorus alloy plating onto polymeric substrates. They used $scCO_2$ as both a solvent for infusing palladium metal complex, $Pd(hfa)_2$, into polymers and as a plasticizer to soften the surface of the polymeric substrates. Furthermore, they also added the $scCO_2$ into an electroless plating solution to enhance the solvency of the solution in polymeric substrate during the conduction of electroless plating reaction, which consequently could increase the adhesiveness between the electrolessly deposited alloy layer and the polymeric substrates.

1.5.2. Palladium-free electroless plating

Furthermore, in the conventional activation processes, noble metal palladium is usually employed as the catalyst sites to initiate the electroless metal plating reaction on the plastic parts. The cost of palladium has increased in recent years, which makes the price for electroless metal deposition rise. Thus, it is very important to develop a cost effective activation techniques. Lu et al. [106, 107] established a new, efficient, palladium- and etchant-free process for the electroless nickel plating of poly(ethylene terephthalate) (PET) fabric. The nickel coating obtained in this palladium-free process can pass through ultrasonic washing challenge, and shows excellent adhesion with the PET substrate. A novel surface activation process has been proposed by Tang et al. [108-110] for plating onto ABS plastics by employing biopolymer chitosan. This proposed method enhanced the adhesive strength of plating layers and plastic substrates by chemical sorption instead of the physical sorption in the conventional sensitizing-activation method. In addition, etching solution without chromium was employed to modify the surface of ABS by an environmental friendly process.

1.6. Scopes and objectives of this study

The aim of this study is to introduce the novel electroless nickel-phosphorus (Ni-P) plating technique into the thermoplastic polymer substrates. This novel electroless plating process technique method was developed for extrusion or injection molded-plastic parts, especially those based on polyamide 6 (PA6), and it was proposed by Ohshima research group [105]. The method mainly consisted of two steps: the first step was the $scCO_2$-assisted impregnation of the polymeric substrate with a catalyst precursor, Pd(II) hexafluoroacetylacetonate ($Pd(hfa)_2$), and the second step was an electroless Ni-P alloy plating reaction. According to Ohshima group's studies, they observed that a Ni-P metal-polymer composite layer was formed between the metal layer and the polymer matrix during the electroless plating reaction and concluded that the thicker metal-polymer composite layer provided stronger adhesion between the metal layer and the polymeric substrate. Moreover, they speculated that the higher mass transfer rate of the plating solution into the polymeric substrate could increase the metal-polymer composite layer thickness and the metal-polymer adhesion. Since the major ingredient in the electroless plating solution is water, the mass transfer rate of the plating solution into the polymer substrate was strongly affected by the degree of hydrophilicity or moisture content of the polymeric substrate. Unfortunately, most polymers are highly hydrophobic; thus, Ohshima research group's method has been limited to polymers with a moderately high water absorption rate, such as poly(methyl methacrylate) (PMMA) or PA6.

This study focused mainly on polypropylene (PP) and acrylonitrile-butadiene-styrene copolymer (ABS) substrates because PP, ABS, and other polyolefin resins have increasingly been used for automotive applications, thus, there is great interest in applying the newly environmentally benign electroless Ni-P alloy plating technique to these polymers. Nevertheless, from the high degree of hydrophobicity, the PP and ABS substrates without the surface conditioning were barely metalized by the novel electroless plating method. The electroless plating reaction occurs only on the surface of the polymeric substrate because the initial electroless-plated metal layer prevents the plating solution from penetrating further inside the polymeric substrate. This mechanism prevents the metal-polymer composite layer from forming inside the substrate. Thus, there was less of an anchoring effect, and the adhesive strength of the metal layer to the polymeric substrate was decreased.

The surface of the PP and ABS substrate, as well as those of other highly hydrophobic polymers, must be modified by a hydrophilic surface treatment to perform the developed electroless plating method. So far, various techniques have been employed to modify the hydrophilicity of the polymer surface as mention in section 1.4. However, most of the environmentally-friendly pre-treatments could modify the hydrophilicity only at short distances from the surface (less than 10 nm) and could not provide metal-polymer adhesion comparable to conventional chemical etching. Thus, in this study, the addition of a block copolymer appears advantageous in case to overcome the problem related to the hydrophilic property of polymer substrate. The block copolymer (Pelestat®, Sanyo Chemical) was dry-blended with PP and ABS resins and the blended polymer was injection-molded to prepare the substrate. The addition of block copolymer into base polymer could significantly increase the hydrophilicity of the blend polymer because this block copolymer was originally developed as an antistatic agent for polymers and could be highly dispersed in a base polymer matrix.

Therefore, in Chapter 2, the hydrophilic modification of PP by blending a polypropylene(PP)-polyethyleneoxide(PEO) block (PP-b-PEO) copolymer with PP, was employed to increase the hydrophilicity of the PP prior to the novel electroless Ni-P alloy deposition. The results showed that blending the PP-b-PEO copolymer with PP increased the diffusion of the plating solution in the PP blend substrate and a uniform Ni-P metal layer was successfully formed onto PP with an average adhesive strength of 7.9±0.5 N/cm to the polymeric substrate. Furthermore, the effects of the process variables and process conditions on the adhesive strength of the Ni-P metal film to the polymeric substrate were investigated.

In Chapter 3, we still mainly discussed about the $scCO_2$-assisted electroless Ni-P plating technique on PP via the hydrophilic modification, however, apart from the previous chapter; the effect of PP/PP-b-PEO copolymer blend morphology on the metal-polymer adhesion was investigated. Thus, in Chapter 3, five grades of PP with different viscosities were used to investigate the effects of the viscosity ratio of PP to PP-b-PEO on the blend morphology and the adhesiveness of the metal to the polymer. The results demonstrated that the blend morphology of PP-b-PEO and PP strongly affected the adhesiveness of the metal layer to the substrate. Moreover, by bringing the viscosity ratio close to a value of approximately twelve, the degrees of elongation

and orientation of the PP-b-PEO copolymer domains near the surface were maximized, resulting in the thickest metal-polymer composite layer, and the highest metal-polymer adhesiveness. By controlling the blend morphology, a uniform Ni-P layer was successfully formed with an average adhesive strength of 8.8±1.8 N/cm to the PP blend substrate.

In Chapter 4, different from the two previous chapters, the aim of this work is to introduce the novel electroless Ni-P plating with co-polymer-based hydrophilic modification into ABS substrates. In this work, a multi-block copolymer poly(ether-ester-amide), (PEEA), and ABS resins was dry-blended and prepared the blend substrate by using injection-molded process as the hydrophilic modification of the ABS-plate surface. The role of PEEA copolymer and butadiene rubbery domains on the metal-polymer adhesion was investigated. The results showed that the amount of PEEA copolymer and butadiene rubbery domain strongly affected the metal-polymer composite layer and consequently the metal-polymer adhesion. In the end, by blending the PEEA copolymer with ABS increased the diffusion of the plating solution in the ABS blend substrate and the Ni-P metal layer was successfully formed onto ABS with an average adhesive strength of 9.1±0.5 N/cm to the polymeric substrate.

In Chapter 5, main points of this study regarding to the results clarified from Chapter 2 to Chapter 4 are summarized.

1.7. References

[1] G. Grundmeier, M. Stratmann, Annu Rev Mater Res, 35 (2005) 571-615.

[2] E. Sacher, Acs Sym Ser, 440 (1990) 1-7.

[3] D. Feldman, Journal of Polymer Science Part A: Polymer Chemistry, 29 (1991) 1834-1834.

[4] S.M. Rossnagel, Journal of Vacuum Science & Technology B, 16 (1998) 2585-2608.

[5] R. Fix, R.G. Gordon, D.M. Hoffman, Chemistry of Materials, 5 (1993) 614-619.

[6] P.R. Willmott, Progress in Surface Science, 76 (2004) 163-217.

[7] P. Holubar, M. Jilek, M. Sima, Surface and Coatings Technology, 133-134 (2000) 145-151.

[8] T. Karasawa, Y. Miyata, Thin Solid Films, 223 (1993) 135-139.

[9] G.A. Krulik, J Chem Educ, 55 (1978) 361-365.

[10] G.O. Mallory, J.B. Hajdu, in, William Andrew Publishing/Noyes, 1990, pp. 377-400.

[11] D. Li, K. Goodwin, C.-L. Yang, J Mater Sci, 43 (2008) 7121-7131.

[12] S.C. Domenech, E. Lima, D. V, J.C. De Lima, N.G. Borges, A.O.V. Avila, S. V, Appl Surf Sci, 220 (2003) 238-250.

[13] J. Sudagar, J. Lian, W. Sha, Journal of Alloys and Compounds, 571 (2013) 183-204.

[14] R.C. Agarwala, V. Agarwala, Sadhana, 28 (2003) 475-493.

[15] B.-H. Woo, M. Sone, A. Shibata, C. Ishiyama, S. Edo, M. Tokita, J. Watanabe, Y. Higo, Surface and Coatings Technology, 204 (2010) 1785-1792.

[16] M. Schlesinger, Electroless Deposition of Nickel, in: Modern Electroplating, John Wiley & Sons, Inc., 2010, pp. 447-458.

[17] G.G. Gavrilov, in, Portcullis Press, Redhill [Eng.], 1979.

[18] A. Brenner, G.E. Riddell, J Res Nat Bur Stand, 37 (1946) 31-34.

[19] A. Brenner, G. Riddell, J Res Nat Bur Stand, 39 (1947) 385-395.

[20] G.O. Mallory, J.B. Hajdu, in, William Andrew Publishing/Noyes, 1990, pp. 1-56.

[21] J.E.A.M. Meerakker, Journal of Applied Electrochemistry, 11 (1981) 395-400.

[22] B. Bozzini, C. Martini, P.L. Cavallotti, E. Lanzoni, Wear, 225–229, Part 2 (1999) 806-813.

[23] A. Srivastava, S. Mohan, V. Agarwala, R.C. Agarwala, Z Metallkd, 83 (1992) 254-257.

[24] F. Pearlstein, R. Wick, A. Gallaccio, Journal of the Electrochemical Society, 110 (1963) 843-846.

[25] D.H. Kim, K. Aoki, O. Takano, Journal of the Electrochemical Society, 142 (1995) 3763-3767.

[26] H. Matsubara, T. Yonekawa, Y. Ishino, H. Nishiyama, N. Saito, Y. Inoue, Electrochimica Acta, 47 (2002) 4011-4018.

[27] Y.M. Chow, W.M. Lau, Z.S. Karim, Surface and Interface Analysis, 31 (2001) 321-327.

[28] K.K. Kar, D. Sathiyamoorthy, J Mater Process Tech, 209 (2009) 3022-3029.

[29] A.S.M.I.H. Committee, in, ASM International, pp. 200.

[30] A.J. Kinloch, J Mater Sci, 15 (1980) 2141-2166.

[31] R. Good, M. Chaudhury, C. Oss, Theory of Adhesive Forces Across Interfaces, in: L.-H. Lee (Ed.) Fundamentals of Adhesion, Springer US, 1991, pp. 153-172.

[32] F. Awaja, M. Gilbert, G. Kelly, B. Fox, P.J. Pigram, Progress in Polymer Science, 34 (2009) 948-968.

[33] K.L. Mittal, J Vac Sci Technol, 13 (1976) 19-25.

[34] K.L. Mittal, Abstr Pap Am Chem S, 210 (1995) 145-IEC.

[35] J.W. McBain, D.G. Hopkins, J Phys Chem-Us, 29 (1925) 188-204.

[36] L. Sharpe, Interfaces, Interphases and "Adhesion": A Perspective, in: G. Akovali (Ed.) The Interfacial Interactions in Polymeric Composites, Springer Netherlands, 1993, pp. 1-20.

[37] V.E. Basin, Progress in Organic Coatings, 12 (1984) 213-250.

[38] C. Boiziau, G. Lecayon, Surface and Interface Analysis, 12 (1988) 475-485.

[39] B.V. Deryagin, N.A. Krotova, Dokl Akad Nauk Sssr+, 61 (1948) 849-852.

[40] S.M. Skinner, R.L. Savage, J.E. Rutzler, Journal of Applied Physics, 24 (1953) 438-450.

[41] A.N. Gent, J. Schultz, J Adhesion, 3 (1972) 281-&.

[42] J. Schultz, A.N. Gent, J Chim Phys Pcb, 70 (1973) 708-716.

[43] N.G. Gaylord, H. Dannenberg, Journal of Polymer Science, 62 (1962) S21-S21.

[44] J.J. Bikerman, Journal of Applied Chemistry, 11 (1961) 81-85.

[45] G. Fourche, Polymer Engineering & Science, 35 (1995) 957-967.

[46] T. Young, Philosophical Transactions of the Royal Society of London, 95 (1805) 65-87.

[47] C.M. Tag, M. Jarn, B. Granqvist, J. Jarnstrom, J. Peltonen, J.B. Rosenholm, Holzforschung, 61 (2007) 516-522.

[48] F.M. Fowkes, Industrial & Engineering Chemistry, 56 (1964) 40-52.

[49] F. Garbassi, M. Morra, E. Occhiello, in, John Wiley & Sons.

[50] D.E. Packham, C. Johnston, Int J Adhes Adhes, 14 (1994) 131-135.

[51] N.H. Ladizesky, I.M. Ward, J Mater Sci, 18 (1983) 533-544.

[52] C.A. Villamizar, L. Feijoo, A. Miller, P. Vazquez, Abstr Pap Am Chem S, 182 (1981) 187-COLL.

[53] M.C. van der Leeden, G. Frens, Advanced Engineering Materials, 4 (2002) 280-289.

[54] K.L. Mittal, Polymer Engineering & Science, 17 (1977) 467-473.

[55] J.J. Pireaux, M. Vermeersch, C. Grégoire, P.A. Thiry, R. Caudano, T.C. Clarke, The Journal of Chemical Physics, 88 (1988) 3353-3362.

[56] P.S. Ho, Appl Surf Sci, 41–42 (1989) 559-566.

[57] D.J. Burnett, F. Thielmann, R.A. Ryntz, Journal of Coatings Technology Research, 4 (2007) 211-215.

[58] G. Fourche, Polymer Engineering & Science, 35 (1995) 968-975.

[59] L.G. Beholz, C.L. Aronson, A. Zand, Polymer, 46 (2005) 4604-4613.

[60] D. Briggs, V.J.I. Zichy, D.M. Brewis, J. Comyn, R.H. Dahm, M.A. Green, M.B. Konieczko, Surface and Interface Analysis, 2 (1980) 107-114.

[61] M. Charbonnier, M. Romand, Int J Adhes Adhes, 23 (2003) 277-285.

[62] W. Gui-xiang, L. Ning, H. Hui-li, Y. Yuan-chun, Appl Surf Sci, 253 (2006) 480-484.

[63] J. Piglowski, M.C. Coen, R. Schäfer, J. Kressler, R. Mülhaupt, Die Angewandte Makromolekulare Chemie, 246 (1997) 97-107.

[64] L.A.C. Teixeira, M.C. Santini, J Mater Process Tech, 170 (2005) 37-41.

[65] Z.X. Li, N. Li, L. Yin, Y. He, Z.L. Wang, Electrochem Solid St, 12 (2009) D92-D95.

[66] Z.L. Wang, Z.X. Li, Y. He, Z.X. Wang, Journal of the Electrochemical Society, 158 (2011) D664-D670.

[67] W.X. Zhao, J. Ding, Z.L. Wang, Langmuir, 29 (2013) 5968-5973.

[68] D. Hegemann, H. Brunner, C. Oehr, Nuclear Instruments and Methods in Physics Research Section B: Beam Interactions with Materials and Atoms, 208 (2003) 281-286.

[69] B. Mutel, J. Grimblot, O. Dessaux, P. Goudmand, Surface and Interface Analysis, 30 (2000) 401-406.

[70] J.F. Friedrich, R. Mix, G. Kühn, Surface and Coatings Technology, 200 (2005) 565-568.

[71] J. Lai, B. Sunderland, J. Xue, S. Yan, W. Zhao, M. Folkard, B.D. Michael, Y. Wang, Appl Surf Sci, 252 (2006) 3375-3379.

[72] Q.F. Wei, Materials Characterization, 52 (2004) 231-235.

[73] K. De Bruyn, M. Van Stappen, H. De Deurwaerder, L. Rouxhet, J.P. Celis, Surface and Coatings Technology, 163–164 (2003) 710-715.

[74] J.E. Gray, P.R. Norton, R. Alnouno, C.L. Marolda, M.A. Valvano, K. Griffiths, Biomaterials, 24 (2003) 2759-2765.

[75] M. Charbonnier, M. Romand, E. Harry, M. Alami, Journal of Applied Electrochemistry, 31 (2001) 57-63.

[76] M. Šimor, J. Ráhel', M. Černák, Y. Imahori, M. Štefečka, M. Kando, Surface and Coatings Technology, 172 (2003) 1-6.

[77] C. Sun, D. Zhang, L.C. Wadsworth, Advances in Polymer Technology, 18 (1999) 171-180.

[78] D. Briggs, D.G. Rance, C.R. Kendall, A.R. Blythe, Polymer, 21 (1980) 895-900.

[79] A.P. Pijpers, R.J. Meier, Journal of Electron Spectroscopy and Related Phenomena, 121 (2001) 299-313.

[80] L.F. MacManus, M.J. Walzak, N.S. McIntyre, Journal of Polymer Science Part A: Polymer Chemistry, 37 (1999) 2489-2501.

[81] H.S. Han, K.L. Tan, E.T. Kang, Journal of Applied Polymer Science, 76 (2000) 296-304.

[82] A. Hartwig, J. Hunnekuhl, G. Vitr, S. Dieckhoff, F. Vohwinkel, O.D. Hennemann, Journal of Applied Polymer Science, 64 (1997) 1091-1096.

[83] H.C. Man, M. Li, T.M. Yue, Int J Adhes Adhes, 18 (1998) 151-157.

[84] O.N. Tretinnikov, S. Ogata, Y. Ikada, Polymer, 39 (1998) 6115-6120.

[85] P.S. Majumder, A.K. Bhowmick, Radiation Physics and Chemistry, 53 (1999) 63-78.

[86] B. Rånby, Int J Adhes Adhes, 19 (1999) 337-343.

[87] G.J. Price, A.A. Clifton, Polymer International, 48 (1999) 1141-1146.

[88] M.D. Green, F.J. Guild, R.D. Adams, Int J Adhes Adhes, 22 (2002) 81-90.

[89] A. Garcia, T. Berthelot, P. Viel, A. Mesnage, P. Jegou, F. Nekelson, S. Roussel, S. Palacin, Acs Appl Mater Inter, 2 (2010) 1177-1183.

[90] M. Kimura, H. Yamagiwa, D. Asakawa, M. Noguchi, T. Kurashina, T. Fukawa, H. Shirai, ACS Applied Materials and Interfaces, 2 (2010) 3714-3717.

[91] G.G. Kim, J.A. Kang, J.H. Kim, K.-y. Lee, S.J. Kim, S.-J. Kim, Scripta Materialia, 56 (2007) 349-351.

[92] L. Magallón-Cacho, J.J. Pérez-Bueno, Y. Meas-Vong, G. Stremsdoerfer, F.J. Espinoza-Beltrán, Surface and Coatings Technology, 206 (2011) 1410-1415.

[93] C. Erkey, The Journal of Supercritical Fluids, 47 (2009) 517-522.

[94] Y. Zhang, C. Erkey, The Journal of Supercritical Fluids, 38 (2006) 252-267.

[95] J.A. Darr, M. Poliakoff, Chemical Reviews, 99 (1999) 495-542.

[96] J. Rosolovsky, R.K. Boggess, A.F. Rubira, L.T. Taylor, D.M. Stoakley, A.K. StClair, J Mater Res, 12 (1997) 3127-3133.

[97] J.J. Watkins, T.J. McCarthy, Chemistry of Materials, 7 (1995) 1991-1994.

[98] H. Yoshida, M. Sone, A. Mizushima, H. Yan, H. Wakabayashi, K. Abe, X.T. Tao, S. Ichihara, S. Miyata, Surface and Coatings Technology, 173 (2003) 285-292.

[99] H. Yan, M. Sone, N. Sato, S. Ichihara, S. Miyata, Surface and Coatings Technology, 182 (2004) 329-334.

[100] B.-H. Woo, M. Sone, A. Shibata, C. Ishiyama, K. Masuda, M. Yamagata, T. Endo, T. Hatsuzawa, Y. Higo, Surface and Coatings Technology, 202 (2008) 3921-3926.

[101] B.-H. Woo, M. Sone, A. Shibata, C. Ishiyama, K. Masuda, M. Yamagata, Y. Higo, Surface and Coatings Technology, 203 (2009) 1971-1978.

[102] B.h. Woo, M. Sone, S. Akinobu, C. Ishiyama, K. Masuda, M. Yamagata, Y. Higo, Microelectronic Engineering, 86 (2009) 1179-1182.

[103] X. Zhao, K. Hirogaki, I. Tabata, S. Okubayashi, T. Hori, Surface and Coatings Technology, 201 (2006) 628-636.

[104] N. Martinez, K. Hisada, I. Tabata, K. Hirogaki, S. Yonezawa, T. Hori, The Journal of Supercritical Fluids, 56 (2011) 322-329.

[105] H. Adachi, K. Taki, S. Nagamine, A. Yusa, M. Ohshima, The Journal of Supercritical Fluids, 49 (2009) 265-270.

[106] Y. Lu, S. Jiang, Y. Huang, Surface and Coatings Technology, 204 (2010) 2829-2833.

[107] Y. Lu, L. Xue, F. Li, Appl Surf Sci, 257 (2011) 3135-3139.

[108] X. Tang, M. Cao, C. Bi, L. Yan, B. Zhang, Materials Letters, 62 (2008) 1089-1091.

[109] X. Tang, C. Bi, C. Han, B. Zhang, Materials Letters, 63 (2009) 840-842.

[110] X. Tang, J. Wang, C. Wang, B. Shen, Surface and Coatings Technology, 206 (2011) 1382-1388.

Chapter II

Electroless Nickel Plating on Polypropylene via Hydrophilic Modification and Supercritical Carbon Dioxide Pd-complex Infusion

2.1. Introduction

In the automotive and electronics industries, plastic parts can be metalized for decorative or functional purposes. A thin metal coating can give polymer parts a glossy appearance and high reflectivity or improve the resistance to abrasion, the electrical conductivity and the electromagnetic shielding [1, 2]. Several techniques to metalize the polymer substrate have been proposed, such as physical–chemical vapor deposition, metal-powder coating, and electroless plating [3]. Among these methods, the electroless plating technique has been widely used in the automotive, aerospace, packaging and microelectronics industries for coating polymer products with sophisticated shapes [4]. The current electroless plating technique comprises a relatively complex multistep process: degreasing, chemical etching, surface seeding of a catalyst for the plating reaction and an electroless plating reaction as shown in the left-hand side of Figure 2.1. In the chemical etching process, harmful oxidative acids such as chromic acid are used to roughen the surface of the polymer substrate to create a strong adhesion of the metal layer [1]. Furthermore, the chemical etching and the catalyst deposition produce a huge amount of wastewater. Thus, from an environmental viewpoint, the conventional electroless plating process must be re-designed so that the amounts of harmful acid and wastewater can be minimized while maintaining a sufficient adhesive strength [5].

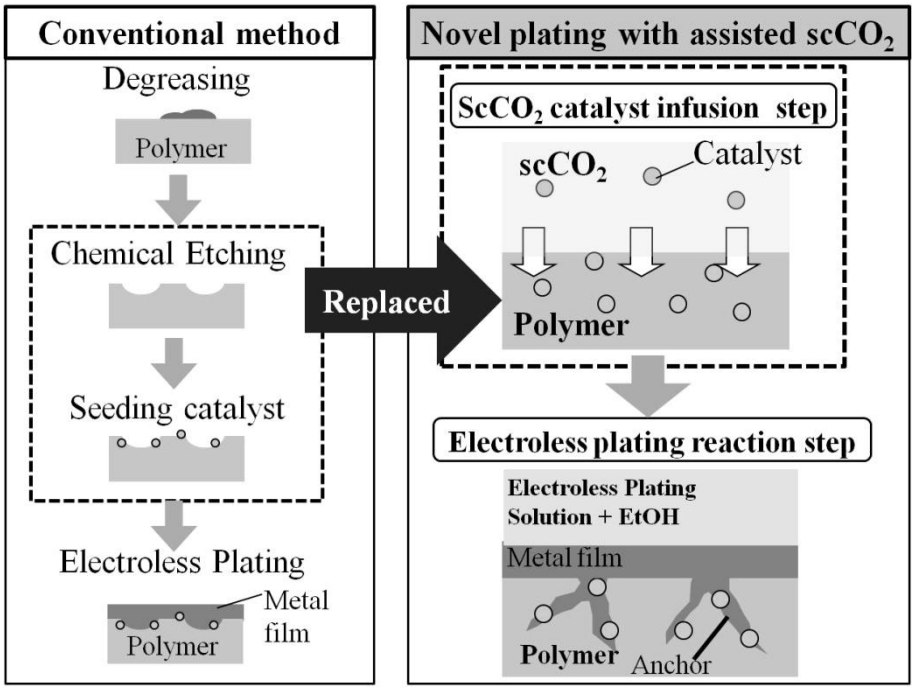

Figure 2.1. Schematics of conventional and developed $scCO_2$-assisted electroless plating processes

Supercritical fluid deposition (SCFD) has attracted attention as an environmentally benign technique for creating metal/polymer and metal/composite materials. The SCFD first dissolves a metallic precursor into the supercritical fluid (SCF) and then the substrate is exposed to the SCF so as to incorporate the metallic precursor on the substrate surface. Then, the metallic precursor is reduced to metal by some methods, such as chemical reduction with a reducing agent, thermal reduction and decomposition by heating, and consequently metal films or nanoparticles are formulated on the surfaces [6]. Supercritical carbon dioxide ($scCO_2$) is often used as a medium in the SCFD process because no liquid waste is generated, no solvent residue is left and the higher mass transfer rate of precursor is realized. Because of these benefits of using $scCO_2$, many researchers have attempted to apply $scCO_2$ in the plating methods for several substrates. Sone's group [7] developed a new electroplating technology for metallic substrates. They combined the conventional electroplating technique with $scCO_2$-SCFD where an electroplating solution was emulsified with a non-ionic surfactant, i.e., dense CO_2 and hexane. They consecutively studied the effects of dense CO_2 on the Ni film and found that low viscosity of dense CO_2 and its miscibility with hydrogen made the surface of the

plated Ni-film surface uniform and smooth [8]. Later, their research group applied their $scCO_2$-emulsification technique to an electroless plating technique for coating a polyimide (PI) substrate with Ni-P metal film [9-11]. They reported the catalyzation in $scCO_2$ with palladium(Pd)-bis(acetylacetonate) influenced the electroless plating mechanism on the PI substrate. They eventually advanced their plating method to a polymer/metal hybridized substrate and prepared a functionally graded Pd/γ-alumina composite membrane [12]. Hori et al. [13] proposed a $scCO_2$-assisted electroless plating method for polymeric substrates, especially polymeric fibers, where Pd(II) hexafluoroacetylacetonate ($Pd(hfa)_2$) was infused into Kevlar® fibers with $scCO_2$ and simultaneously activated by over-heating to use the complex as a catalyst of the plating reaction. The Kevlar was then immersed in an electroless copper (Cu) plating solution to coat the Kevlar with a Cu metal layer. They extended their plating technique to several polymeric fibers and studied the effect of a thermal treatment on the adhesion strength of the metal to poly-(p-phenylene terephthalamide) (PPTA), i.e., aramid fibers [14]. Ohshima research group proposed a novel process of electroless nickel–phosphorus (Ni-P) metal plating onto polymeric substrates as shown in the right-hand side picture of Figure 2.1 [5]. They used $scCO_2$ as both a solvent for infusing $Pd(hfa)_2$ into polymers and as a plasticizer to soften the surface of the polymeric substrates and increase the adhesiveness between the Ni-P metal layer and the polymeric substrates. One of the differences in Ohshima group's method from Hori group's method [13, 14] was to add alcohol in the plating solution for further softening the surface of polymer substrates. With the addition of alcohol, Ohshima research group's method could achieve a strong adhesiveness of the metal film to the polymer without using any harmful acids and water to etch the polymer surface and rinse the acid from the polymer substrate. Ohshima and co-workers found that a Ni-P metal-polymer composite layer was formed between the metal layer and the polymer matrix during the electroless plating reaction, and concluded that the thicker composite layer provided a stronger adhesion of the metal layer to the polymeric substrate. Moreover, they speculated that the higher mass transfer rate of the plating solution in the polymer substrate can make the Ni-P metal/polymer composite layer thicker and increase the adhesive strength of the Ni-P metal layer to polymer. Because the major ingredient of the plating solution is water, the mass transfer rate of the plating solution into the polymer substrate was strongly affected by the hydrophilicity or moisture content of the polymer. Unfortunately, because most polymers are highly

hydrophobic, Ohshima research group's method was limited to poly(methyl methacrylate) (PMMA) and polyamide 6 (PA6).

Polypropylene (PP) and acrylonitrile-butadiene-styrene (ABS) are two of the most commonly used polymers for automotive parts, and thus, there is great interest in applying the newly-developed environmentally benign electroless metal plating technique. However, the contact angle between PP and water is 102º±1 [15], whereas the contact angles for PI-water and PPTA-water are both 74º [10, 16], and the contact angle for PA6-water is only 69.2º [17]. Because of this higher degree of hydrophobicity, the PP substrate was barely metalized by the novel electroless Ni-P metal plating method. The plating reaction occurs only on the surface of the PP substrates, and the composite layer does not form inside the substrate. Thus, a lesser anchor effect is provided and the adhesive strength of metal layer to polymeric substrate is reduced [5]. Therefore, the surface of the PP substrate must be modified to be hydrophilic to promote a stronger adhesion, which would result in the success of the proposed plating technique for PP as well as for other highly hydrophobic polymers.

The hydrophilic modification of polymers can be achieved by several methods, such as flame treatment [18], corona discharge [19], or plasma treatment [20]. These modifications chiefly introduce polar functional groups onto the polymer surfaces to improve the wetting and adhesive properties [15], but they cannot provide the same strength of adhesion as that of the chemical etching method. In this study, the hydrophilic property of polypropylene (PP) was modified by the addition of a polypropylene(PP)-polyethyleneoxide(PEO) block (PP-b-PEO) copolymer. The PP-b-PEO copolymer was blended with PP and the blended polymer was injection-molded to prepare the substrate. The PEO block provides a hydrophilic nature to PP, and the injection molding preparation brings the PP-b-PEO domains near the substrate surface by exploiting the differences in the viscosities and flow mechanisms of the injected polymers. The electroless Ni-P metal alloy plating method was then applied to the PP substrate modified with PP-b-PEO, after the substrate was impregnated with $Pd(hfa)_2$ by using $scCO_2$. Ohshima group's method [5] used high pressure CO_2 as both a solvent for infusing $Pd(hfa)_2$ into polymers and as a plasticizer to soften the polymeric substrates in electroless plating solution. However, since the usage of high pressure CO_2 in practice would increase the equipment cost as well as the risk of safety. Therefore, in this study, the usage of $scCO_2$ to the $Pd(hfa)_2$ infusion process was

limited and carried out electroless plating without using CO_2 but alcohol.

The blend morphology as well as the interface of the metal plating and polymer surface was observed by transmission electron microscope (TEM) to confirm the location of the PP-b-PEO domains and the thickness of the composite layer. The increase in the mass transfer of plating solution in the modified PP substrate was confirmed by the sorption test and the adhesive strength of the Ni-P metal layer to the polymeric surface was measured by peel-off testing after the metal layer was thickened by Cu electroplating. Furthermore, the effects of the process variables and process conditions on the adhesive strength of the Ni-P metal film to the polymer substrate were investigated.

2.2. Experimental section

2.2.1. Materials

The isotactic polypropylene (PP, tacticity=97%, Prime Polymer, F133A), polyamide 6 (PA6: Unitika, A1025NO, Mw 14,000) and polypropylene(PP)-polyethyleneoxide(PEO) block copolymer (PP-b-PEO: Sanyo Chemical Industries, Pelestat® 300) were used to prepare the polymeric substrate. Neat PP and PA6 substrates were prepared and used for comparison. Pd(II) hexafluoroacetylacetonate ($Pd(hfa)_2$) was used as the catalyst precursor and was purchased from Sigma-Aldrich, USA. CO_2 (99.95% in purity) was supplied from Showa-Tansan, Japan. The electroless Ni–P metal plating solutions (ICP Nicoron DK-M and DK-1) were purchased from Okuno Chemical Industry Co., Ltd. DK-M contains phosphoric acid (16%), adipic acid (4%), the complexing agent (16%) and water (64%), and DK-1 contains nickel sulfate (35%) and water (65%). A standard solution was prepared by mixing DK-M (10%) and DK-1 (5%) with distilled water (85%). Ethanol (99.5% in purity, Wako Pure Chemical) was added to the standard plating solution as an additional plasticizer of the polymer surface [5]. All chemicals were used as received.

2.2.2. Substrate preparation

The PP-b-PEO copolymer was blended with PP at four different ratios of PP to copolymer (95/5, 90/10, 85/15 and 75/25) and was injection-molded into a flat plate. The sample substrates were prepared by cutting the molded flat plate into four

rectangle-shaped pieces. Each piece was 2 mm in thickness, 15 mm in width and 50 mm in length as illustrated in Figure 2.2. Molding was conducted by a 35-ton injection molding machine (J35ELIII-F, Japan Steel Works Ltd.) at 210 ºC barrel and 100 ºC mold cavity temperatures. The reference substrates were prepared from both neat PP and PA6 under the same injection molding conditions.

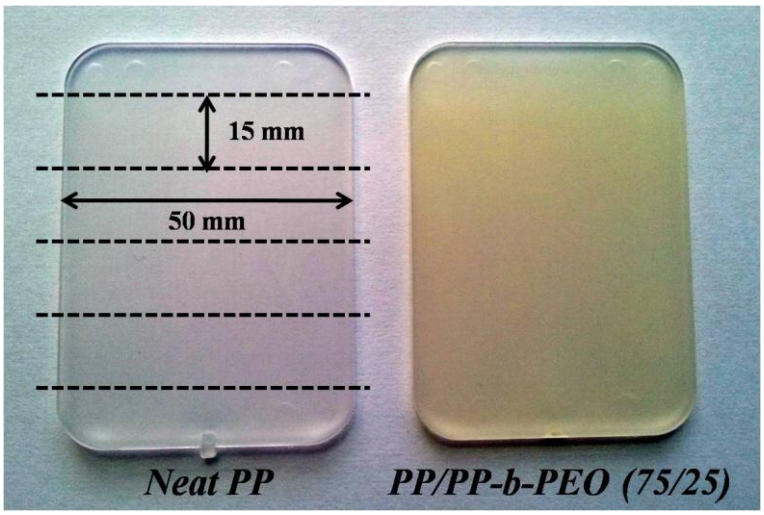

Figure 2.2. Injection-molded neat PP and PP/PP-b-PEO (75/25) blend substrates, which were prepared by cutting these molded flat substrates into four rectangle-shaped pieces as shown by the guidance dotted-lines. The cutting piece was 2 mm in thickness, 15 mm in width and 50 mm in length.

2.2.3. Supercritical CO_2 assisted infusion of $Pd(hfa)_2$

Polymer substrates were placed in an high pressure autoclave (70 cm^3 in volume) and the catalyst precursor, $Pd(hfa)_2$, was infused in the substrates. The autoclave temperature was controlled at 80 ºC during the $Pd(hfa)_2$ infusion and was pressurized by a pump (ISCO, Japan) to 10 MPa with CO_2. The dissolution of $Pd(hfa)_2$ in $scCO_2$ and its infusion into the substrate with $scCO_2$ were simultaneously conducted for 120 min. To observe the effect of the Pd on the plating, the amount of $Pd(hfa)_2$ loaded in the autoclave was varied at six different levels: 0.5, 1, 5, 15, 25, and 50 mg. With the assumption that all of the loaded $Pd(hfa)_2$ dissolved into the $scCO_2$, the concentration of the $Pd(hfa)_2$ in the $scCO_2$ was estimated and varied in the range from 3.17×10^{-5} to 3.17×10^{-3} g-$Pd(hfa)_2$ / g-$scCO_2$. The reduction of the Pd-complex was performed thermally by increasing the autoclave temperature to 120 ºC; this temperature was

maintained for 45 min while maintaining the CO_2 pressure at 10 MPa.

2.2.4. Electroless plating reaction

A Pd-infused polymer substrate was placed in a vacuum chamber for more than 48 h to remove the CO_2 from the substrate and was then immersed in the electroless Ni-P plating solution, which is a mixture of a standard plating solution (60%) and ethanol (40%). The addition of ethanol to the electroless plating solution enhanced the diffusivity of the plating solution due to the effect of solvent swelling in the polymer substrate [5]. As the diffusivity of the plating solution increases, electroless plating reaction occurs around the Pd nanoparticles embedded deeper inside the polymer. The Ni–P particles grow, agglomerate among others and form the anchors in the substrate. This provides stronger adhesiveness of the metal film to the polymer. The temperature of the plating solution was maintained at 65 ºC by using a water bath. The plating reaction time was set to be 60 min as a reference and was varied in association with the infused Pd and copolymer amount to determine the optimal plating conditions.

2.2.5. Evaluation of the morphology of the surface and cross-section

An optical microscope with digital camera (DP21, Olympus) was used to observe the surface morphology of the Ni-P metal plated samples as well as non-plated samples. The cross-sectional area of the plated substrate was observed by a TEM (TEM-1010, JEOL) after slicing the sample using an ultra-microtome (ULTRACUT-J, Leica). Slicing was conducted by the ultra-microtome at the rate of 2 mm/s at room temperature. The thickness of the sliced sample was 70 nm. The blend morphology was observed with a different TEM (H-7100, Hitachi High-Technology) at a 75 kV accelerating voltage after staining the sliced sample with a 2% phosphotungstic acid solution for 20 s.

2.2.6. Measurement of the sorption amounts of the plating solution and Pd metal

Without infusing the Pd complex, the polymer substrate alone was immersed in the plating solutions at 65°C to evaluate the solubility and diffusivity of the plating solution in the polymer. The weight change of the substrates was measured using an electronic balance with 10 μg resolution (AUW220D, Shimadzu) after wiping any

residual solution from the substrates. The amount of the infused Pd-complex in the substrate was calculated by measuring the weight change of the substrate before and after the Pd-infusion and vacuum treatment.

2.2.7. Measurement of adhesiveness of the metal layer to the polymer substrate

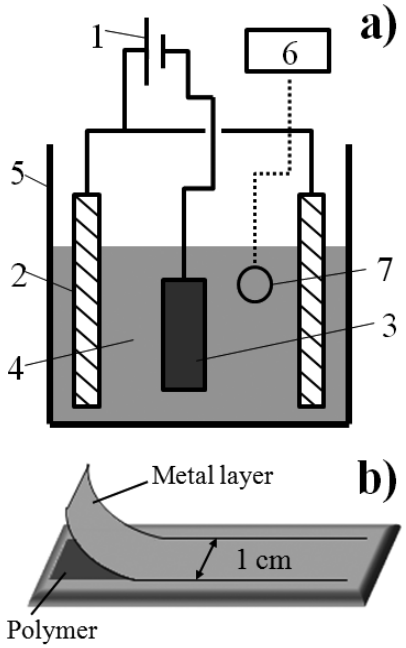

Figure 2.3. (a) A schematic diagram of the Cu electroplating apparatus: 1) DC power supply; 2) Anode; 3) Cathode (Ni-P plated polymer); 4) Plating solution; 5) Glass bath; 6) Air pump; 7) Air bubble stone; (b) Prepared sample for peeling-test machine

Immediately after the electroless plating, the Ni-P plated polymer was coated with a copper (Cu) layer by electroplating to increase the thickness of the metal layer and perform the peeling test. The schematic diagram of the Cu plating apparatus is shown in Figure 2.3(a). The Cu plates that were used as the anode were located vertically on either side of the bath. The Ni-P plated polymer substrates were used as the cathode. An aqueous mixture of 180 g/L $CuSO_4 \cdot 5H_2O$ and 60 g/L of H_2SO_4 was used as the plating solution. All of the electroplating was carried out in a bath made of glass at room temperature for 45 min with 1 A of applied electric current.

Before measuring the adhesive strength between the metal film and polymer, the Cu-plated samples were dried at room temperature for more than 24 h and approximately 1 cm in length of the Cu-coated Ni-P metal layer was manually peeled by cutting with a knife as shown in Figure 2.3(b). The peeled metal layer was

clamped and further peeled by applying peeling forces with a peel-off testing machine (Autograph AGS-J, Shimadzu). For the machine to appropriately clamp the metal layer, a certain layer thickness was required, thus requiring Cu-electroplating. The applied force per unit peeled length was used evaluate the adhesiveness of the Ni-P metal layer to the polymer substrate.

2.3. Results and discussion

2.3.1. Amount of infused catalyst precursor

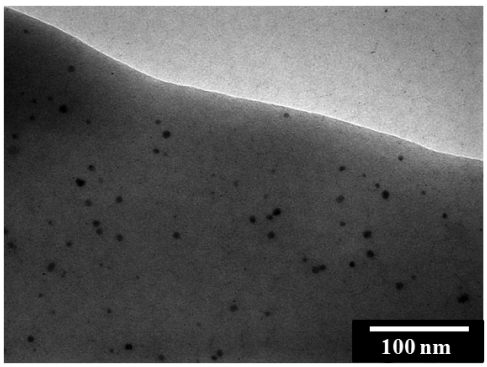

Figure 2.4. TEM micrograph of a cross-section of the PP/PP-b-PEO (75/25) blend substrate where Pd nanoparticles (black dots) were infused and embedded by using $scCO_2$ with the concentrations of the Pd catalyst precursor of 3.17×10^{-3} g-$Pd(hfa)_2$/g-CO_2.

Figure 2.4 shows a TEM micrograph of the cross-sectional area of a PP/PP-b-PEO (75/25) blend substrate in which $Pd(hfa)_2$ was infused by $scCO_2$. The black dots are Pd nanoparticles and they are dispersed inside the polymer. Figure 2.5 shows the weight gain of the polymer substrates by infused Pd catalyst precursor against the blended copolymer wt. percentages. The measurement was conducted after infusion of the Pd catalyst precursor at different loadings of $Pd(hfa)_2$. The weight of Pd infused in the polymer substrate could be measured by a 10 μg resolution balance. At the $scCO_2$ assisted infusion of $Pd(hfa)_2$ process, some of the loaded $Pd(hfa)_2$ in the autoclave were infused in the polymer substrates and others were left in the autoclave. When the $Pd(hfa)_2$ loaded in the infusion autoclave was less than 15 mg, the amount of the Pd-complex infused into the substrate was too small to be detected by the balance because of the resolution limitation. When the loaded $Pd(hfa)_2$ was over 15

mg, the weight of the infused Pd complex was detectable. The amount of Pd infused in polymer substrate slightly increased with the increase of the PP-b-PEO contents in the blend, but leveled off once the PP-b-PEO content was greater than 5 wt%. The amount of Pd infused in PP substrate increased proportionally to the amount of $Pd(hfa)_2$ loaded in the autoclave, and blending the PP with more than 10 wt% of the PP-b-PEO copolymer did not affect the amount of infused $Pd(hfa)_2$.

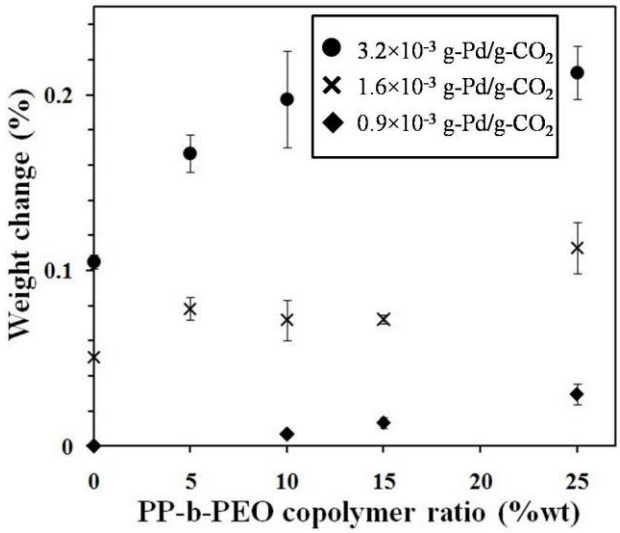

Figure 2.5. Weight gain by the infused Pd complex. The measurements were conducted after the $scCO_2$ impregnation step at different three levels of the loaded concentrations of $Pd(hfa)_2$ in $scCO_2$. (A data point was given by averaging 4-8 samples)

2.3.2. Sorption of the plating solution to the polymer substrates

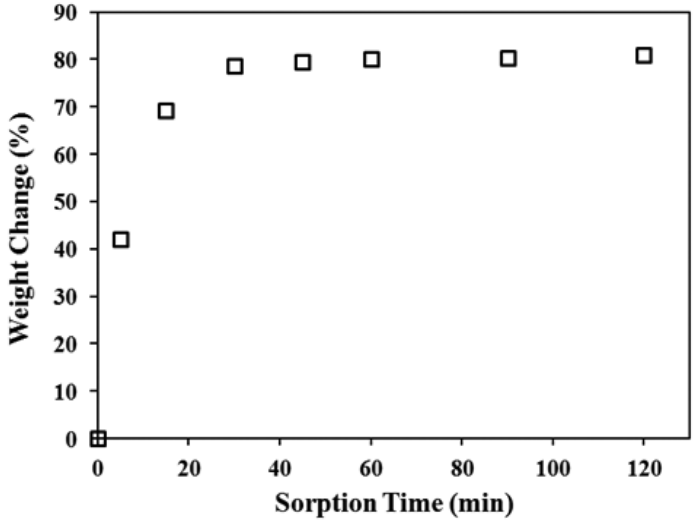

Figure 2.6. Intake of the plating solution in the PP-b-PEO copolymer alone (averaging 4 samples data for each condition)

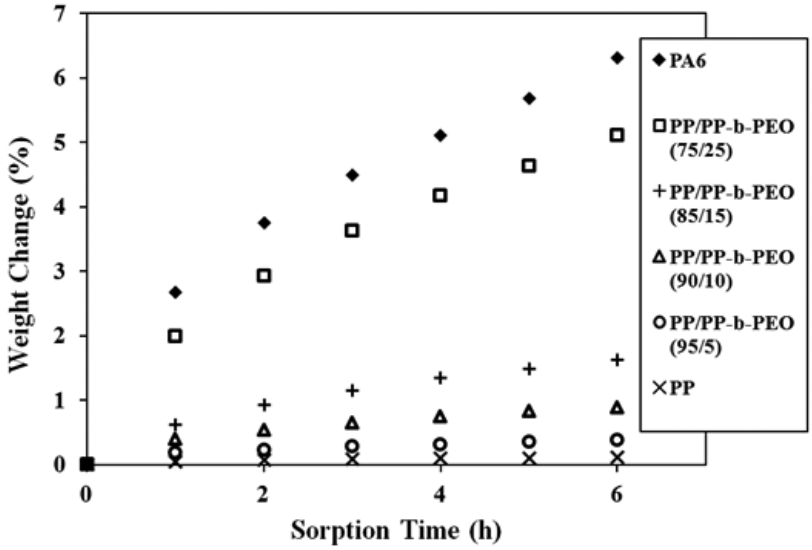

Figure 2.7. Intake of the plating solution in the polymer substrates (averaging 4 samples data for each condition)

Figures 2.6 and 2.7 show the intake of the plating solution in neat PP, neat PP-b-PEO copolymer and PP/copolymer-blended substrates. All substrates were immersed in the plating solution, i.e., a mixture of 60% standard plating solution and 40% ethanol at 65 °C. The solubility of the plating solution in the polymer substrate was determined by measuring the weight gain of the polymer substrates after immersing

the substrate in the plating solution. The weight gain is calculated by the following equation.

$$\text{weight change (\%)} = \frac{\text{weight of substrate after sorption} - \text{weight of substrate before sorption}}{\text{weight of substrate before sorption}} \times 100\%$$

Figure 2.6 shows that the PP-b-PEO copolymer alone could significantly absorb the plating solution and was saturated within 40 min. Figure 2.7 clearly shows that the solubility of the plating solution in the polymer blend substrate increased with the increasing copolymer content in the polymer substrate. The increase in solubility of plating solution directly indicates the improvement of the mass transfer of the solution in polymer substrate.

2.3.3. Morphology of the PP and PP-b-PEO copolymer blend

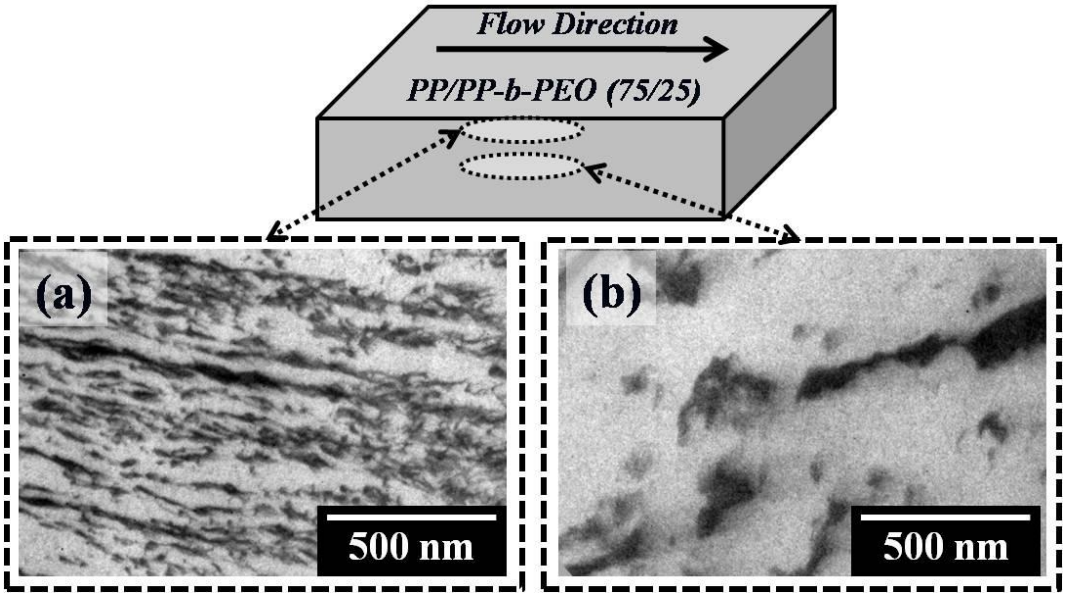

Figure 2.8. TEM micrographs of the cross-sectional area of PP/PP-b-PEO (75/25) blend substrate at (a) the skin region near the surface of substrate and (b) the center region, the PP blend sample was stained with phosphotungstic acid solution at the TEM observation. The dark regions represent the copolymer domains and the white regions represent the PP matrix.

In this study, a PP-b-PEO copolymer was used to increase the hydrophilicity of the PP substrate although it was originally developed as an antistatic agent for PP. PP-

b-PEO is immiscible with PP, but it is highly dispersed in the PP matrix due to the PP block [21]. When the polymer blend was molded by the injection molding machine, the PP-b-PEO copolymer domain was elongated in the flow direction of injected polymer and the surface of the polymer product became rich in this domain due to the viscosity difference between the matrix PP polymer and the copolymer [21]. Figure 2.8 shows TEM micrographs of the cross-sectional area (a) near the surface of an injection-molded PP/copolymer with a 75/25 blend ratio and (b) in the center region of the PP blend substrate. The black regions represent the PP-b-PEO domains and the white regions represent the PP matrix. The flow direction of the injected polymer was the horizontal direction of the TEM micrograph from right to left. As seen in Figure 2.8(a), the PP-b-PEO copolymer domains were elongated in the flow direction and a thin layer of the copolymer domain was formed near the surface of the substrate. However, the PP-b-PEO copolymer domain became the spherical shape in the center region of the substrate as illustrate in Figure 2.8(b).

2.3.4. Electroless plating of the PP and PP/copolymer substrates

Figure 2.9 shows an image from a digital camera and an optical microscope with digital camera of the surface of the non-plated polymer substrates, the electroless plated neat PP substrate and PP/PP-b-PEO blend substrate with 75/25 weight ratio. As can be observed from the optical microscope images of Figures 2.9(a) and (b), the surface roughness of the samples were not different each other. This is because the injection molding machine was used to mold and prepare the substrates under the same molding condition. The surface roughness of all polymeric substrates was determined by the mold cavity roughness and the molding condition. The copolymer content ratio may change the microscopic roughness of blended polymeric substrates but the change was not detected at the microscope magnification level.

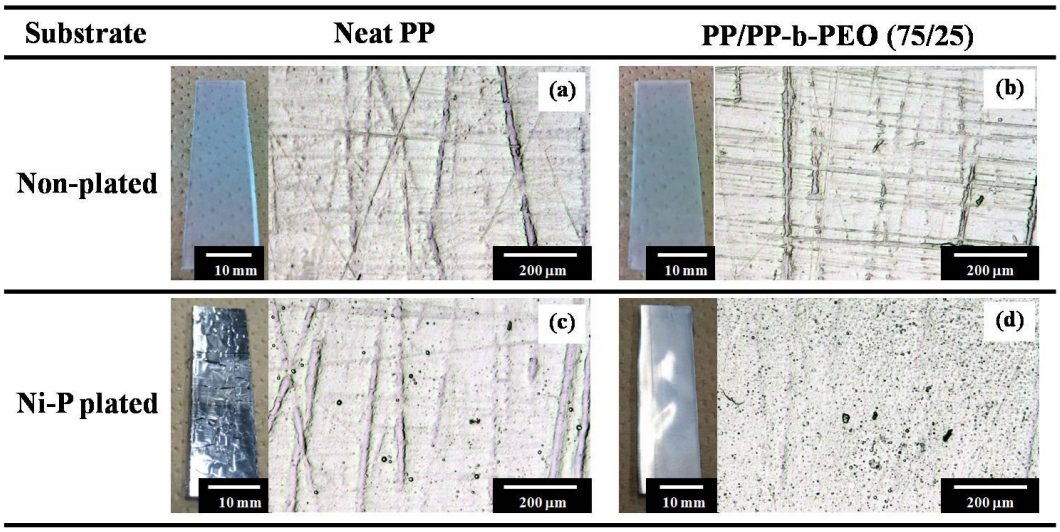

Figure 2.9. Images of a digital camera (left) and an optical microscope image (right) of the surface of (a) a non-plated neat PP substrate, (b) a non-plated PP/PP-b-PEO blend (75/25) substrate, (c) a Ni-P plated PP substrate and (d) a Ni-P plated PP/PP-b-PEO (75/25) blend substrate

More than 240 min of electroless plating time was required to coat the entire surface area of the neat PP substrate with the Ni-P metal. However, only 30 min of plating time was required to uniformly coat the PP/PP-b-PEO blends. This could be due to the higher solubility of the plating solution in the PP/PP-b-PEO blend substrates. Because of the higher hydrophobicity of PP, the Ni-P metal layer has many cracks on the neat PP substrate and peeled off easily when cooled down to room temperature as shown in Figure 2.9(c). Figure 2.9(d) clearly shows that a substantially uniform thin Ni–P film could be formed on the PP/PP-b-PEO copolymer blend substrates.

2.3.5. Adhesive strength of the Ni-P metal to the polymer substrates

The adhesiveness of the Ni-P metal layer to the polymer substrate was quantitatively measured by a peel-off testing machine (Autograph AGS-J, Shimadzu) to investigate the effect of the copolymer on electroless plating. Figure 2.10 shows the measured adhesive strength of the Ni-P metal film to the PP/PP-b-PEO blend substrates, which were plated using the optimal Pd infusion concentration. For comparison, the peeling force for the PA6 substrate is also illustrated in Figure 2.10. The PA6 substrate was prepared for comparison via Ohshima research group's method

[5], and treated under the same conditions as the PP/copolymer blend (except for the amount of infused Pd). The data for the neat PP substrate could not be obtained due to the weak adhesiveness of the metal layer. The samples were prepared from the PA6 and PP/PP-b-PEO blend substrates via $scCO_2$ infusion of $Pd(hfa)_2$ with 1.59×10^{-3} and 6.35×10^{-5} g-$Pd(hfa)_2$/g-$scCO_2$ for the PA6 and the PP/copolymer blend, respectively, and the plating reaction was conducted at the same conditions, i.e., 65 °C for 60 min. The highest adhesive strength data were selected and shown in Figure 2.10 to compare both polymers.

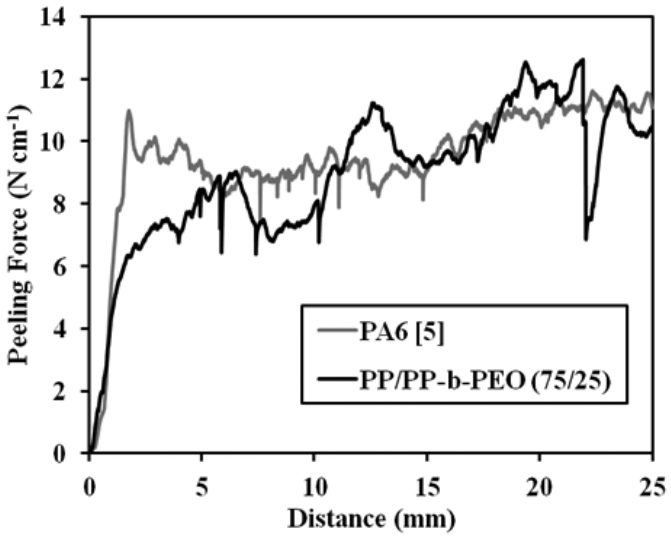

Figure 2.10. Adhesiveness of the Ni-P metal layer to the PA6 [5] and PP/copolymer (75/25) blend substrates prepared by $scCO_2$ infusion of $Pd(hfa)_2$ with concentrations of 1.59×10^{-3} and 6.35×10^{-5} g-$Pd(hfa)_2$/g-CO_2 for impregnation of the PA6 and the PP/copolymer blend, respectively

As seen in Figure 2.10, blending the PP with PP-b-PEO improved the peeling force to 7.9±0.5 N/cm. The solubility of the plating solution in the PA6 and the PP/PP-b-PEO (75/25) blend substrates were similar, as shown in Figure 2.7. This indicated that the adhesive strength was controlled by the mass transfer of the plating solution in polymer.

Figure 2.11 shows the average peeling forces for the PP/PP-b-PEO blend substrates prepared with different blend ratios and different amounts of infused Pd. As shown in Figure 2.11, at the lower concentration of the PP-b-PEO copolymer in the PP matrix, 15 %, the adhesiveness of metal layer was not improved compared to

that of PA6, and the infused Pd concentration had little observed effect. The adhesiveness dramatically increased when the copolymer blend ratio was increased to 25 %. From the results of adhesive strength of the PP/PP-b-PEO (75/25) blend substrates (Figure 2.11), it could be found that there exists an optimal Pd catalyst concentration at 6.35×10^{-5} g-Pd(hfa)$_2$/g-CO_2 for producing a strongly adhesive metal coating layer.

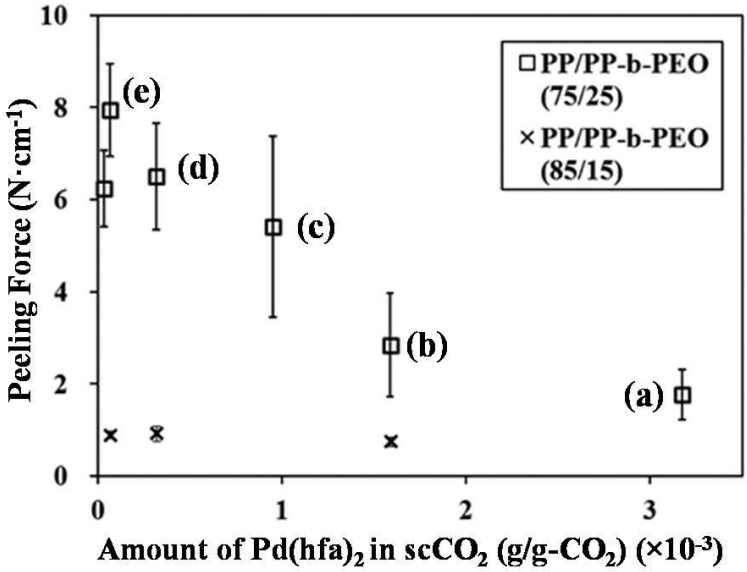

Figure 2.11. Adhesive strength of the Ni-P metal film to the PP/PP-b-PEO blend substrates at two different blend ratios, 85:15 and 75:25. Both of blend substrates were treated under scCO_2 conditions with different amounts of Pd in the CO_2. (Averaging 10 samples for each condition) (a, b, c, d and e, they are indicated and related with the data in section 3.6 and Figure 2.12)

As observed in previous study [5], in the region close to the metal layer, we could also observe that the metallic nanoparticles were dispersed and the density of nanoparticle was increased as the location was closer to the metal layer. This is the composite layer of polymer and Ni-P metal. The thickness of the metal/polymer composite layer was determined by a competitive relationship between the mass transfer of the plating solution and the plating reaction. When the plating reaction rate was faster than mass transfer rate of the plating solution, the plating reaction occurred on the surface of the substrates, the metal/polymer composite layer was not created and the metal layer was formed on the surface. The metal layer formed on the surface

prevented the plating solution from diffusing into the interior of the substrate and the composite layer was thin. As the infused Pd content increased in the polymer substrate, the electroless plating reaction rate increased. The increase in reaction rate reduced the adhesiveness of metal layer to polymer. Thus, the concentration of the infused Pd metal in the polymer substrate as well as the hydrophilicity must be optimally controlled to increase the adhesive strength.

2.3.6. Metal-polymer composite layer

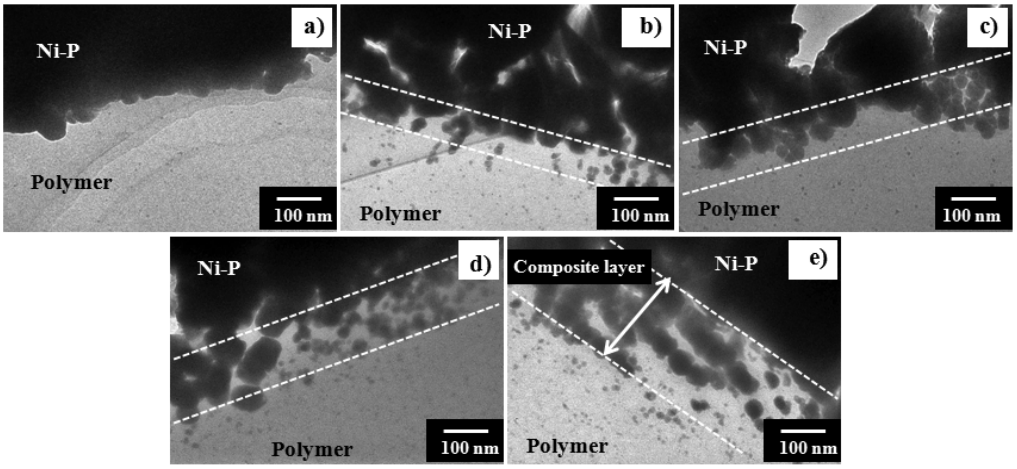

Figure 2.12. TEM micrographs of the cross-section of the interface between the Ni-P film and the PP/PP-b-PEO (75/25) blend substrate using concentrations of the Pd catalyst precursor of (a) 3.17×10^{-3}, (b) 1.59×10^{-3}, (c) 0.95×10^{-3}, (d) 0.32×10^{-3} and (e) 6.35×10^{-5} g-Pd(hfa)$_2$/g-CO_2

Figure 2.12 shows the TEM micrographs of the cross-sectional area near the surface of the electroless plated PP/PP-b-PEO (75/25) substrates. The samples were impregnated with the catalyst precursor at five different concentrations, 3.17×10^{-3}, 1.59×10^{-3}, 0.95×10^{-3}, 0.32×10^{-3} and 6.35×10^{-5} g-Pd(hfa)$_2$/g-CO_2, and were electroless-plated at 65 ºC for 60 min. In Figure 2.12, the black region represents the Ni–P metal film, gray is the composite layer and the white region is the polymer. As shown in Figures 2.12(a), (b) and (c), the thickness of the metal/polymer composite layer was approximately 0~100 nm when the higher concentration of the Pd catalyst precursor was used. On the other hand, it became 200~300 nm when the Pd catalyst precursor concentration was in the optimal range as shown in Figures 2.12(d) and (e). The

thickness of the composite layer in these samples corresponds to the adhesive strength of Ni-P metal film to the polymer substrate shown in Figure 2.11.

2.4. Conclusion

By modifying the hydrophilicity of PP by blending it with a PP-b-PEO copolymer, the supercritical carbon dioxide ($scCO_2$) assisted electroless Ni-P plating technique could be applied to PP-made plastic products. The technique could successfully produce a markedly uniform Ni-P metal film on a PP-based substrate with sufficiently strong adhesion. The adhesiveness of the Ni-P metal film to the polymer substrate was affected by the thickness of the metal/polymer composite layer. Because the thickness of the composite layer was determined by the rate of mass transfer of the plating solution and the rate of the plating reaction, the adhesiveness could be controlled by adjusting the copolymer weight percentage and the concentration of the infused Pd complex in the polymer. The supercritical carbon dioxide ($scCO_2$)-assisted electroless Ni-P plating technique with modification of the hydrophilicity can increase the potential for applying this technique to other polymers.

2.5. References

[1] G.O. Mallory, J.B. Hajdu, in, William Andrew Publishing/Noyes, 1990, pp. 1-56.

[2] S.H. Cho, S.H. Kim, J.G. Lee, N.E. Lee, Microelectronic Engineering, 77 (2005) 116-124.

[3] S.M. Rossnagel, Journal of Vacuum Science & Technology B, 16 (1998) 2585-2608.

[4] B.-H. Woo, M. Sone, A. Shibata, C. Ishiyama, S. Edo, M. Tokita, J. Watanabe, Y. Higo, Surface and Coatings Technology, 204 (2010) 1785-1792.

[5] H. Adachi, K. Taki, S. Nagamine, A. Yusa, M. Ohshima, The Journal of Supercritical Fluids, 49 (2009) 265-270.

[6] C. Erkey, The Journal of Supercritical Fluids, 47 (2009) 517-522.

[7] H. Yoshida, M. Sone, A. Mizushima, H. Yan, H. Wakabayashi, K. Abe, X.T. Tao, S. Ichihara, S. Miyata, Surface and Coatings Technology, 173 (2003) 285-292.

[8] H. Yan, M. Sone, N. Sato, S. Ichihara, S. Miyata, Surface and Coatings Technology, 182 (2004) 329-334.

[9] B.-H. Woo, M. Sone, A. Shibata, C. Ishiyama, K. Masuda, M. Yamagata, T. Endo, T. Hatsuzawa, Y. Higo, Surface and Coatings Technology, 202 (2008) 3921-3926.

[10] B.-H. Woo, M. Sone, A. Shibata, C. Ishiyama, K. Masuda, M. Yamagata, Y. Higo, Surface and Coatings Technology, 203 (2009) 1971-1978.

[11] B.h. Woo, M. Sone, S. Akinobu, C. Ishiyama, K. Masuda, M. Yamagata, Y. Higo, Microelectron. Eng., 86 (2009) 1179-1182.

[12] M. Seshimo, T. Hirai, M.M. Rahman, M. Ozawa, M. Sone, M. Sakurai, Y. Higo, H. Kameyama, Journal of Membrane Science, 342 (2009) 321-326.

[13] X. Zhao, K. Hirogaki, I. Tabata, S. Okubayashi, T. Hori, Surface and Coatings Technology, 201 (2006) 628-636.

[14] N. Martinez, K. Hisada, I. Tabata, K. Hirogaki, S. Yonezawa, T. Hori, The Journal of Supercritical Fluids, 56 (2011) 322-329.

[15] J. Long, P. Chen, Langmuir, 17 (2001) 2965-2972.

[16] N. Inagaki, S. Tasaka, H. Kawai, Journal of Polymer Science Part A: Polymer Chemistry, 33 (1995) 2001-2011.

[17] C.W. Extrand, Journal of Colloid and Interface Science, 248 (2002) 136-142.

[18] H.Y. Nie, M.J. Walzak, B. Berno, N.S. McIntyre, Applied Surface Science, 144–145 (1999) 627-632.

[19] R.J. Good, L.K. Shu, H.-C. Chiu, C.K. Yeung, The Journal of Adhesion, 59 (1996) 25-37.

[20] K. Harth, H. Hibst, Surface and Coatings Technology, 59 (1993) 350-355.

[21] T. Yabuta, Polymer Preprints, 58 (2009) 87.

Chapter III

Supercritical Carbon Dioxide-assisted Electroless Nickel Plating on Polypropylene —The effect of Copolymer Blend Morphology on Metal-Polymer Adhesion—

3.1. Introduction

The metallization of plastic surfaces is of great interest for various applications [1], such as printed circuits, diffusion barrier coatings, decorative coatings and wear protective coatings. For example, aluminum coated foils are used for food packaging, copper plated housings shield computers from electromagnetic radiation and precious metals are layered on jewels for finishing [2]. Several techniques such as physical–chemical vapor deposition, metal-powder coating and electroless plating have been proposed to metalize polymer substrates [3]. Among these methods, electroless plating has been the most widely used technique, especially in the automotive, aerospace and microelectronics industries [4]. The electroless plating process has several advantages, such as the possibility of a partial coating, flexibility in the plating volume and thickness, automatic monitoring of chemical replenishment and controllability of surface brightness [1]. The conventional electroless plating technique consists of a multistep processes: cleaning or degreasing, chemical etching, seeding of a catalyst for the electroless plating reaction and the electroless plating reaction, as shown in the left-hand side picture of Figure 2.1.

In the chemical etching process of conventional electroplating technique, strong oxidative acids such as sulfuric acid or chromic acid roughen the surface of the plastic parts [1]. The surface treatment is needed before metal deposition to ensure stronger metal-polymer adhesion [5]. Because these strong acids are harmful to humans, as well as environments, surface treatment using such strong acids creates one of the major issues in conventional electroless plating processes. In addition to harmful acids,

wastewater treatment is another issue to consider because chemical etching and catalyst deposition produce a huge amount of wastewater. From an environmental protection viewpoint, these chemical-etching stages should be eliminated. An electroless metal plating technique that does not require chemical etching is desired as an environmentally benign production process.

Hori et al. [6, 7] and Ohshima's group [8] have been independently developing a so-called supercritical carbon dioxide ($scCO_2$)-assisted electroless plating scheme for polymeric materials, in which no acid is needed for roughening the substrate surface and infusing the catalyst into the polymer substrate. Hori's $scCO_2$-assisted electroless plating method was developed mainly for polymeric fibers. For example, Pd(II) hexafluoroacetylacetonate $Pd(hfa)_2$ was infused into Kevlar® fibers with $scCO_2$ and simultaneously activated by over-heating to use the complex as a catalyst for the plating reaction [6]. The Kevlar was then immersed in an electroless copper (Cu) plating solution to coat the Kevlar with a Cu metal layer. In contrast, Ohshima and co-workers developed an electroless plating technique method for extrusion or injection molded-plastic parts, especially those based on Polyamide 6 (PA6) [8]. The method consisted of two steps, as illustrated in the right hand side picture of Figure 2.1: the first step was the $scCO_2$-assisted impregnation of the substrate with a catalyst precursor, $Pd(hfa)_2$, and the second step was an electroless nickel-phosphorus (Ni-P) plating reaction. In the first step, the $scCO_2$ was used as a solvent for the catalyst precursor and a plasticizer to soften the surface of the polymeric substrates. The catalyst precursor was dissolved in $scCO_2$, and the substrate was exposed to the $scCO_2$, impregnating the substrate with the catalyst precursor. Then, the precursor was thermally reduced [9]. One of the differences between Ohshima research group's method and the approach used by Hori's group [6, 7] was the addition of alcohol in the plating solution to further soften the polymeric substrates during the electroless plating reaction. With the addition of alcohol, Ohshima research group's method could achieve strong adhesion of the metal film to the polymer.

As mentioned in previous chapter, a Ni-P metal-polymer composite layer was formed between the metal layer and the polymer matrix during the electroless plating reaction, and it could be said that the thicker composite layer provided stronger adhesion between the metal layer and the polymeric substrate. Moreover, the higher mass transfer rate of the plating solution into the polymeric substrate was speculated that it could increase the metal-polymer composite layer thickness and the adhesive

strength of the metal layer to the polymer. Because the major ingredient in the plating solution is water, the mass transfer rate of the plating solution into the polymer substrate was strongly affected by the hydrophilicity or moisture content of the polymer. Unfortunately, most polymers are highly hydrophobic; thus, the developed electroless plating method has been limited to polymers with a moderately high water absorption rate, such as PMMA or PA6 [8].

Polypropylene (PP), acrylonitrile-butadiene-styrene (ABS) and other polyolefin resins have increasingly been used for automotive applications; thus, there is great interest in applying this newly developed and environmentally benign electroless plating technique to these polymers. The contact angle between PA6 and water is only 69.2º [10]. On the other hand, the contact angle between PP and water is ranging between 87.5º to 116.2º [11-13]. Due to the higher degree of hydrophobicity, the PP substrate was barely metalized by the novel electroless Ni-P metal plating method which is proposed by Ohshima research group. The electroless plating reaction occurs only on the surface of the PP substrate because the initial electroless-plated metal layer prevents the plating solution from penetrating further inside the polymeric substrate. This mechanism prevents the metal-polymer composite layer from forming inside the substrate. Thus, there was less of an anchor effect, and the adhesive strength of the metal layer to the polymeric substrate was reduced [8].

The surface of the PP substrate, as well as those of other highly hydrophobic polymers, must be modified by a hydrophilic surface treatment to perform the novel electroless plating method. So far, various techniques have been employed to modify the hydrophilicity of the polymer surface such as flame treatment [14], corona discharge [15], plasma treatment [16], mechanical abrasion and wet-chemical treatment [17]. Green et al. [18] have investigated several surface pre-treatment schemes, including corona discharge, flame, fluorination, vacuum plasma and air plasma for polyolefin and PP in particular. Most of the effective pre-treatments introduced different functional groups to the polymer surface, induced molecular modification and improved the wetting and adhesive properties of the material [11]. However, these pre-treatments could modify the hydrophilicity only at short distances from the surface (less than 10 nm) and could not provide adhesive strength comparable to conventional chemical etching.

In Chapter 2, a co-polymer was used to solve this problem, and Chapter 2 showed that the addition of PP-polyethylene oxide (PEO) block copolymer (PP-b-PEO) into

PP could significantly increase the hydrophilicity of PP. PP-b-PEO was originally developed as an antistatic agent for PP and could be highly dispersed in a PP matrix [19]. When the PP/PP-b-PEO polymer blend was molded by an injection molding machine, copolymer multilayers formed and were elongated in either the flow direction (FD) or the machine direction (MD) and the copolymer concentration in the region near the surface of the injected product increased due to the viscosity difference between the matrix PP polymer and the PP-b-PEO copolymer [19]. Not only the copolymer concentration in the PP blend substrate but also the multilayer blend morphology of the copolymer and PP affects the thickness of the metal-polymer composite layer and the adhesive strength of the metal.

In this follow-up chapter, PP/PP-b-PEO blend substrates were prepared from five PP grades with different viscosities, and then we investigated the effect of the viscosity ratios of PPs to the PP-b-PEO copolymer on the multilayer blend morphology, the concentration of PP-b-PEO near the surface and the adhesion strength of the Ni-P metal layer to the polymer substrate. Additionally, we clarified the existence of an optimal viscosity ratio of PP to PP-b-PEO copolymer to hydrophilically modify the surface, a maximum PP-b-PEO concentration near the surface of the plastic blend substrate and a strongest adhesive strength for the Ni-P metal layer.

3.2. Experimental section

3.2.1. Sample preparation and experimental procedure

Polypropylene (PP)-polyethylene oxide (PEO) block copolymer (PP-b-PEO: Sanyo Chemical Industries, Japan, Pelestat® 300), which was developed as an antistatic agent for PP, was used as a copolymer to modify the hydrophilicity of PP. The copolymer was dry-blended with different PPs and different blend ratios of PP to PP-b-PEO (PP/PP-b-PEO = 95/5, 85/15 and 75/25). As listed in Table 3.1, five different PPs were investigated. Two of these PPs were high tacticity isotactic homo-polypropylene (i-PP-A and i-PP-B) with tacticities of 97% and 90% (Prime Polymer, Japan, F-133A and F-300SP), other two were low-viscosity homo-PPs (v-PP) with different melt mass flow rates, 30 and 60 g/10 min (Prime Polymer, Japan, J-782HV and Y-6005GM) and one random PP (r-PP) (Prime Polymer, Japan, E-330GV). Neat

PP substrates were prepared from each of these grades and Polyamide 6 (PA6: Unitika, Japan, A1025NO, Mw 14,000) substrate was also prepared as a reference. iPP-A, iPP-B, vPP-A and vPP-B are homo polypropylene but different tacticity and viscosity. rPP was produced by randomly polymerizing ethylene monomer with polypropylene homopolymer to decrease the crystallinity of polymer.

Table 3.1. Material Properties of the PPs and the copolymer used in this chapter

Properties	Polymer (Grade No./Trade name)					
	iPP-A (F133A)	iPP-B (F300SP)	rPP (E-330GV)	vPP-A (J782HV)	vPP-B (Y6005)	PP-b-PEO (Pelestat)
Tacticity [mmmm] (%)	97	90	----	----	----	----
[a]Tm (ºC)	165.9	163.5	142.8	167.1	162.7	135.0
[b]Crystallinity (%)	39.5	33.9	25.4	34.8	39.2	----
[c]MFR (g/10 min)	3	3	3	30	60	31
[d]Water adsorption (%)	0.030 ±0.021	0.032 ±0.021	0.027 ±0.018	0.079 ±0.015	0.024 ±0.009	71.35 ±0.87

[a] Melting Temperature: Tm was measure at the rate of 10 ºC/min by the differential scanning calorimeter (DSC: Pyris 1, Perkin Elmer).

[b] Crystallinity was calculated by the ratio of the measured heat of fusion (ΔH_m) to the heat of fusion of perfect crystals (ΔH_m^0 = 209 J/g). The heat of fusion (ΔH_m) was measured by the DSC at the rate of rate of 10ºC/min.

[c] Melt flow rate: MFR data for PPs and PP-b-PEO are provided from Prime Polymer (Japan) and Sanyo Chemical Industries (Japan), respectively.

[d] ASTM D570: Test specimens were immersed in distilled water at 23 ºC (73.4 ºF) for 24 h.

[e] iPP = high tacticity isotactic PP; rPP = random PP; vPP = low-viscosity homo-PP; PP-b-PEO = PP-polyethylene oxide (PEO) block copolymer

An injection molding machine with a rectangular plate-shaped mold cavity prepared every polymer substrate. The injection molding was conducted by a 35-ton injection molding machine (J35ELIII-F, Japan Steel Works Ltd., Japan). The temperatures of the solid conveying, compression and metering zones in the injection machine were kept at 190, 210 and 210 ºC, respectively, while the mold cavity temperature was changed to three different levels, 40, 70 and 100 ºC, to observe the effect of the mold cavity temperature on the blend morphology. Rectangular shaped substrates 2 mm in thickness, 15 mm in width and 50 mm in length were then

prepared by cutting out the molded plate as shown in Figure 2.2.

After the substrates were impregnated with Pd(II) hexafluoroacetylacetonate, $Pd(hfa)_2$, the electroless Ni-P metal alloy plating method was applied to the substrates. $Pd(hfa)_2$ was used as a catalyst precursor, which was purchased from Sigma-Aldrich, USA. CO_2 (99.95% in purity) was supplied from Showa Gas Products, Japan. In case of Ohshima group's method [8], they used high pressure CO_2 as both a solvent for infusing $Pd(hfa)_2$ into the polymers and as a plasticizer to soften the polymeric substrates in the electroless plating solution. However, the usage of high pressure CO_2 increases the equipment cost and poses a safety risk. Therefore, in this study, the usage of $scCO_2$ was limited to the $Pd(hfa)_2$ infusion process and carried out electroless plating without using CO_2, but using ethanol instead. The electroless Ni–P metal plating solutions (ICP Nicoron DK-M and DK-1) were purchased from Okuno Chemical Industry Co., Ltd., Japan. DK-M contains phosphoric acid (16%), adipic acid (4%), a complexing agent (16%) and water (64%), while DK-1 contains nickel sulfate (35%) and water (65%). A standard plating solution was prepared by mixing DK-M (10%) and DK-1 (5%) with distilled water (85%). Ethanol (99.5% purity, Wako Pure Chemical, Japan) was added to the standard plating solution as an additional plasticizer of the polymer surface [8]. All chemicals were used as received.

The blend morphology of the PP/copolymer composite was strongly influenced by the PP viscosity and the sorption rates of the $Pd(hfa)_2$ as well as the plating solution in PP substrate would be changed by the blend morphology. The blend morphology and the interface between the metal and polymer were observed by a transmission electron microscope (TEM) to confirm the location of the dispersed PP-b-PEO domains and the thickness of the metal-polymer composite layer. The increase in the mass transfer of the plating solution in the PP/PP-b-PEO substrate was confirmed by a sorption test. The amount of Pd catalyst infused in the polymeric substrates was measured by using X-ray photoelectron spectroscopy (XPS). The adhesive strength of the Ni-P metal layer to the polymeric surface was measured by peel-off testing after the metal layer was thickened by Cu electroplating. Furthermore, the effects of the process variables and process conditions on the adhesive strength of the Ni-P metal layer to the polymer substrate were investigated.

3.2.2. Rheological measurement

The viscoelasticity of the samples was measured by a rheometer (ARES, Rheometric Scientific, TA Instrument, USA) equipped with parallel plate geometry. The dynamic temperature ramp tests were started at 220 ºC and then cooled to 110 ºC at a cooling rate of 2 ºC/min with a 1 rad/s frequency and a 5% strain rate.

3.2.3. Supercritical CO_2-assisted infusion of $Pd(hfa)_2$

Polymer substrates were placed in a high pressure autoclave (70 cm^3 in volume) and the catalyst precursor, $Pd(hfa)_2$, was infused into the substrates by $scCO_2$: the autoclave temperature was kept constant at 80 ºC during infusion and the pressure was controlled by a pump (ISCO, Japan) with a 10 MPa of CO_2 set point. The impregnation of $Pd(hfa)_2$ into the substrate with $scCO_2$ was conducted for 120 min. To observe the effect of Pd on the plating process, the amount of $Pd(hfa)_2$ loaded in the autoclave was varied between six different levels: 0.5, 1, 5, 15, 25 and 50 mg. Assuming that all of the loaded $Pd(hfa)_2$ dissolved into the $scCO_2$, the concentration of $Pd(hfa)_2$ in the $scCO_2$ was estimated to vary in a range from 3.17×10^{-5} to 3.17×10^{-3} g-$Pd(hfa)_2$/g-$scCO_2$. The Pd-complex was thermally reduced by increasing the autoclave temperature to 120 ºC; this temperature was maintained for 45 min while maintaining the CO_2 pressure at 10 MPa.

3.2.4. Electroless plating reaction

A Pd-infused polymer substrate was placed in a vacuum chamber for more than 48 hr to remove the CO_2 from the substrate and was then immersed in the electroless Ni-P plating solution, which was a mixture of the standard plating solution (60%) and ethanol (40%), as described in the previous section. The addition of ethanol to the electroless plating solution enhanced the diffusivity of the plating solution due to the effect of solvent swelling on the polymer [8]. As the diffusivity of the plating solution increases, the electroless plating reaction occurs around the Pd nanoparticles impregnated inside the polymer substrate. The Ni–P grows around the particles, agglomerates among other particles and forms a semi-continuous composite layer in the substrate. This layer provides an anchoring structure and stronger adhesiveness of the metal layer to the polymer. The temperature of the plating solution was maintained at 65 ºC using a water bath. The plating reaction time was initially 60 min, but was

varied according to the amount of infused Pd and copolymer to carry out the plating reaction at optimal conditions.

3.2.5. Evaluation of the morphology

An optical microscope with a digital camera (DP21, Olympus, Tokyo, Japan) was used to observe the surface morphology of the Ni-P metal plated samples as well as the non-plated samples. The cross-sectional area of the plated substrate was observed by a transmission electron microscopy (TEM) (JEM-1010, JEOL, Japan) after slicing the sample. Slicing was conducted by an ultra-microtome (ULTRACUT-J, Leica, Austria) at a rate of 2 mm/s at room temperature. The thickness of the sliced sample was 70 nm. TEM observations were conducted at a 100 kV accelerating voltage after staining the sliced sample with a 2% phosphotungstic acid solution for 20 s. The morphology of the blends was also observed with scanning-electron microscopy (SEM) (JSM-6700F, JOEL, Japan) at an acceleration voltage of 10 kV, a current of 5 μA and 8 mm in the working distance (WD). The SEM observations were conducted on samples stained with Ruthenium (III) chloride for 60 min and sliced by the ultra-microtome.

3.2.6. Measurement of the sorption amounts of the plating solution and water contact angle

Without carrying out the Pd complex infusion, the polymer substrate was immersed in the plating solutions at 65 ºC to measure the solubility and diffusivity of the plating solution in the polymer substrate. The weight change of the substrates before and after sorption was measured using an electronic balance with 10 μg resolution (AUW220D, Shimadzu, Japan) after wiping out any residual solution from the substrates. The static water contact angle on the polymer substrates was measured by the sessile drop method under condition of room temperature.

3.2.7. X-ray photoelectron spectroscopy (XPS)

The surface composition and depth concentration profile of Pd were measured using X-ray photoelectron spectroscopy (XPS) analysis with ion gun etching. For XPS, an ESCA-3400 spectrometer (Kratos analytical, Japan) with excitation (Acc.

HT.: 10 kV, Emission current: 20 mA) under a vacuum pressure of 1×10^{-6} Pa was used. The samples with etched with an ion gun under vacuum pressure (5×10^{-4} Pa) and an etching rate of 40 Å/min.

3.2.8. Measurements of the adhesiveness of the metal layer to the polymer substrate

Immediately after electroless plating, the Ni-P plated polymeric substrate was coated with Cu in an electroplating process. The purpose of the Cu coating is to increase the thickness of the metal layer to a thickness suitable for a peeling test. The schematic diagram of the Cu plating apparatus is shown in Figure 3.1(a). The Cu plates that were used as the anode were located vertically on either side of the bath. The Ni-P plated polymer substrates were used as the cathode. An aqueous mixture of 180 g/L $CuSO_4\cdot5H_2O$ and 60 g/L of H_2SO_4 was used as the plating solution. All of the electroplating was carried out in a glass bath at room temperature for 35 min with 1 A of applied electric current. Before measuring the adhesive strength between the metal film and polymer, the Cu-plated samples were dried at room temperature for more than 24 hr. An approximately 1 cm length of the Cu-coated Ni-P metal layer was peeled by cutting with a knife as shown in Figure 3.1(b). Then, a 90 degree adhesive peel strength test was conducted to measure the adhesiveness at room temperature, where the partially peeled metal layer was clamped, and peeling was sustained by the application of force on the peel-off testing machine (Autograph AGS-J, Shimadzu, Japan). To appropriately clamp the metal layer, a certain layer thickness was required. The applied force per unit peeling length was used as a measure of the adhesive strength of the Ni-P metal layer to the polymer substrate.

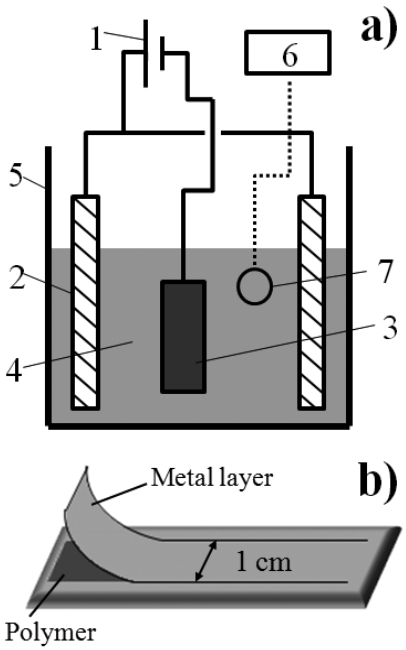

Figure 3.1. (a) A schematic diagram of the Cu electroplating apparatus: 1) DC power supply; 2) Anode; 3) Cathode (Ni-P plated polymer); 4) Plating solution; 5) Glass bath; 6) Air pump; 7) Air bubble stone; (b) Prepared sample for peeling-test machine

3.3. Results and discussion

Hydrophilic modification and blend morphology

3.3.1. Sorption of the plating solution to the polymer substrates substrates and wettability of the polymer surfaces

Figures 3.2 and 3.3 show the intake of the plating solution in the neat PA6, neat PP and PP/copolymer-blended substrates. All of the substrates were immersed in the same plating solution, i.e., a mixture of 60% standard plating solution and 40% ethanol at 65 ºC. The solubility of the plating solution in the polymer substrate was determined by measuring the weight gain of the polymer substrates after immersing the substrate in the plating solution. The weight change was calculated by the following equation.

$$\text{weight change (\%)} = \frac{\text{weight of substrate after sorption} - \text{weight of substrate before sorption}}{\text{weight of substrate before sorption}} \times 100\%$$

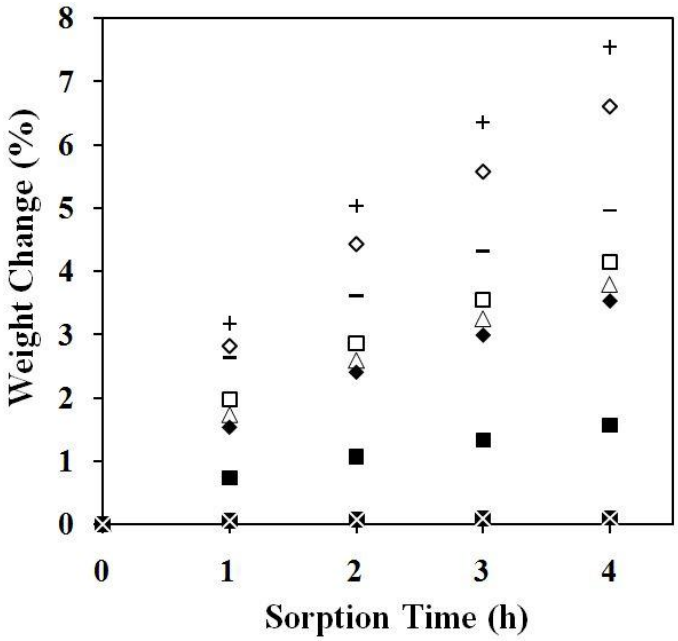

Figure 3.2. Intake of the plating solution in the polymer substrates (averaging 4 samples data for each condition) (Polymer substrates: ▬ = PA6; + = rPP/PP-b-PEO (75/25); ◇ = iPP-B/PP-b-PEO (75/25); △ = vPP-A/PP-b-PEO (75/25); ◆ = vPP-B/PP-b-PEO (75/25); □ = iPP-A/PP-b-PEO (75/25); ■ = iPP-A/PP-b-PEO (85/15); ⊠ = iPP-A)

Figure 3.2 shows the sorption behaviors of the plating solution in polymer blend substrates. The solubility and diffusivity of the plating solution in the substrates increased with increasing PP-b-PEO copolymer content in the polymer blend. The increase in both the solubility and diffusivity of the plating solution clearly indicated the increased mass transfer rate of the plating solution in the polymer substrate. When the blend ratio of PP-b-PEO to PP was 25/75, the solubility and diffusivity became high enough to conduct electroless plating with a satisfactory level of peeling force.

As listed in Table 3.1, the five grades of PP had water adsorption values that ranged between 0.024 and 0.079%, which were very low. By blending the PP-b-PEO with PP at a 25/75 weight ratio, the solubility of the plating solution was dramatically increased in all five PP grades, however, the amounts of plating solution absorbed in the PP/PP-b-PEO (75/25) blend substrates were slightly changed by the base PP resins and the mold cavity temperatures of the injection molding machine, as illustrated in Figure 3.3.

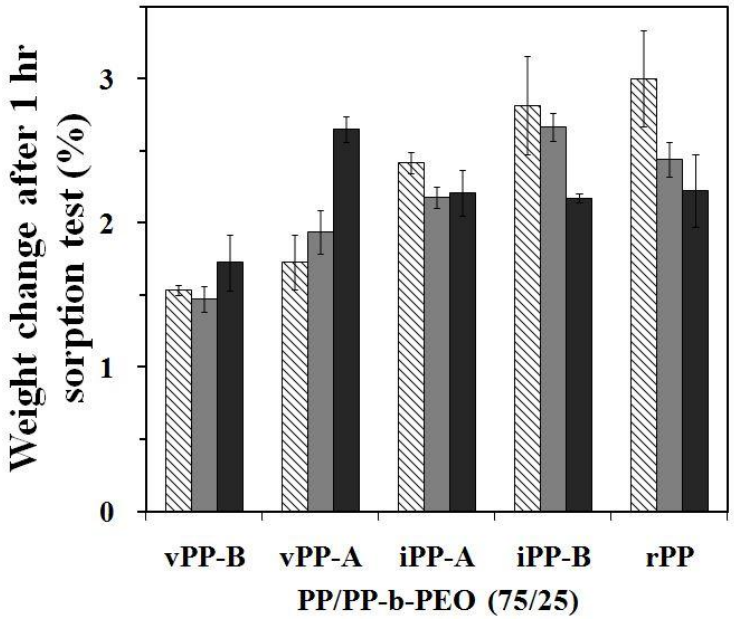

Figure 3.3. Intake of the plating solution in the PP/PP-b-PEO (75/25) blend substrates (averaging 4 samples data for each condition) (Mold cavity temperature: ▨ = 40 ºC; ■ = 70 ºC; ■ = 100 ºC)

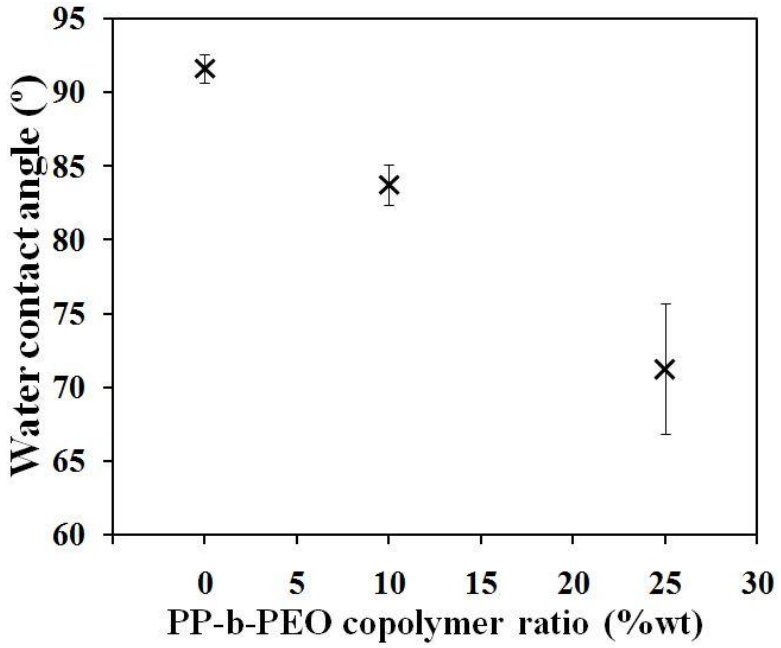

Figure 3.4. Water contact angle on neat iPP-A and iPP-A/PP-b-PEO blend substrates with different blend ratios (average of 5 measurements)

Figure 3.4 shows the contact angle of water on neat iPP-A and iPP-A/PP-b-PEO blend substrates with two different blend weight percentages (10 and 25 wt%).

The contact angle on the blend substrates was lower than that on the neat iPP-A substrate and it decreased with the increase of the percentage of PP-b-PEO copolymer in the blend. The same effect of copolymer blending could be observed for other PP grades. On the other hand, the PP grade difference and the mold cavity temperature did not affect the water contact angle significantly. The contact angles of water on the five grades of PP with 25% PP-b-PEO blend were in the range from 70.3º to 72.2º.

3.3.2. Rheology data of the PP and PP-b-PEO copolymer

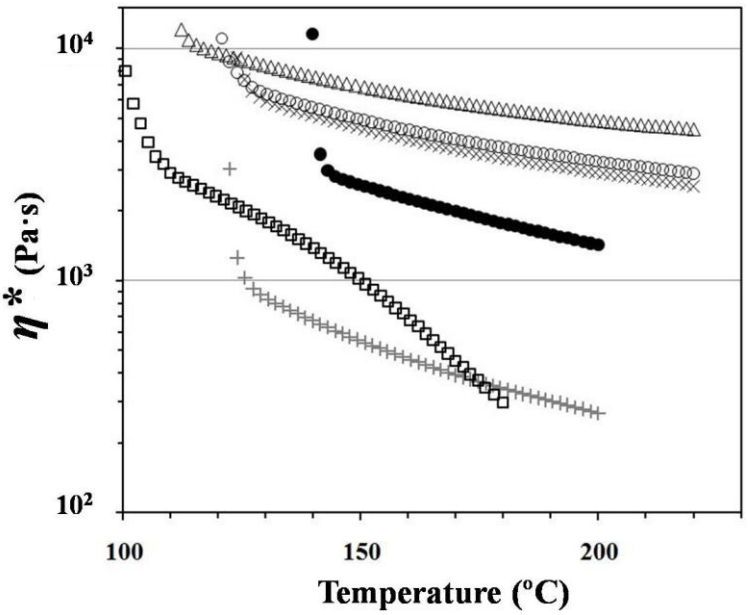

Figure 3.5. Temperature – complex viscosity, | η*|, data of five grades of PP and PP-b-PEO (Polymers: △ = rPP; ○ = iPP-B; × = iPP-A; ● = vPP-A; + = vPP-B; □ = PP-b-PEO)

Because blending in the injection molding machine was conducted at temperatures that ranged from 190 to 210 ºC, the viscosity ratio between the PP-b-PEO and the matrix PP at the blending temperature was a key factor in determining the blend morphology. Figure 3.5 shows the temperature dependency of the absolute value of complex viscosity, η*, of the five grades of PP, as well as the PP-b-PEO. The viscosities of four of the PP grades (vPP-A, iPP-A, iPP-B and rPP) were higher than that of PP-b-PEO, while the viscosity of vPP-B was closer to the PP-b-PEO than the other PP grades. In general, when the viscosity ratio is close to 1, the two polymers tend to be well mixed. From the viewpoint of blend-ability, the vPP-B could be

blended with the PP-b-PEO better than the other PPs. However, during electroless plating of the PP substrate, hydrophilic modification on near the surface of the PP substrate is a key factor in determining the mass transfer rate and adhesiveness of the plating solution in the substrate. The blend-ability of two polymers in an entire region does not directly lead to stronger adhesiveness between the Ni-P metal layer and the PP blend substrate. To bring the copolymer domain close to the substrate surface and increase the concentration of the PP-b-PEO copolymer in the PP matrix near the surface of the PP blend substrate, the viscosity ratio of PP to PP-b-PEO copolymer is an important variable.

3.3.3. Morphology of the PP and PP-b-PEO copolymer blend

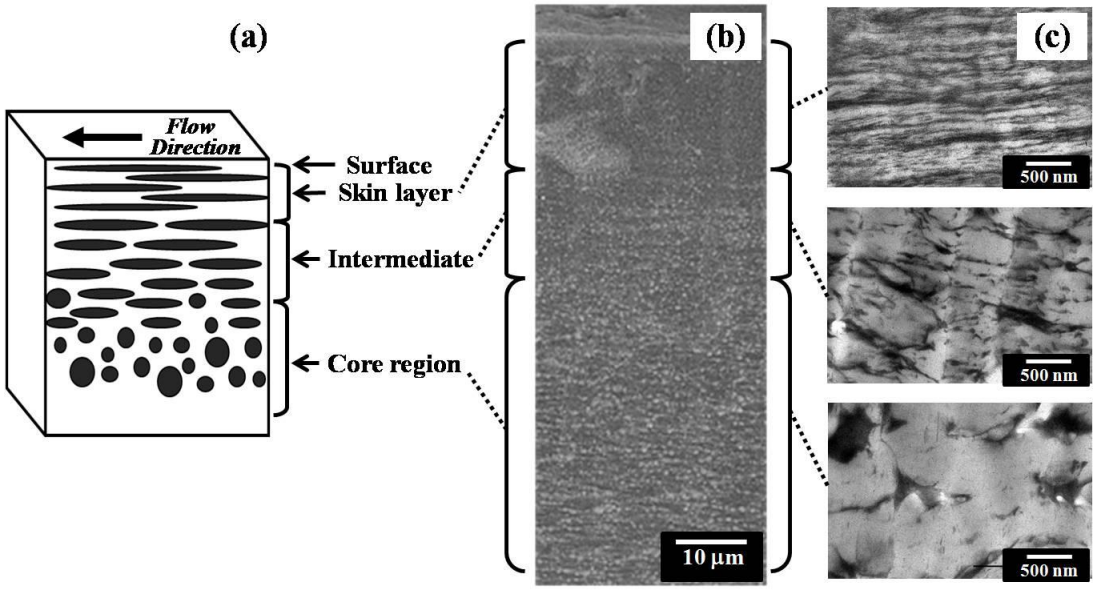

Figure 3.6. (a) Schematic of the skin/core structure of injection-molded blend substrate; (b) the SEM micrograph of the cross-sectional area of the stained iPP-B/PP-b-PEO (75/25) blend substrate, the white regions represent PP-b-PEO domains and the grey regions represent PP matrix; and (c) the TEM micrographs of the cross-sectional area of stained iPP-B/PP-b-PEO (75/25) blend substrate, the dark regions represent PP-b-PEO domains and the white regions represent PP matrix.

To see PP-b-PEO dispersed in PP, SEM and TEM of ultrathin sections were conducted. Figure 3.6 shows the typical skin/core morphology observed at the cross-sectional area of the polymer blend substrate prepared by injection molding. The SEM

and TEM micrographs were taken from an iPP-B/PP-b-PEO (75/25) blend. The black domain in the TEM micrograph represents the PP-b-PEO, while the white domain is the PP matrix. As shown in the TEM micrograph, the PP-b-PEO domain was elongated in the flow direction and the degree of orientation increased close to the surface. In the region approximately 20 μm beneath the surface, the domains were highly oriented and showed a platelet-like nanostructure. In the center region of the substrate, the degrees of orientation of the domains were completely lost, and the shapes of the domains became spherical.

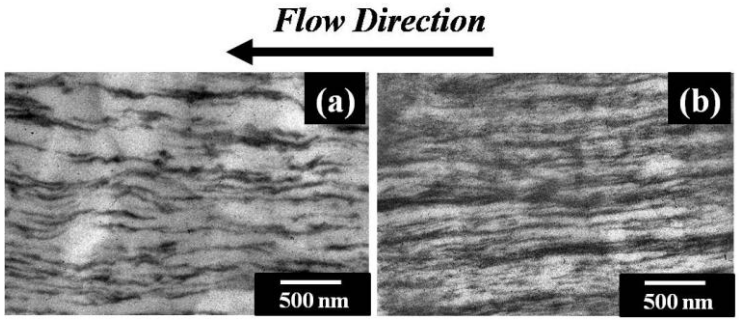

Figure 3.7. TEM micrographs of the cross-sectional area at the skin layer of the stained iPP-B/PP-b-PEO blend substrates prepared by blending iPP-B with different weight percentage of the PP-b-PEO, (a) 15% and (b) 25%, at mold temperature, 40 ºC. (black: PP-b-PEO, white: PP)

Figures 3.7(a) and 7(b) show the TEM micrographs of the cross-sectional area near the surface of the iPP-B/PP-b-PEO blend substrates with different blend ratios, 15% and 25%. Both of the substrates were prepared at the same molding temperature, 40 ºC. The PP-b-PEO layers were oriented in flow direction of the polymer injected in mold cavity. The orientation is parallel to the substrate surface. As shown in these images, the degrees of enrichment and orientation of the PP-b-PEO domains near the surface increased as the PP-b-PEO weight percentage in the blend samples was increased.

Figure 3.8 shows TEM micrographs of the PP/PP-b-PEO blend substrates of the PP-b-PEO copolymer, 25%, with five different PP grades ((a) vPP-B, (b) vPP-A, (c) iPP-A, (d) iPP-B and (e) rPP) prepared by injection molding at a mold cavity temperature of 40 ºC. All of the TEM micrographs were taken from the cross-sectional region near the substrate surface. These images clearly indicate that the

concentrations of the PP-b-PEO domains and their orientations near the surface regions were changed by the different PP grades. As shown in Figure 3.5, the absolute value of the complex viscosity, η^*, of vPP-B was closer to the PP-b-PEO copolymer than the other PP grades. However, the blend of vPP-B/PP-b-PEO did not show the highest degree of concentration as well as orientation of the PP-b-PEO domains near the surface of substrate.

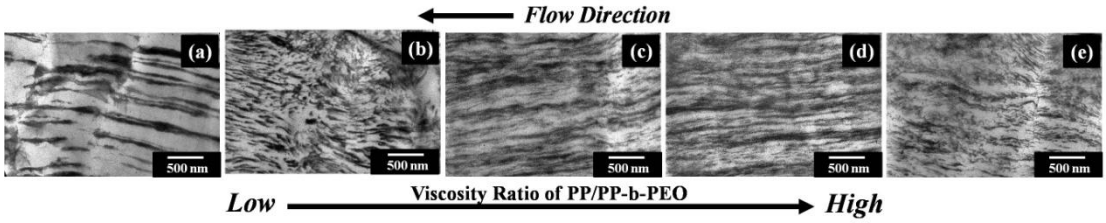

Figure 3.8. TEM micrographs of the cross-sectional area at the skin layer of stained PP/PP-b-PEO (75/25) blend substrates prepared by blending PP-b-PEO, 25%, with the different PP, (a) vPP-B, (b) vPP-A, (c) iPP-A, (d) iPP-B and (e) rPP, and the blend samples were injection molded at mold cavity temperature, 40 ºC. The dark regions represent as PP-b-PEO domains and the white regions represent as PP matrix.

Figure 3.9 shows the relationship between the viscosity ratio of PP to PP-b-PEO and the average percentage of the PP-b-PEO copolymer domains as well as the average distance between the oriented PP-b-PEO layers. The distance of two oriented layers, Y_2, was measured from micrographs as shown in Figure 3.9. The viscosity ratio was calculated from the ratio of the absolute value of the complex viscosity of PP to PP-b-PEO measured at a temperature of 180 ºC. The average percentage of the PP-b-PEO domains in the PP, Y_1, was calculated from the ratio of black to white areas in the TEM micrographs. The average distance between the PP-b-PEO elongated domains was also measured from the TEM micrographs. As illustrated in Figure 3.9, the average percentage of the PP-b-PEO domains in the PP and the average distance of the oriented domains a reached maximum in the iPP/PP-b-PEO blends, whose viscosity ratio was close to a value of approximately twelve. The difference between the viscosities should sufficiently minimal for the polymers to be well blended but large enough to bring the lower viscosity polymer to the surface of injection-molded parts. Therefore, these conditions suggested there was an optimal viscosity difference

between the PP-b-PEO and the PP that achieved the highest concentration and the highest degree of orientation of the copolymer domains in the PP matrix. However, when the viscosity ratio of PP to copolymer are increased until beyond the optimal range such in case of the rPP/PP-b-PEO (75/25) blend sample, as results in Figures 3.8 and 3.9, the concentration and the degree of orientation of the copolymer were decreased.

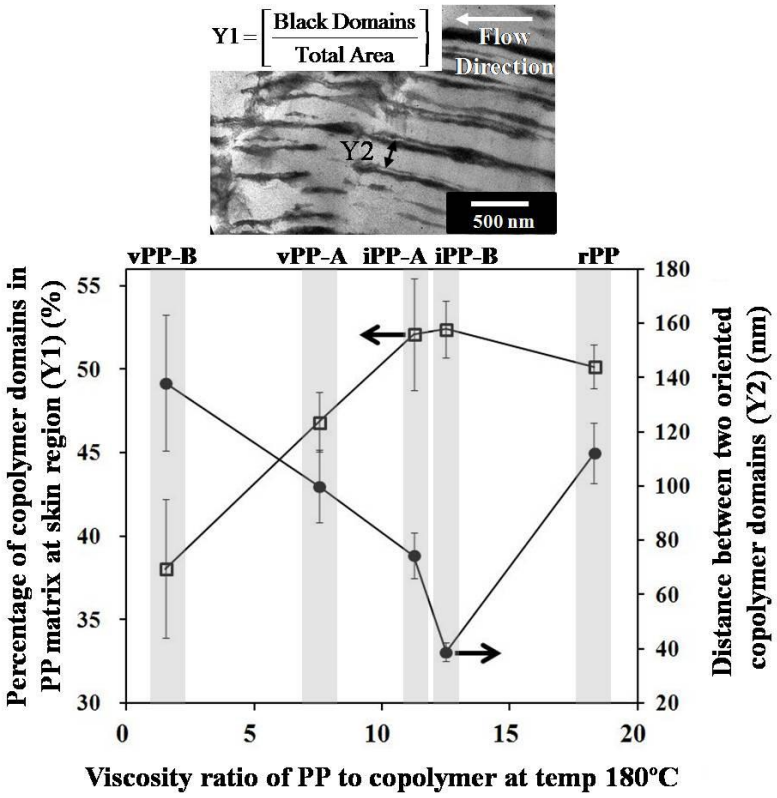

Figure 3.9. Relationship between viscosity ratio of PP to PP-b-PEO and the average percentage of the PP-b-PEO domains in PP (Y1) and the average distance between the oriented PP-b-PEO layers (Y2) (PP/PP-b-PEO ratio = 75/25 prepared by injection-molded at mold cavity temperature, 40 ºC)

Figure 3.10 shows the TEM micrographs of the cross-sectional area near the surface of the PP/PP-b-PEO (75/25) blend substrates. The samples were prepared by injection molding at three different mold cavity temperatures, 40, 70 and 100 ºC, from PP-b-PEO copolymer and three different PP grades (iPP-A, iPP-B and rPP) to investigate the effect of mold cavity temperature on the degree of orientation and concentration of the PP-b-PEO domains in the PP matrix.

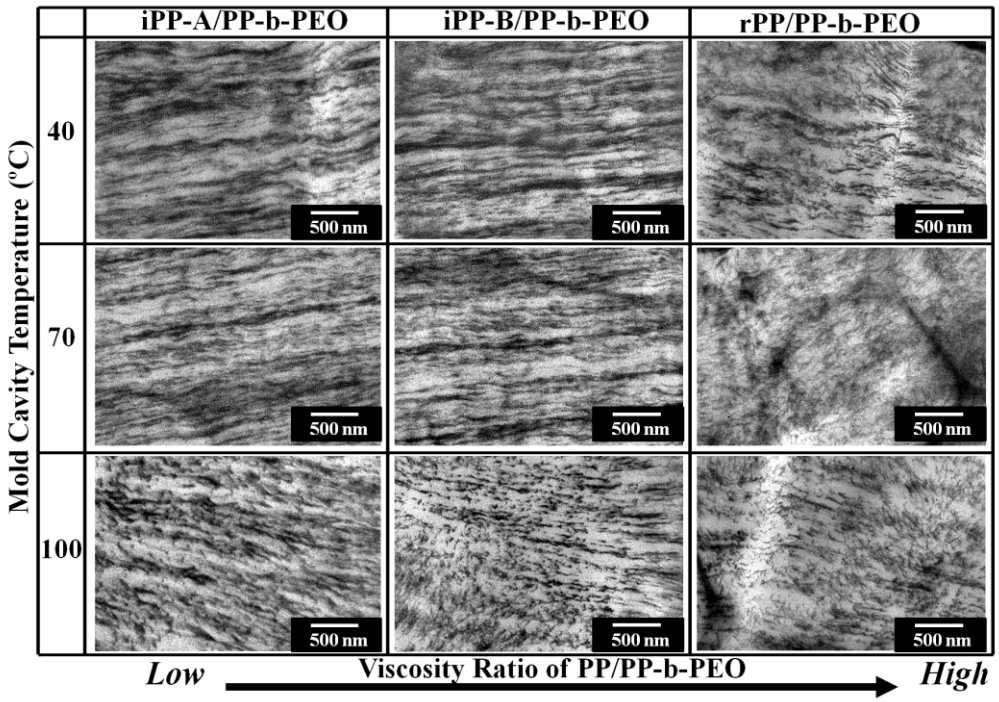

Figure 3.10. TEM micrographs of the cross-sectional area near the surface of PP/PP-b-PEO (75/25) blend substrates with different PP, iPP-A (left), iPP-B (middle) and rPP (right) and different molding temperature, 40 ºC (top), 70 ºC (middle) and 100 ºC (bottom)

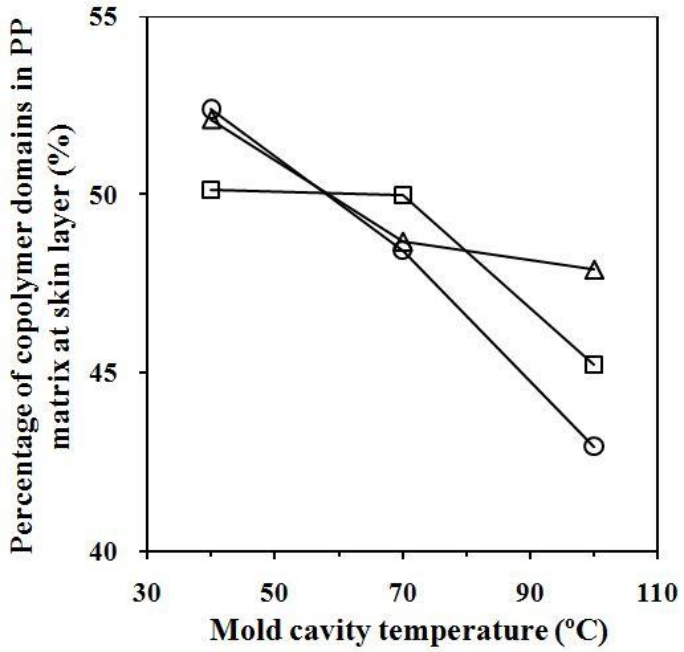

Figure 3.11. Effect of the mold cavity temperature on the average percentage of the PP-b-PEO copolymer domains in PP matrix (PP/PP-b-PEO (75/25) blend samples: □ = rPP; ○ = iPP-B; △ = iPP-A)

Figure 3.11 shows the average percentage of the PP-b-PEO domains in the PP matrix near the substrate surface. The substrates were prepared by blending 25% PP-b-PEO with iPP-A, iPP-B and rPP, individually, at different molding temperatures of 40, 70 and 100 ºC, respectively. The lowest molding temperature provides the highest percentage of copolymer domains in the PP matrix near the surface of the injection-molded parts.

Figure 3.12(a) shows how the amount of PP-b-PEO in PP (Y1) affected the sorption behaviors of the plating solution in PP/PP-b-PEO (75/25) blend. It was clearly illustrated that the increase in the amount of PP-b-PEO copolymer near the surface of PP/PP-b-PEO (75/25) blend substrates, Y1, could increase the weight gain, i.e., the diffusion rate and solubility of electroless plating solution in the polymer substrate. Because PEO polymer chain in PP-b-PEO is hydrophilic, thus the increase in the amount of PP-b-PEO near the surface of the substrate increased the diffusion rate and solubility of electroless plating solution in polymer substrate. The amount of PEO content near the surface of the substrate was changed with the dispersed morphology of PP-b-PEO domain in PP matrix. The morphology was changed by the blend ratio as well as the flow condition of polymer injected in mold cavity, such as mold temperature and viscosity ratio of the polymers as shown in Figures 3.7-3.10. In the injection molding process, the low viscosity polymer was enriched near the surface of the molded products by a fountain flow in the cavity. The viscosity ratio of PP to PP-b-PEO is the key factor of controlling the flow behavior. Figure 3.12(b) shows the effect of viscosity ratio of PP to PP-b-PEO copolymer on the sorption behaviors of plating solution in the PP/copolymer (75/25) blend substrate. Therefore, as illustrated in Figure 3.12(b), the viscosity ratio is the dominant polymer property of differentiating the sorption behaviors as well as the peeling strength of the Ni-P metal. Moreover, the presence of crystalline phase in PP matrix might affect the sorption behavior. The diffusion rate and solubility of the plating solution to the iPP-B and rPP blend substrates were higher than those to the iPP-A blend substrate. Thus, the crystallinity of PP matrix could be another polymer property of determining the sorption behavior of plating solution.

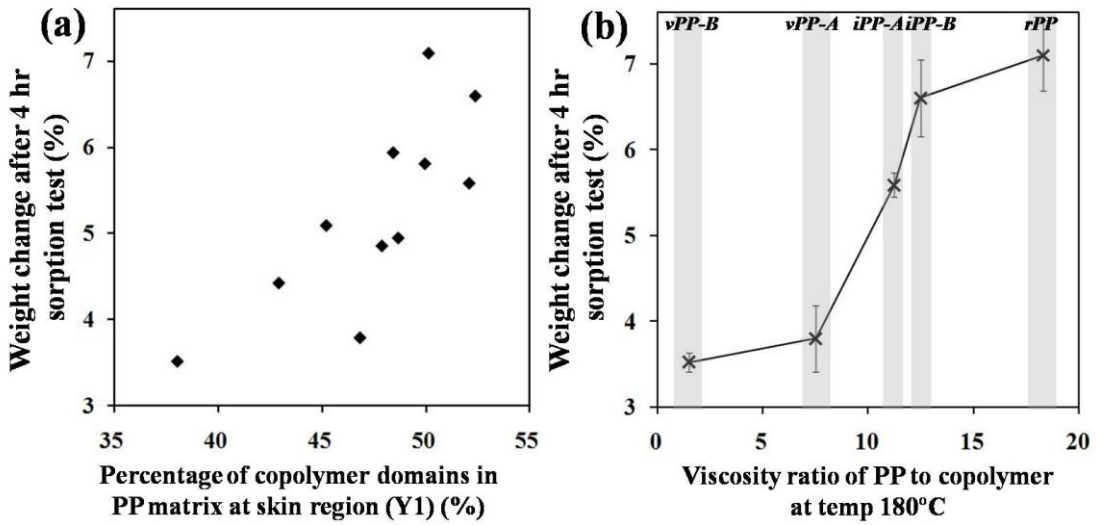

Figure 3.12. (a) Relationship between average percentage of the PP-b-PEO domains in PP (Y1) and sorption behaviors of the plating solution in PP/PP-b-PEO blend substrates, and (b) the effect of viscosity ratio of PP to PP-b-PEO on the sorption behaviors of plating solution in PP/PP-b-PEO blend samples (PP/PP-b-PEO ratio = 75/25 prepared by injection-molded at mold cavity temperature, 40 ºC)

3.3.4. Amount of infused catalyst precursor

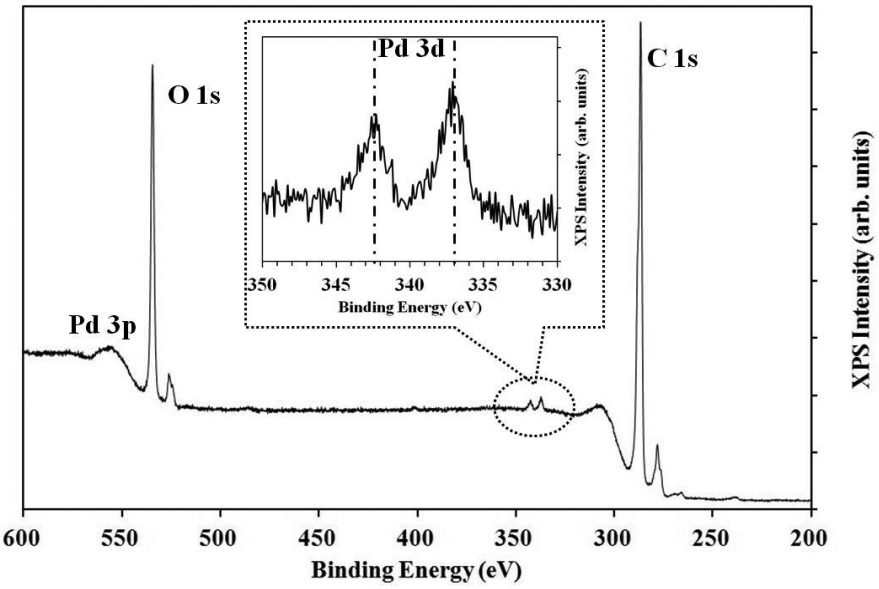

Figure 3.13. XPS spectra of a iPP-A/PP-b-PEO (75/25) blend substrate after impregnation of $Pd(hfa)_2$ under loading $Pd(hfa)_2$ concentration of 3.17×10^{-3} g-$Pd(hfa)_2$/g-CO_2

After $scCO_2$-assisted impregnation at 80 ºC and 10 MPa for 120 min, thermal reduction was conducted to transform the $Pd(hfa)_2$ complex into an activated Pd catalyst at 120 ºC under 10 MPa CO_2 for 45 min. Figure 3.13 shows the XPS spectra of an iPP-A/PP-b-PEO (75/25) blend substrate after impregnation and reduction of the $Pd(hfa)_2$. The peaks were detected at 337 and 342.5 eV, which corresponds to the emission from the 3d levels of the Pd metal. These emission peaks indicated the presence of reduced Pd on the substrate.

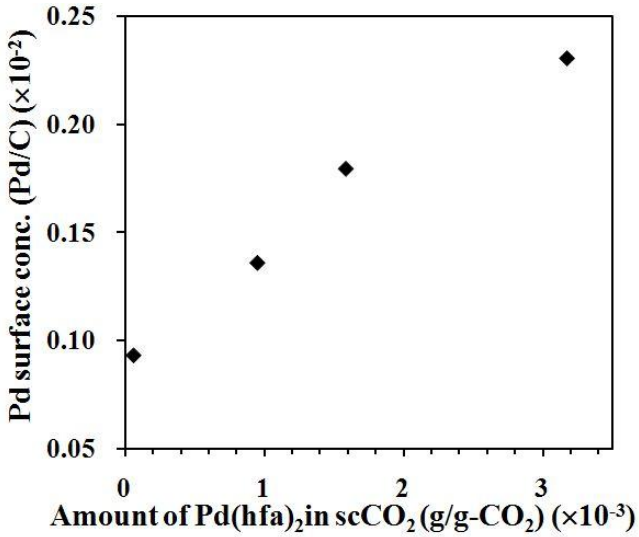

Figure 3.14. Concentration of Pd on the surface of the iPP-A/PP-b-PEO (75/25) blend substrates, Pd catalyst was impregnated at different loading concentrations of $Pd(hfa)_2$ in $scCO_2$

From this XPS analysis, the Pd concentration (Pd per carbon) on the surface and inside of the PP/PP-b-PEO (75/25) blend substrate was measured as illustrated in Figures 3.14 and 3.15. Figure 3.14 illustrates the resulting XPS analysis of the iPP-A/PP-b-PEO (75/25) blend substrate and shows that the Pd concentration increased with an increase in the loading concentration of the $Pd(hfa)_2$ in the $scCO_2$ infusion process. Figure 3.15 illustrates the concentration profiles of Pd along the distance from the surface to the inside of the PP/PP-b-PEO (75/25) blend substrates. The profiles were obtained by etching the substrate with an ion gun layer by layer. The substrates were prepared by blending PP-b-PEO with the different PP grades, iPP-A, iPP-B and rPP. For all of the samples, Pd impregnation was conducted at a loading $Pd(hfa)_2$ concentration of 1.59×10^{-3} g-$Pd(hfa)_2$/g-$scCO_2$, under $scCO_2$ with the same

pressure and temperature as described previously. Interestingly, the Pd concentration reached its maximum not at the surface but slightly inside the substrate. This result might be due to some $Pd(hfa)_2$ diffusing out when the temperature was increased for the reduction process. The XPS analysis confirmed that the Pd catalyst was successfully infused by the $scCO_2$ infusion and thermal reduction processes.

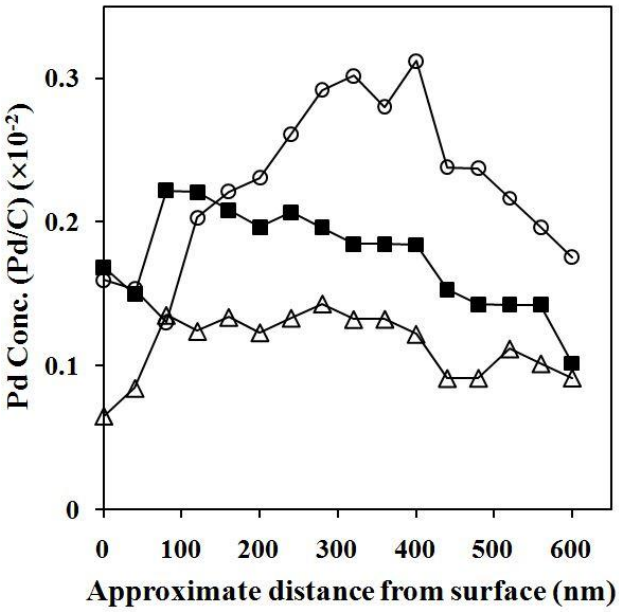

Figure 3.15. Pd metal concentration profile along the distance from the surface of three different PP/PP-b-PEO (75/25) blend substrates (mold cavity temperature = 40 ºC, loading $Pd(hfa)_2$ concentration = 1.59×10^{-3} g-$Pd(hfa)_2$/g-CO_2) (PP/PP-b-PEO (75/25) substrates: ■ = iPP-A; ○ = iPP-B; △ = rPP)

Electroless plating of the hydrophilicity-modified polymer substrates

3.3.5. Electroless plating of the PP and PP/copolymer substrates

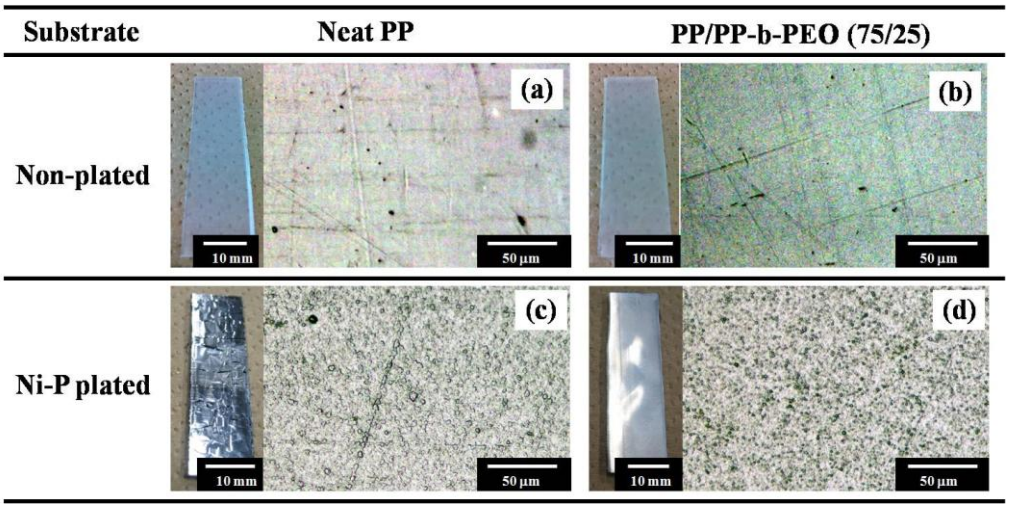

Figure 3.16. Digital camera images (left) and optical microscope images (right) of the substrate surface; (a) a non-plated neat iPP-A substrate, (b) a non-plated iPP-A/PP-b-PEO blend (75/25) substrate, (c) a Ni-P plated iPP-A substrate and (d) a Ni-P plated iPP-A/PP-b-PEO (75/25) blend substrate

Figure 3.16 shows digital camera and optical microscope images of the substrate surface of the non-plated polymer substrates (Figure 3.16(a) and 3.16(b)) and the electroless-plated neat iPP-A and iPP-A/PP-b-PEO (75/25) blend substrates (Figure 3.16(c) and 3.16(d)). A comparison of Figure 3.16(a) with 3.16(b) clearly shows that the surface roughness of the blended polymer substrate did not differ substantially from the neat PP substrate. The surface roughness of the polymer substrate was determined principally by the roughness of the mold cavity.

As shown in Figures 3.16(c) and 3.16(d), the electroless-plated neat iPP-A substrate without hydrophilic modification and blended with the PP-b-PEO had many cracks and the resulting Ni-P metal layer could be peeled off easily (Figure 3.16(c)). On the other hand, a uniform Ni-P metal layer could be formed on the iPP-A/PP-b-PEO (75/25) blend substrates (Figure 3.16(d)).

3.3.6. Adhesive strength of the Ni-P metal to the polymer substrates

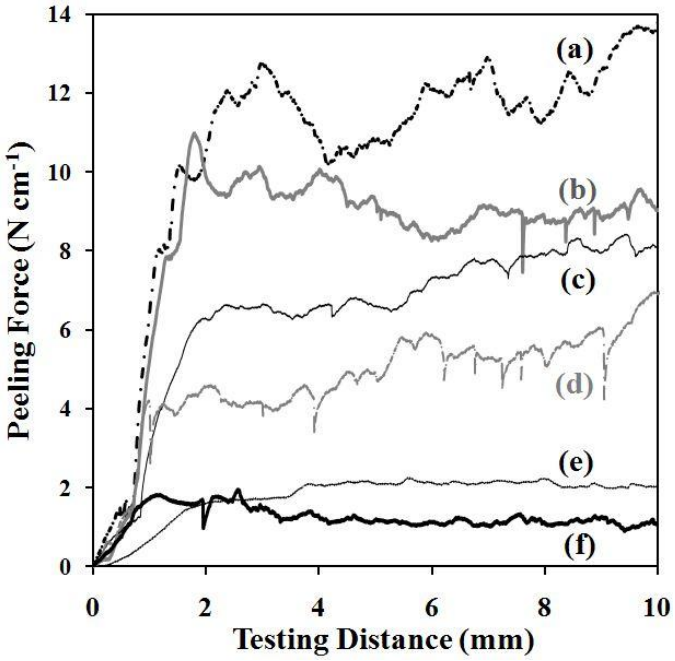

Figure 3.17. Peeling force of the Ni-P plated PP/PP-b-PEO (75/25) blend substrates prepared from different PP grade after $scCO_2$ infusion of $Pd(hfa)_2$ with loading concentration, 0.317×10^{-3} g-$Pd(hfa)_2$/g-CO_2, and the electroless-plated PA6 substrate prepared from $scCO_2$ infusion of $Pd(hfa)_2$ with loading concentration of 1.587×10^{-3} g-$Pd(hfa)_2$/g-CO_2 [Polymer substrates: (a) iPP-B/PP-b-PEO (75/25); (b) PA6; (c) rPP/PP-b-PEO (75/25); (d) = vPP-A/PP-b-PEO (75/25); (e) vPP-B/PP-b-PEO (75/25); (f) iPP-B/PP-b-PEO (85/15)]

The adhesiveness of the Ni-P metal layer to the polymer substrate was measured by peel-off testing to quantitatively evaluate the peeling force. Figure 3.17 shows the measured peeling force of the Ni-P metal layer from the substrates. The PP/PP-b-PEO substrates were prepared from different PP grades at a molding temperature of 40 ºC and impregnated with Pd with a $Pd(hfa)_2$ concentration of 0.317×10^{-3} g-$Pd(hfa)_2$/g-CO_2. The PA6 substrate was also electroless-plated after $scCO_2$ infusion of $Pd(hfa)_2$ with a $Pd(hfa)_2$ loading concentration of, 1.587×10^{-3} g-$Pd(hfa)_2$/g-CO_2, and the plating reaction occurred at 65 ºC for 60 min as conducted in Ohshima group's report [8]. The peeling force of the Ni-P plated neat PP substrates was too weak to be detected by the peeling test. The Ni-P metal layer could be uniformly formed on the surface of both of the PP/PP-b-PEO (85/15) and (75/25) blend substrates. The average peeling force of the iPP-B/PP-b-PEO (85/15) blend substrate was 1.3 N/cm and

dramatically increased when the PP-b-PEO percentage became 25%. As shown in Figure 3.17, the peeling force of iPP-B, rPP, v-PP-A and vPP-B base substrates blended with 25% PP-b-PEO, increased to 12.9, 7.5, 5.8 and 1.9 N/cm, respectively.

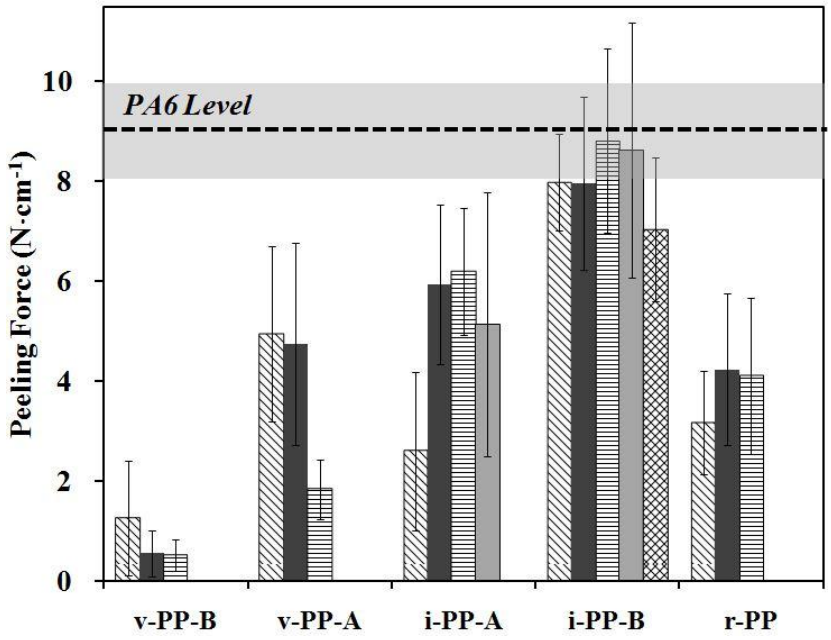

Figure 3.18. Peeling force of the PP/PP-b-PEO (75/25) blend substrates preparing with different PP grades and under different loading $Pd(hfa)_2$ concentrations in $scCO_2$ infusion process (mold cavity temperature = 40 ºC) (Amount of $Pd(hfa)_2$ in $scCO_2$ (g/g-CO_2) ($\times 10^{-3}$): ▨ = 0.063; ■ = 0.317; ▭ = 0.952; ▩ = 1.587; ▨ = 3.175) (Viscosity ratios of PP to PP-b-PEO are in order from low (left side of x-axis) to high (right side of x-axis): vPP-B < vPP-A < iPP-A < iPP-B < rPP) (averaging 8 samples data for each condition)

To observe the effect of infused $Pd(hfa)_2$ concentration on the peeling force or adhesive strength of the Ni-P layer, the $scCO_2$ infusion was conducted at several $Pd(hfa)_2$ loading concentrations for each sample. Figure 3.18 shows the average peeling forces for the PP/PP-b-PEO (75/25) blend substrates that were prepared with five different PP grades and then injection molded at a mold cavity temperature of 40 ºC. The peeling forces were different depending on the PP grades as well as the loading concentration of $Pd(hfa)_2$: the iPP-A/PP-b-PEO and iPP-B/PP-b-PEO blend substrates showed larger peeling forces than the other PP grade-base blend substrates. The loading $Pd(hfa)_2$ concentration changed the peeling force. The highest loading

concentration did not always provide the strongest peeling force. The metal-polymer composite layers were formed at the interface between the electroless-plated metal layer and the polymer substrate. In Ohshima group's report [8], it clarified that the adhesive strength of the Ni-P metal layer was strongly related with the thickness of the composite layer. When the loading concentration of $Pd(hfa)_2$ was high, the plating reaction rate became faster than the mass transfer rate in the plating solution, with the plating reaction occurring on the surface of the substrates. The Ni-P metal layer that formed on the surface prevented the plating solution from diffusing into the interior of the substrate. When the metal-polymer composite layer was not added to surface and instead a metal layer formed on the surface, this metal layer reduced the adhesiveness between the metal layer and the polymeric substrate. Figure 19 clearly shows the existence of an optimal concentration of Pd catalyst for each blend system to produce a strongly adhesive Ni-P metal layer.

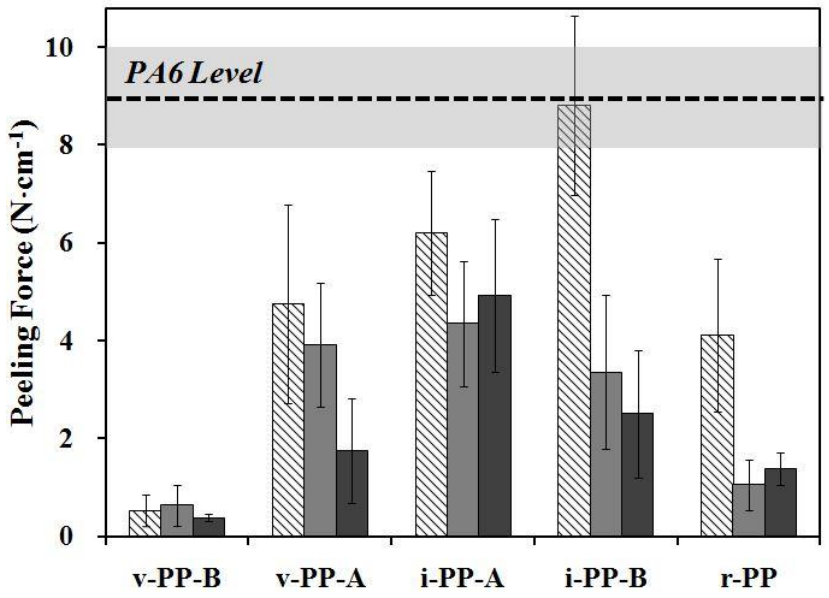

Figure 3.19. Peeling force of the PP/PP-b-PEO (75/25) blend substrates preparing with different PP grades and different molding temperatures, ▨ = 40, ■ = 70 and ■ = 100 ºC (loading $Pd(hfa)_2$ concentration = 0.952×10^{-3} g-$Pd(hfa)_2$/g-CO_2.) (Viscosity ratios of PP to PP-b-PEO are in order from low (left side of x-axis) to high (right side of x-axis): vPP-B < vPP-A < iPP-A < iPP-B < rPP) (averaging 8 samples data for each condition)

The effect of mold cavity temperature was also investigated by preparing the PP/PP-b-PEO substrate at different molding temperatures (40, 70 and 100 ºC) and impregnating Pd catalyst into the blend samples under $scCO_2$ infusion of $Pd(hfa)_2$ with a loading $Pd(hfa)_2$ concentration of 0.952×10^{-3} g-$Pd(hfa)_2$/g-CO_2. Figure 3.19 shows the average peeling forces for the PP/PP-b-PEO (75/25) blend substrates prepared with different PP grades. The PP/PP-b-PEO blend substrates prepared at a mold cavity temperature of 40 ºC clearly showed a higher peeling force than the blend substrates molded at 70 or 100 ºC, especially on the rPP, iPP-B and vPP-A base blend substrates. Figure 3.11 shows that the percentage of PP-b-PEO copolymer domains in the PP matrix near the substrate surface were reduced as the mold temperature increased from 40 to 100 ºC. This result indicates that there is strong relationship between the concentration of copolymer in the PP matrix near the surface and the adhesive strength of the Ni-P metal layer or the thickness of the metal-polymer composite layer.

3.3.7. Metal-polymer composite layer

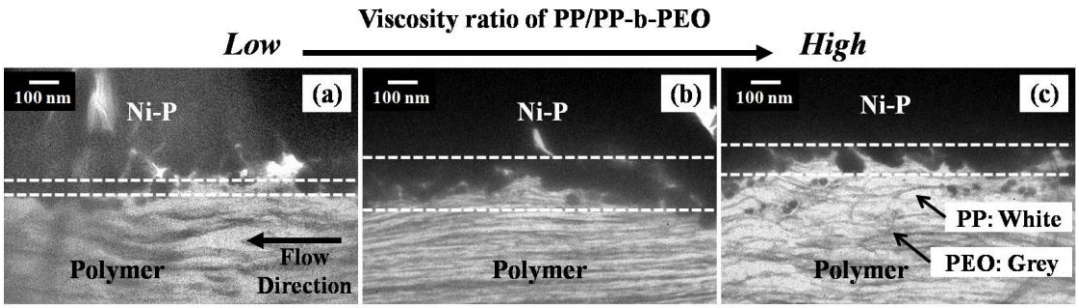

Figure 3.20. TEM images of the cross-section of the interface between the Ni-P film and the stained (a) vPP-B, (b) iPP-B and (c) rPP blended with 25% PP-b-PEO (mold cavity temperature = 40 ºC, loading $Pd(hfa)_2$ concentration = 6.35×10^{-5} g-$Pd(hfa)_2$/g-CO_2)

Figure 3.20 shows the TEM micrographs of the cross-sectional area near the surface of the electroless Ni-P plated PP/PP-b-PEO (75/25) substrates. The samples were prepared by blending different PP grades, (a) vPP-B, (b) iPP-B and (c) rPP with 25% PP-b-PEO, and injection molding at a mold cavity temperature of 40 ºC, infusing $Pd(hfa)_2$ at a loading concentration of 6.35×10^{-5} g-$Pd(hfa)_2$/g-CO_2, and electroless-

plating at 65 ºC for 60 min. In Figure 3.20, the black area represents the Ni–P metal layer as well as the Ni-P metal nanoparticles, the gray layers are the PP-b-PEO dispersed domains and the white is the polymeric substrate. The Ni-P metal nanoparticles seemed to be in or nearby the PP-b-PEO dispersed domains. The thickness of the metal-polymer composite layer was determined from the TEM micrographs as shown by the white dotted lines. The metal-polymer composite layer of the iPP-B/PP-b-PEO (75/25) substrate was thickest among those of the rPP and vPP-B/copolymer blend substrates and showed the strongest peeling force.

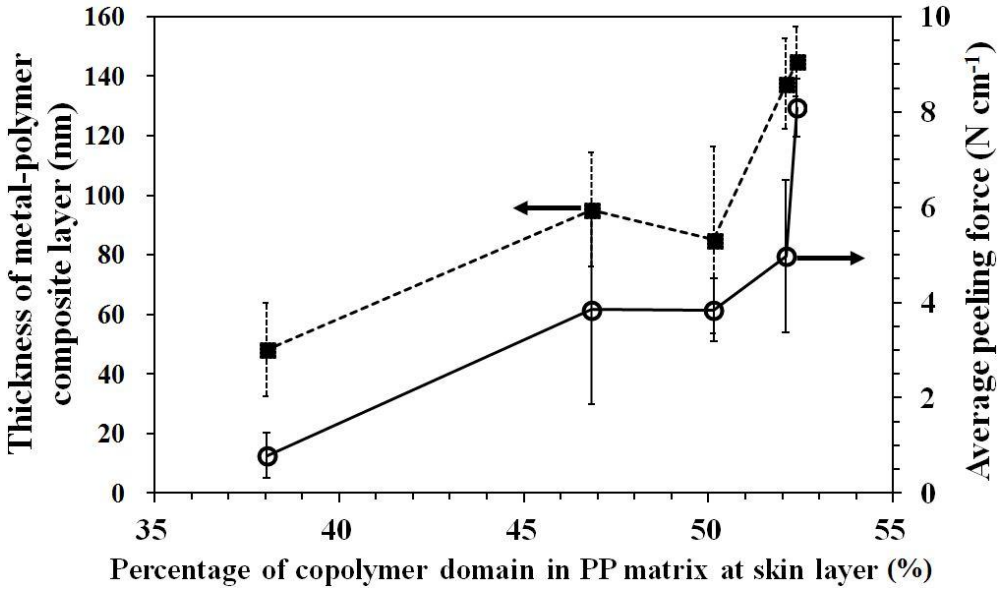

Figure 3.21. Relationship between the thicknesses of metal-polymer composite layer and the peeling forces of the Ni-P metal layer as well as the concentration of PP-b-PEO domains in PP matrix near the surface of the PP/PP-b-PEO (75/25) blend substrates

Similarly, the thickness of the metal-polymer composite layer was measured for all of the electroless-plated blend substrates. Figure 3.21 shows the relationship between the thicknesses of the metal-polymer composite layer and the peeling forces of the Ni-P film as well as the concentration of the PP-b-PEO copolymer domains in the PP matrix near the surface of the PP/PP-b-PEO (75/25) blend substrates investigated in this study. This figure clearly shows that the thickness of the metal-polymer composite layer increased as the concentration of the PP-b-PEO domains

near the substrate surface increased and that the peeling force increased as the thickness of the composite layer increased.

3.4. Conclusion

The hydrophilic property of the surface of the PP substrate was modified by blending the base polymer with a PP-b-PEO copolymer in the injection molding machine and then a supercritical carbon dioxide ($scCO_2$) assisted electroless Ni-P plating technique could be applied to the PP-made plastic products. The technique successfully prepared a remarkably uniform Ni-P metal layer on a PP-based substrate with sufficiently strong adhesion. The adhesiveness of the Ni-P metal layer to the polymer substrate was dominated by the thickness of the metal-polymer composite layer. The thickness of the metal-polymer composite layer could be controlled by the degree of the hydrophilic modification and the amount of infused catalyst in the polymeric substrate. The orientation and concentration of the PP-b-PEO (hydrophilicity modifier) in the PP matrix near the surface were the most important factors for determining the thickness of the metal-polymer composite layer. The orientation and concentration of the PP-b-PEO were determined by the flow behavior of the injection molding process, which was changed by altering the viscosity ratio of PP to copolymer and the mold cavity temperature. The $scCO_2$-assisted electroless Ni-P plating technique when combined with hydrophilic modification of the surface can increase the potential for applying this technique to other polymers.

3.5. References

[1] G.O. Mallory, J.B. Hajdu, in, William Andrew Publishing/Noyes, 1990, pp. 1-3.

[2] D. Schröer, R.J. Nichols, H. Meyer, Electrochimica Acta, 40 (1995) 1487-1494.

[3] S.M. Rossnagel, Journal of Vacuum Science & Technology B, 16 (1998) 2585-2608.

[4] B.-H. Woo, M. Sone, A. Shibata, C. Ishiyama, S. Edo, M. Tokita, J. Watanabe, Y. Higo, Surface and Coatings Technology, 204 (2010) 1785-1792.

[5] V. Zaporojtchenko, J. Zekonyte, S. Wille, U. Schuermann, F. Faupel, Nuclear Instruments and Methods in Physics Research Section B: Beam Interactions with Materials and Atoms, 236 (2005) 95-102.

[6] X. Zhao, K. Hirogaki, I. Tabata, S. Okubayashi, T. Hori, Surface and Coatings Technology, 201 (2006) 628-636.

[7] N. Martinez, K. Hisada, I. Tabata, K. Hirogaki, S. Yonezawa, T. Hori, The Journal of Supercritical Fluids, 56 (2011) 322-329.

[8] H. Adachi, K. Taki, S. Nagamine, A. Yusa, M. Ohshima, The Journal of Supercritical Fluids, 49 (2009) 265-270.

[9] C. Erkey, The Journal of Supercritical Fluids, 47 (2009) 517-522.

[10] C.W. Extrand, Journal of Colloid and Interface Science, 248 (2002) 136-142.

[11] J. Long, P. Chen, Langmuir, 17 (2001) 2965-2972.

[12] E. Occhiello, M. Morra, G. Morini, F. Garbassi, P. Humphrey, Journal of Applied Polymer Science, 42 (1991) 551-559.

[13] M. Strobel, M.C. Branch, M. Ulsh, R.S. Kapaun, S. Kirk, C.S. Lyons, Journal of Adhesion Science and Technology, 10 (1996) 515-539.

[14] H.Y. Nie, M.J. Walzak, B. Berno, N.S. McIntyre, Applied Surface Science, 144–145 (1999) 627-632.

[15] R.J. Good, L.K. Shu, H.-C. Chiu, C.K. Yeung, The Journal of Adhesion, 59 (1996) 25-37.

[16] K. Harth, H. Hibst, Surface and Coatings Technology, 59 (1993) 350-355.

[17] A. Shojaei, R. Fathi, N. Sheikh, Surface and Coatings Technology, 201 (2007) 7519-7529.

[18] M.D. Green, F.J. Guild, R.D. Adams, International Journal of Adhesion and Adhesives, 22 (2002) 81-90.

[19] T. Yabuta, Polymer Preprints, 58 (2009) 87.

Chapter IV

Environmentally Benign Electroless Nickel Plating using Supercritical Carbon-Dioxide on Hydrophilically Modified Acrylonitrile-Butadiene-Styrene

4.1. Introduction

Plastic surfaces are metalized for use in various industrial applications ranging from the fabrication of printed circuits to decorative coatings for plastic parts. Metallization provides the plastic parts with metallic characteristics, such as reflectivity, abrasion resistance, electrical conductivity and a decorative luster [1, 2]. Several techniques have been developed for metalizing the surfaces of plastic parts, such as physical–chemical vapor deposition, metal-powder coating and electroless plating [3]. Electroless plating is the most widely used of these methods in industry, especially in the automotive, aerospace and microelectronics industries [4]. Electroless metal plating offers several advantages, such as the option of forming partial coatings, flexibility in the plating volume and thickness, automatic monitoring of chemical replenishment and surface brightness control [5, 6].

In electroless metal plating, a catalytic redox reaction of a metal ion in an aqueous solution occurs in the presence of a reducing chemical agent but without an external electrical field [6-8]. The process consists of three primary steps: (i) surface treatment or conditioning; (ii) the application of an appropriate catalyst (typically a noble metal catalyst, such as tin or palladium) onto the substrate surface; and (iii) metal electroless deposition. The substrate must be rinsed between the steps. In the first step, harsh and/or toxic surface conditioning, i.e., chemical-etching, is usually used to modify the substrate surface characteristics such that the catalyst firmly attaches to the surface. However, chemical-etching is environmentally harmful. Thus, the exclusion of chemical etching would make the electroless metal plating

environmentally benign.

Hori et al. [9, 10] and Ohshima's group [11] have independently developed a so-called supercritical carbon dioxide ($scCO_2$)-assisted electroless plating scheme for polymeric materials, in which acid is not used to roughen and condition the plastic substrate surface. Hori's $scCO_2$-assisted electroless plating method was primarily developed for application to polymeric fibers. For example, Pd(II) hexafluoroacetylacetonate $Pd(hfa)_2$ was infused into Kevlar® fibers using $scCO_2$ and simultaneously activated by over-heating to reduce the metal complex to a catalyst for the plating reaction [9]. The Kevlar was then immersed in an electroless copper (Cu) plating solution to coat the Kevlar with a Cu metal layer. Ohshima and co-workers developed an electroless plating technique method for use with extrusion or injection molded-plastic parts, especially plastic parts made from polyamide 6 (PA6) [11]. This method comprised two steps: the first step consisted of the $scCO_2$-assisted impregnation of the substrate with a catalyst precursor, $Pd(hfa)_2$, and the second step consisted of an electroless nickel-phosphorus (Ni-P) plating reaction. In the first step, $scCO_2$ served as a solvent for the catalyst precursor and as a plasticizer to soften the surface of the polymeric substrates. The catalyst precursor was dissolved in $scCO_2$. The substrate was impregnated with the catalyst precursor by exposure to $scCO_2$ containing $Pd(hfa)_2$. The catalyst precursor was then thermally reduced [12]. One of the differences between Ohshima group's method and that of Hori's group [9, 10] was that the addition of alcohol to the plating solution to further soften the polymeric substrates during the electroless plating reaction. The addition of alcohol resulted in strong adhesion between the metal film and the polymer.

In Ohshima group's method, a Ni-P metal-polymer composite layer was formed between the Ni-P alloy layer and the polymer matrix during the electroless plating reaction, resulting in a high adhesive strength between the metal layer and the polymeric substrate. Increasing the mass transfer rate of the plating solution into the polymeric substrate increased the thickness of the metal-polymer composite layer and strengthened the adhesion between the metal layer and the polymer. The electroless plating solution consisted primarily of water; thus, the mass transfer rate of the plating solution into the polymer substrate was strongly affected by the hydrophilicity of the polymer substrate. Unfortunately, most thermoplastic polymers are highly hydrophobic, thereby limiting the direct application of Ohshima group's method to polymers with a moderately high water absorption rate, such as poly(methyl

methacrylate) (PMMA) or PA6 [11].

Acrylonitrile-butadiene-styrene (ABS) is one of the most commonly used polymers in the automotive industry because of its excellent toughness, good dimensional stability, good processability, chemical resistance and low cost [13, 14]. However, ABS is hydrophobic. The contact angle between PA6 and water is only 69.2º [15]. However, the contact angle between ABS and water is 81.0º±0.6º [16]. When the developed electroless Ni-P alloy plating method was applied to ABS, the high hydrophobicity of the substrate prevented the water-based plating solution from penetrating into the polymeric substrate. Thus, only the surface of the ABS substrate was covered with the metal, and the metal-polymer composite layer did not form. This mechanism prevented a metal-polymer composite layer from forming in the substrate interior. Thus, the anchoring effect was diminished, which weakened the adhesive strength between the metal layer and the polymeric substrate [11]. There is considerable interest in developing an environmentally benign electroless plating technique that can be applied to ABS polymers.

The surface of the ABS substrate must be modified to convert the hydrophobic polymer into a hydrophilic polymer to ensure good performance for the developed electroless plating method. Several techniques have been used to modify the hydrophilicity of the polymer, such as flame treatment [17], ion-assisted laser treatment [18] and plasma modification [19]. However, many of these techniques can only modify the hydrophilicity of the polymer substrate at short distances from the surface (i.e., less than 10 nm) and do not provide the same adhesive strength as conventional chemical etching [20]. Conventional chemical etching, i.e., etching with chromic/sulfuric acid solutions, can increase the wettability of ABS plastics [21]. Chromic/sulfuric acid also dissolves the polybutadiene nodes in ABS and increases the surface roughness, which significantly increases mechanical adhesion [7]. There have been continuing efforts to develop a non-toxic environmentally benign surface modification technique. Recently, Kim et al. [22] and Magallón-Cacho et al. [23] used a photocatalytic reaction in a titanium dioxide (TiO_2) solution to modify the ABS surface as an alternative to etching with chromic/sulfuric acid solutions. Garcia et al. [24] developed a poly(acrylic acid) covalent grafting technique to deposit Cu by electroless plating onto ABS. Ohshima's group has developed a copolymer-based modification technique coupled with injection molding. As resulted in previous chapter that demonstrated the effectiveness of this modification technique for

polypropylene (PP): the addition of a PP-polyethylene oxide (PEO) block copolymer (PP-b-PEO) into PP significantly increased the hydrophilicity of PP. The PP-b-PEO copolymer was originally developed as an antistatic agent for PP and can be highly dispersed in a PP matrix [25]. Plastic parts were fabricated from PP blended with the PP-b-PEO copolymer in an injection molding machine; the copolymer content was enriched near the surface of the injected plastic parts because of a fountain flow and the viscosity difference between the copolymer and the matrix polymer. In a 20-μm region from the surface of the plastic substrate, dense copolymer domains formed in a multilayered structure that either oriented in the flow direction (FD) or the machine direction (MD). This surface enrichment and the oriented structure of the hydrophilic copolymer facilitated a high mass transfer rate of the plating solution and created strong adhesion between the polymer and the Ni-P metal layer.

In this chapter, the effectiveness of developed electroless plating technique combined with the polymer modification technique was investigated for ABS. A poly(ether-ester-amide)s (PEEA) copolymer [25, 26], which is an antistatic agent for the family of styrene-based polymers, was used to modify the ABS hydrophilicity. ABS consists of an elastomer (butadiene) in a styrene and acrylonitrile copolymer (SAN) matrix [13], and the ratio of butadiene to SAN can be varied to produce different mechanical properties. The effects of the morphology of ABS and ABS/PEEA were investigated. The effects of the processing conditions on the adhesion between the Ni-P metal film and the polymer substrate were also investigated. Transmission electron microscopy (TEM) was used to determine the location of the butadiene and PEEA domains and the thickness of the composite layer. The effect of modification by the PEEA copolymer on the mass transfer of plating solution was studied using a sorption test, and the adhesive strength of the contact between the Ni-P metal layer and the polymeric surface was measured using a peel-off test.

4.2. Experimental section

4.2.1. Sample preparation and experimental procedure

General-purpose grade acrylonitrile-butadiene-styrene (ABS: Daicel Polymer, Japan, Cevian V 320SF), styrene-acrylonitrile copolymer (SAN: Daicel Polymer,

Japan, Cevian N 070SF) and poly(ether-ester-amide)s (PEEA) multi-block copolymer (PEEA: Sanyo Chemical Industries, Japan, Pelestat® NC6321) were used to prepare the polymeric substrates. PEEA copolymer, Pelestat® NC6321, was developed as an antistatic agent for styrene resins and was used in this study to modify the hydrophilicity of ABS. PEEA copolymer has a high melting point ($T_m \approx 203$ ºC) because of the crystallization of the polyamide blocks, and the polyether block imparts a hydrophilic nature to ABS [26]. The pelletized PEEA copolymer was dry-blended with ABS at ABS to PEEA different blend ratios (ABS/PEEA = 95/5, 90/10, 85/15 and 80/20). Neat ABS and SAN substrates and a Polyamide 6 (PA6: Unitika, Japan, A1025NO, Mw 14,000) substrate were prepared for use as references. The SAN copolymer was dry-blended and injection molded with ABS at different ABS to SAN weight ratios (i.e., ABS/SAN = 25/75, 50/50 and 75/25) to prepare ABS substrates with different butadiene volume percentages. A 35-ton injection molding machine (J35ELIII-F, Japan Steel Works Ltd., Japan) with a rectangular plate-shaped mold cavity was used to prepare the polymer substrate. The temperatures of the solid conveying, compression and metering zones in the injection machine were set at 205, 215 and 230 ºC, respectively, and the mold cavity temperature was maintained at 60 ºC. Rectangular-shaped substrates that were 2 mm in thickness, 15 mm in width and 50 mm in length were then cut out of the injection molded plate as shown in Figure 2.2.

Pd(II) hexafluoroacetylacetonate, ($Pd(hfa)_2$) (99.95% purity, Sigma-Aldrich, USA) was used as a catalyst precursor. CO_2 (Showa Gas Products, Japan) was used as a solvent and a $Pd(hfa)_2$-carrier for the polymers. The electroless Ni–P metal plating solutions used in this study were ICP Nicoron DK-M and DK-1 (Okuno Chemical Industry, Japan). DK-M contains phosphoric acid (16%), adipic acid (4%), a complexing agent (16%) and water (64%), and DK-1 contains nickel sulfate (35%) and water (65%). A standard plating solution was prepared in this study by mixing DK-M (10%) and DK-1 (5%) with distilled water (85%). Ethanol (99.5% purity, Wako Pure Chemical, Japan) was added to the standard plating solution as an additional plasticizer for the polymer surface [11]. All the chemicals were used as received.

4.2.2. Supercritical CO_2-assisted infusion of $Pd(hfa)_2$

The polymer substrates were placed in a high pressure autoclave (with a 70-cm^3 volume), and the $Pd(hfa)_2$ catalyst precursor was infused into the substrates using $scCO_2$: the autoclave temperature was maintained constant at 80 ºC during the infusion process, and the pressure was controlled by a pump (ISCO, Japan) at 10 MPa CO_2. The infusion was conducted for 60 min. To observe the effect of Pd on the plating process, the four different masses of $Pd(hfa)_2$ were loaded into the autoclave: 1, 2.5, 5 and 15 mg. The $Pd(hfa)_2$ concentration in $scCO_2$ was estimated assuming that all the loaded $Pd(hfa)_2$ dissolved in the $scCO_2$. The Pd-complex was thermally reduced in the polymer substrate by increasing the autoclave temperature to 120 ºC; this temperature was maintained for 35 min while maintaining the CO_2 pressure at 10 MPa to prevent foaming of the substrate.

4.2.3. Electroless plating reaction

The Pd-infused polymer substrate was placed in a vacuum chamber for over 24 h to remove CO_2 from the substrate and was then immersed into the electroless Ni-P plating solution. Ethanol was added to the electroless plating solution. Ethanol enhanced the diffusivity and solubility of the plating solution by swelling the polymer [11]. Consequently, the electroless plating reaction occurred around the Pd nanoparticles that had impregnated into the polymer substrate. The Ni–P metal phase grew around the nanoparticles, agglomerated with the other metal phases and formed a semi-continuous structure near the substrate surface. This structure had an anchoring effect and increased the adhesive strength of the contact between the metal layer and the polymer. During the plating process, the temperature of the plating solution was maintained at 65 ºC using a water bath. The minimum plating reaction time was 30 min; however, this time was adjusted depending on the infused Pd concentration.

4.2.4. Morphology evaluation

An optical microscope with a digital camera (DP21, Olympus, Tokyo, Japan) was used to observe the surface morphology of the Ni-P metal plated samples and the unplated samples. Cross-sections of the plated substrate were observed using a TEM (JOEL-1010, JEOL, Japan) after slicing the sample. An ultra-microtome (ULTRACUT-J, Leica, Austria) was used to perform the slicing at a rate of 2 mm/s at

room temperature. The sliced Ni-plated samples were 70 nm thick. The TEM observations were conducted at a 100 kV accelerating voltage after the sliced sample was stained with a 2% phosphotungstic acid (PTA) solution for 20 s. TEM was also used to observe the dispersed butadiene domains in the ABS matrix after staining the sliced sample with osmium tetroxide (OsO_4). The OsO_4 staining was performed by dropping 2% aqueous OsO_4 solution onto the ultra-thin microtomed section of the sample and leaving the sample undisturbed for 6 min. PTA solution was used to selectively stain the PEEA copolymer domains. The staining was performed by floating the ultra-thin microtomed samples in a 2% aqueous PTA solution for 30 s.

4.2.5. Mechanical measurement

A tensile test was performed on the neat ABS substrate and the ABS/PEEA blend substrate using an Autograph (Shimadzu, AGS-J Series, Japan) at the ambient temperature and a strain rate of 1 $mm \cdot min^{-1}$. Following ISO 527-2, the ABS/PEEA blend samples were prepared using the injection molding machine, after which the test piece was cut out from the solid sample: the test piece was 2 mm thick and 6 mm wide with an overall length of 50 mm (the gauge length was 10 mm).

4.2.6. Measurement of the sorption amounts of the plating solution and the water contact angle

The polymer substrate (which was not infused with the Pd complex) was immersed in the plating solutions at 65 ºC to measure the solubility and diffusivity of the plating solution in the polymer substrate. The weight of the substrates before and after sorption was measured using an electronic balance with a 10-μg resolution (AUW220D, Shimadzu, Japan) after wiping out any residual solution from the substrates. The static water contact angles on the surface of the polymer substrates were measured using the sessile drop method at room temperature.

4.2.7. X-ray photoelectron spectroscopy (XPS)

The Pd surface composition and concentration depth-profile were measured using X-ray photoelectron spectroscopy (XPS) in conjunction with ion gun etching. The XPS measurements were performed using an ESCA-3400 spectrometer (Kratos

analytical, Japan) with excitation (Acc. HT.: 10 kV, emission current: 20 mA) under a vacuum pressure of 1×10^{-6} Pa. The samples with etched with an ion gun under vacuum pressure (5×10^{-4} Pa) at an etching rate of 40 Å /min.

4.2.8. Measurements of the adhesiveness of the metal layer to the polymer substrate

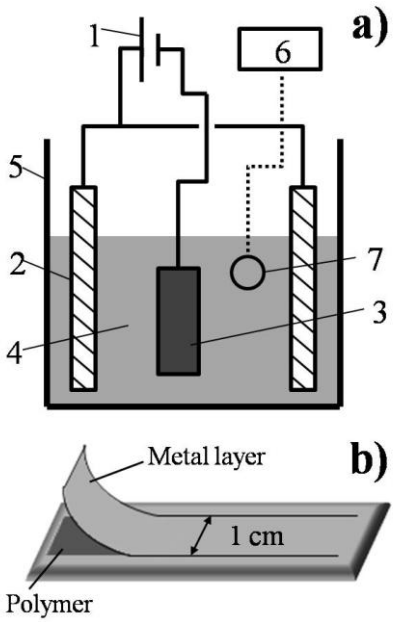

Figure 4.1. (a) Schematic of Cu-electroplating apparatus: 1) DC power supply; 2) anode; 3) cathode (Ni-P plated polymer); 4) plating solution; 5) glass bath; 6) air pump; and 7) air bubble stone; and (b) prepared sample for peeling-test machine

Immediately following Ni-P electroless plating, the plated polymeric substrate was electroplated with Cu. The purpose of the Cu coating was to increase the thickness of the metal layer for a peeling test. Figure 4.1(a) is a schematic of the Cu plating apparatus. A Cu plate was located vertically on either side of the bath and served as an anode. The Ni-P plated polymer substrate served as a cathode. The plating solution was an aqueous mixture of 180 g/L $CuSO_4\cdot5H_2O$ and 60 g/L of H_2SO_4. The entire electroplating process was performed in a glass bath at room temperature for 35 min with a 1-A applied electric current. Before measuring the adhesive strength of the contact between the metal film and the polymer, the Cu-plated samples were dried at room temperature for over 24 h. An approximately 1-cm length of the Cu-coated Ni-P metal layer was peeled using a knife, as shown in Figure

4.1(b). The partially peeled metal layer was clamped, and a 90º peel test was then used to measure the adhesive strength at the ambient temperature (Autograph AGS-J, Shimadzu, Japan). A certain layer thickness was required to properly clamp the metal layer. The force needed to peel the metal layer per unit length was considered to be the adhesive strength of the contact between the Ni-P metal layer and the polymer substrate.

4.3. Results and discussion

Hydrophilic modification and blend morphology

4.3.1. Sorption of the plating solution by the polymer substrates and wettability

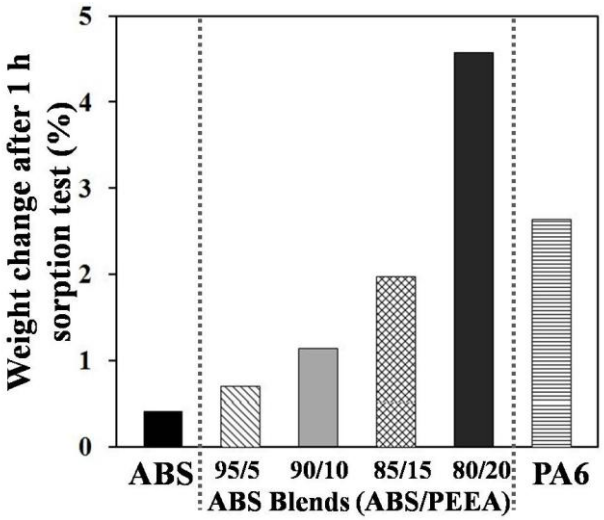

Figure 4.2. Intake of plating solution by polymer substrates (each data point is an average for 4 samples for each case)

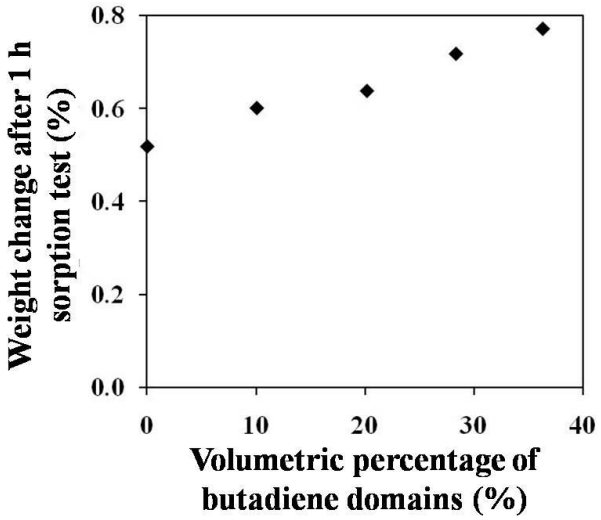

Figure 4.3. Relationship between the amount of plating solution absorbed by the polymer substrate and the volumetric percentage of butadiene in the SAN matrix near the surface of the polymer substrate (each data point is an average for 4 samples for each case)

Figures 4.2 and 4.3 show the intake of the plating solution by the neat ABS and neat PA6 substrates and the ABS/copolymer-blended substrate. All the substrates were immersed in the same plating solution, i.e., a mixture of 60% standard plating solution and 40% ethanol at 65 ºC. The solubility of the plating solution in the polymer substrate was determined by measuring the weight gained by the polymer substrates after immersion in the plating solution for 1 h. The weight change was calculated using the following equation:

$$\text{weight change (\%)} = \frac{\text{weight of substrate after sorption} - \text{weight of substrate before sorption}}{\text{weight of substrate before sorption}} \times 100\%$$

Figure 4.2 shows that the solubility and diffusivity of the plating solution in the substrates increased with the proportion of the PEEA copolymer in the polymer blend. The increase in the solubility and diffusivity of the plating solution reflected the increase in the mass transfer rate of the plating solution into the polymer substrate. When the PEEA to ABS blend ratio was 5/95 or more, the solubility and diffusivity became sufficiently high to facilitate electroless plating and increased the adhesive strength to a satisfactory level. Figure 4.3 shows that the amount of the plating solution that was absorbed by the polymer substrate varied with the butadiene volume

percentage in the skin region near the polymer surface.

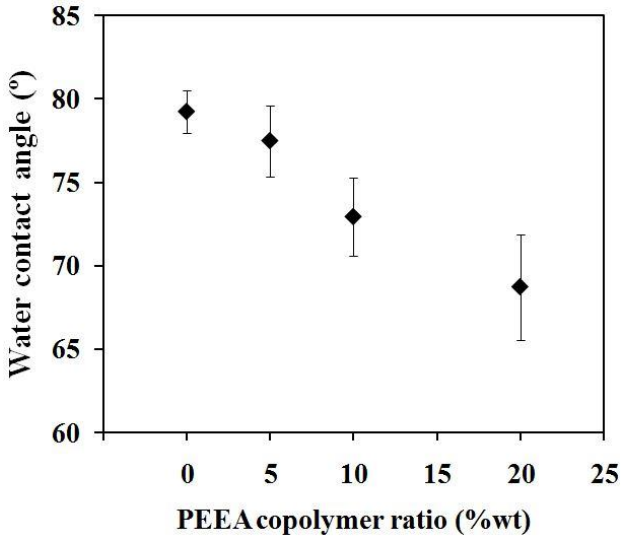

Figure 4.4. Water contact angle on the surface of the neat ABS substrate and the ABS/PEEA blend substrate for different PEEA blend ratios (each data point is an average of 5 measurements)

Figure 4.4 shows the water contact angle at the surface of the neat ABS substrate and the ABS/PEEA blend substrate for different PEEA blend ratios (5, 10 and 20 wt%). The water contact angle at the surface of the ABS/PEEA blend was lower than that at the surface of the neat ABS substrate and decreased as the percentage of PEEA copolymer in the polymer blend increased. The water contact angle at the surface of the neat ABS substrate measured in this study agreed with the literature values [16]. Adding the PEEA copolymer to the ABS substrate increased the wettability and the hydrophilicity of the polymer substrate.

4.3.2. Morphology of ABS and PEEA copolymer blend

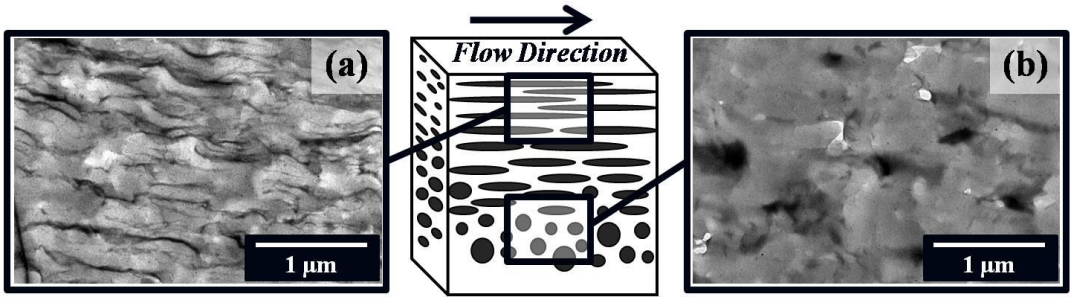

Figure 4.5. Schematic of skin/core structure of injection-molded blend substrate (center) and TEM micrographs of cross-section of ABS/PEEA (80/20) blend substrate for (a) the skin region and (b) the core region: dark regions correspond to PEEA domains and grey regions correspond to the ABS matrix

Figure 4.5 shows the skin/core structure in a cross-section of the injection molded polymer blend substrate. The black regions correspond to the PEEA copolymer domains, and the grey regions correspond to the ABS matrix. The TEM micrograph shows that the PEEA domains elongated in the flow direction and that the domains were more highly oriented closer to the surface. In a region approximately 20 μm beneath the surface, the copolymer domains were highly oriented, and a platelet-like nanostructure was formed as illustrated in Figure 4.5(a). In contrast, the domain orientation completely vanished in the central region (core region) of the substrate, and spherical domains were observed as shown in Figure 4.5(b). This result was attributed to the viscosity difference between the PEEA copolymer and the ABS matrix. When a low viscosity polymer was blended with a higher viscosity polymer and injected into the mold cavity, the low viscosity polymer segregated preferentially to the surface [25, 26].

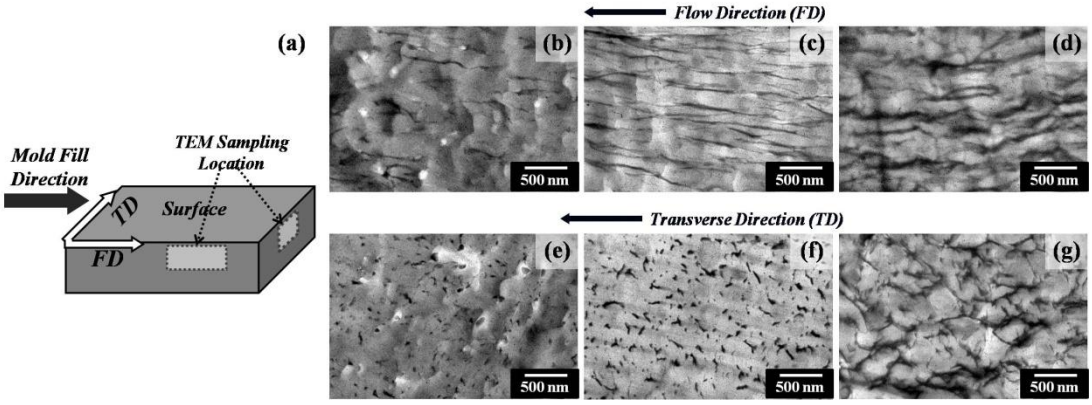

Figure 4.6. Illustration of (a) TEM sampling location relative to the flow direction (FD) and the transverse direction (TD) of an injection molded sample and TEM micrographs of the cross-section of the skin layer of stained ABS/PEEA blend substrates prepared by blending ABS with different PEEA weight percentages: (b) and (e) 5%, (c) and (f) 10%, (d) and (g) 20%; (b), (c) and (d) viewed parallel to the FD, and (e), (f) and (g) viewed parallel to the TD; (black strips: PEEA; grey region: ABS)

Figure 4.6 shows the TEM micrographs for a cross-section near the surface of the ABS/PEEA blend substrates for blend ratios of 5%, 10% and 20%, in which all the samples were observed in the flow direction (FD) and the transverse direction (TD). Figures 4.6(b), (c) and (d) show that the degrees of enrichment and orientation of the PEEA domains in the FD below the molded surface increased with the PEEA weight percentage in the blend samples. The PEEA domains away from the molded surface became longer and thicker strips as the PEEA content in the ABS/PEEA blends increased. Figures 4.6(e) and (f) show that the PEEA copolymer domains in the ABS/PEEA (95/5) and (90/10) blends were stick-shaped and dispersed in the ABS matrix; however, Figures 4.6(d) and (g) show strips of PEEA copolymer domains in both the FD and TD directions, indicating that plane PEEA layers may have formed for the blend sample with a 20% PEEA copolymer content.

ABS is a thermoplastic copolymer that consists of a dispersed butadiene phase in a styrene acrylonitrile copolymer (SAN) matrix. Figure 4.7 shows TEM micrographs of a cross-section near the surface of the ABS substrate and the ABS/PEEA (95/5) blend substrate before and after $scCO_2$ infusion of Pd. The grey region corresponds to the SAN copolymer matrix, and the black spherical regions correspond to the butadiene domains. For the ABS/PEEA blends, in addition to the black spherical

butadiene domains, black strings were also observed, corresponding to PEEA domains that were elongated in the flow direction. Figure 4.7 shows dispersed PEEA copolymer domains in the SAN matrix, where the distribution of the PEEA domains is such that they appear to be connecting the butadiene domains to each other.

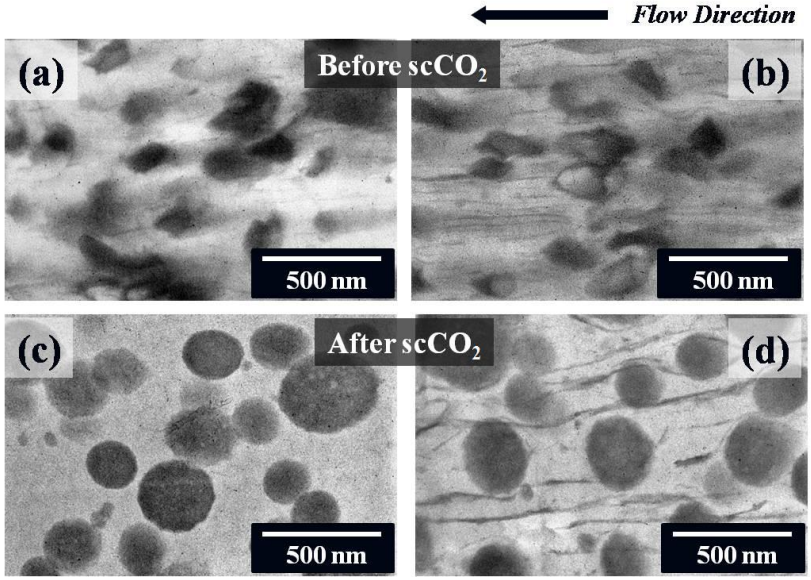

Figure 4.7. TEM micrographs of (a) neat ABS substrate and (b) ABS/PEEA (95/5) blend substrate without $scCO_2$ treatment and in contrast, $scCO_2$-infused blend substrates of (c) neat ABS and (d) ABS/PEEA (95/5): black spherical regions correspond to butadiene domains, black strips correspond to PEEA domains, and grey regions correspond to SAN matrix

Figure 4.8 shows TEM micrographs of the neat ABS substrate and the ABS/SAN blend substrate for three different weight ratios of ABS to SAN. All the substrates were prepared by injection molding, where the mold temperature was controlled at 60 ºC. All the TEM micrographs correspond to cross-sections near the substrate surface. The images clearly show that the density of butadiene domains decreased, whereas the size of the butadiene domains did not change significantly as the SAN weight ratio increased. The measured average volume percentage and the size of the butadiene domains are given in Table 4.1.

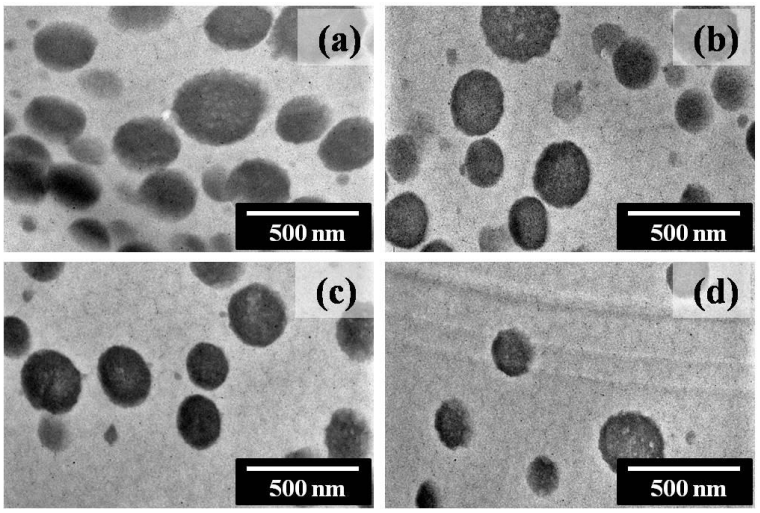

Figure 4.8. TEM micrographs of (a) neat ABS substrate and ABS/SAN blend substrates for different ABS to SAN blend ratios (ABS/SAN = (b) 25/75, (c) 50/50 and (d) 75/25); (black region: butadiene phase; grey region: SAN matrix)

Table 4.1. Volume percentage and size of butadiene domains (each data point is the average of 6 samples for each case)

Polymer grade	ABS	ABS/SAN		
		75/25	50/50	25/75
Volume % of Butadiene domain	36.3±3.0	28.3±3.1	20.2±3.9	10.1±0.8
Butadiene domain size (nm)	225±10	206±15	214±15	233±23

4.3.3. Polymer blend mechanical properties

Table 4.2. Mechanical properties of ABS/PEEA blends for various blend ratios (each data point is an average of 4 samples for each case)

Polymer grade	ABS / PEEA copolymer			
	100/0	95/5	90/10	80/20
Tensile strength (MPa)	41.0±2.7	39.5±0.8	37.0±1.0	30.3±0.7

Table 4.2 shows the tensile strengths of the ABS and the ABS/PEEA blends for different ABS ratios. The tensile strength of the ABS/PEEA blends decreased as the PEEA blend ratio increased. The mechanical properties of the blend samples deteriorated, because the degree of compatibility between ABS and PEEA decreased. That is, the interfacial tension of the ABS/PEEA (95/5) blend substrate was smaller than that of the ABS/PEEA (80/20) blend, and the ABS/PEEA (95/5) blend exhibited more uniformly dispersed domains and a higher mechanical strength [26-29].

4.3.4. Quantity of infused catalyst precursor

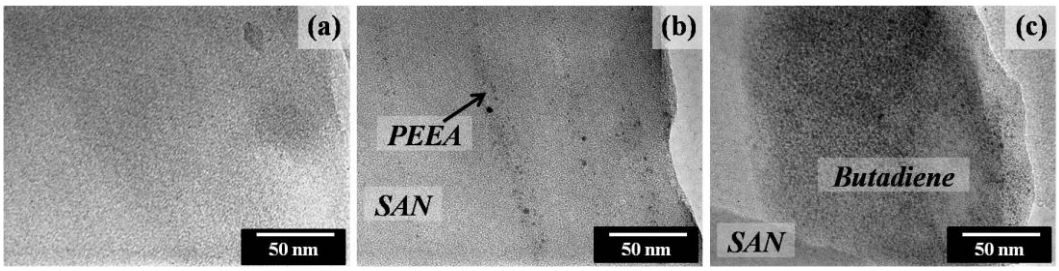

Figure 4.9. TEM micrographs of Pd-infused substrates: (a) neat SAN, (b) SAN/PEEA (95/5) blend and (c) neat ABS; Pd nanoparticles (black dots) were infused and embedded using $scCO_2$ at a Pd catalyst precursor concentration of 1.59×10^{-3} g-$Pd(hfa)_2$/g-$scCO_2$

After conducting the $scCO_2$-assisted Pd-complex impregnation at 80 ºC and 10 MPa for 60 min, thermal reduction was performed at 120 ºC under 10 MPa CO_2 for 35 min. Figure 4.9 shows TEM micrographs of cross-sections for the following substrates: (a) neat SAN, (b) the SAN/PEEA (95/5) blend and (c) neat ABS, for which $Pd(hfa)_2$ was impregnated using $scCO_2$. The black dots correspond to the Pd nanoparticles. Figure 4.9(a) shows a few Pd nanoparticles in the neat SAN substrate. However, nanoparticles were observed in the SAN/PEEA blend substrate and in the ABS substrate. Figure 4.9(c) shows Pd nanoparticles in the PEEA domains as well as in butadiene domains in the SAN matrix. Thus, the Ni-P plating reaction could occur in the PEEA copolymer and/or the butadiene domains, and these domains could affect the adhesive strength of the contact between the Ni-P metal layer and the polymer substrate.

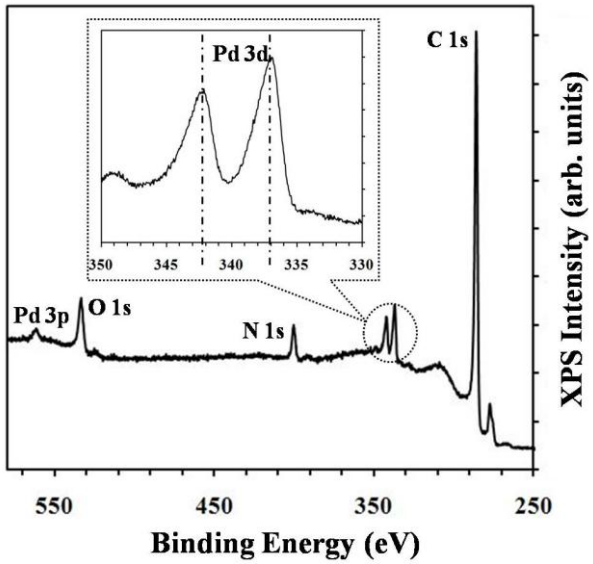

Figure 4.10. XPS spectra of neat ABS substrate after impregnation with $Pd(hfa)_2$ at a loading concentration of 1.59×10^{-3} g-$Pd(hfa)_2$/g-CO_2

Figure 4.10 shows the XPS spectra of a neat ABS substrate after impregnation and reduction of $Pd(hfa)_2$. Peaks were detected at 337 and 342.3 eV, corresponding to emissions from the 3d levels of the Pd metal. These emission peaks indicated the presence of reduced Pd on the substrate. The XPS analysis was used to determine the Pd concentration (i.e., the number of Pd atoms per carbon atom) on the surface and the interior of the polymeric substrates, as shown in Figure 4.11. Figure 4.11 shows the Pd concentration profiles as a function of the distance from the surface to the interior of the neat ABS and neat SAN substrates and the SAN/PEEA (95/5) blend substrate. The profiles were obtained by etching the substrate with an ion gun layer by layer. For all the samples, Pd impregnation was conducted at a $Pd(hfa)_2$ loading concentration of 1.59×10^{-3} g-$Pd(hfa)_2$/g-$scCO_2$ under $scCO_2$ at the same pressure and temperature as previously described. Figure 4.11 shows that the maximum Pd concentration was not attained at the surface but slightly inside the substrate. This result may have been obtained because some of the $Pd(hfa)_2$ diffused out of the substrate when the temperature was increased for the reduction process. Figure 4.11 shows that the Pd concentration varied for the different polymer substrates, showing the importance of the role played by the butadiene and PEEA copolymer domains in the electroless Ni-P plating reaction, because these domains were able to attract the Pd catalyst precursor. The XPS analysis also confirmed that the Pd catalyst was

successfully infused into the substrates by the $scCO_2$ infusion and thermal reduction processes.

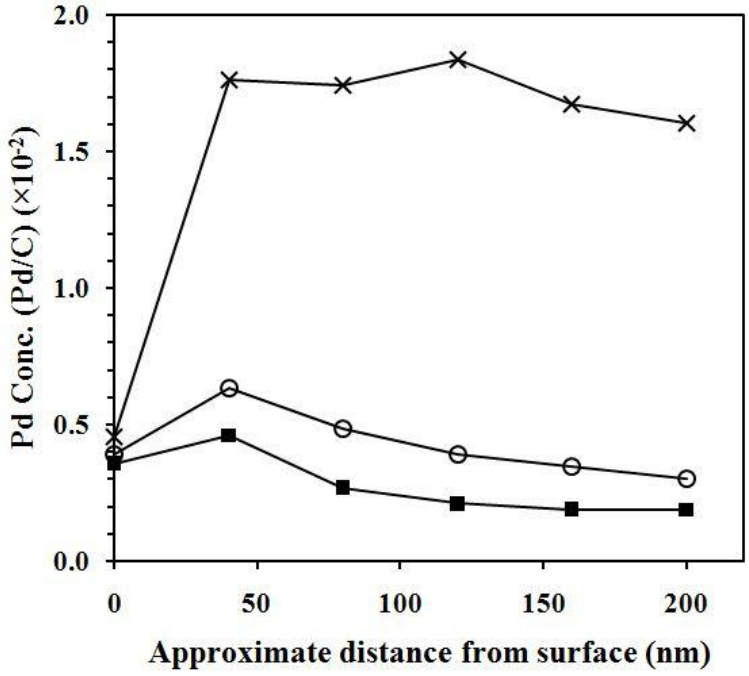

Figure 4.11. Pd metal concentration profile as a function of distance from the substrate surface for (×) neat ABS, (■) neat SAN and (○) SAN/PEEA (95/5) blend ($Pd(hfa)_2$ loading concentration = 1.59×10^{-3} g-$Pd(hfa)_2$/g-CO_2)

4.3.5. Electroless plating of ABS and ABS/ PEEA copolymer substrates

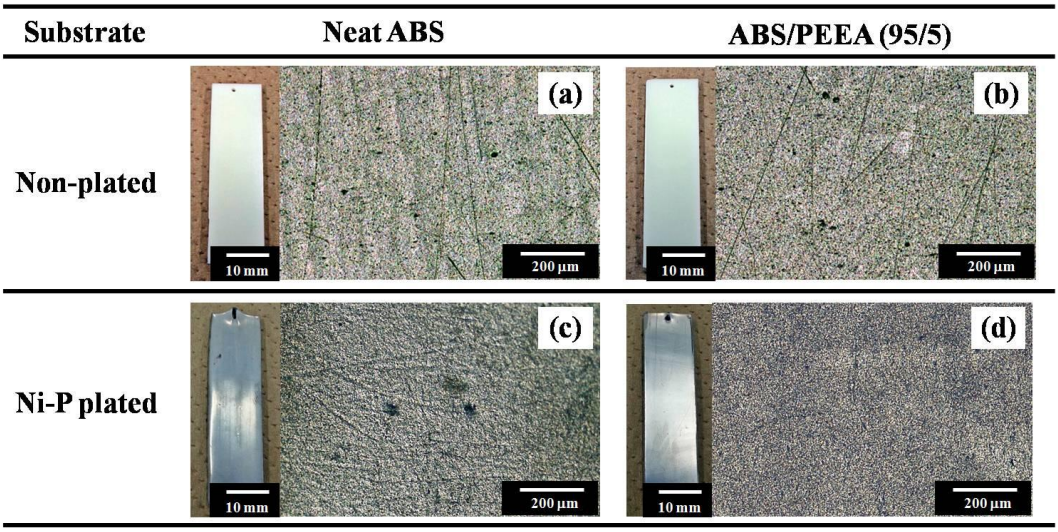

Figure 4.12. Digital camera (left) and optical microscope images (right) of the following substrate surfaces: (a) unplated neat ABS, (b) unplated ABS/PEEA blend (95/5), (c) Ni-P-plated ABS and (d) Ni-P-plated ABS/PEEA (95/5) blend

Figure 4.12 shows digital camera and optical microscope images of the substrate surface before electroless plating (Figures 4.12(a) and (b)) and after electroless plating (Figures 4.12(c) and (d)). Comparing Figure 4.12(a) with Figure 4.12(b) clearly shows that the surface roughness of the PEEA-blended polymer substrate did not differ substantially from that of the neat ABS substrate. The surface roughness of the polymer substrate was primarily determined by the roughness of the mold cavity. Figures 4.12(c) and (d) show several pinholes on the surface of the electroless-plated neat ABS substrate that was not modified with the PEEA copolymer (Figure 4.12(c)). After PEEA modification, a uniform Ni-P metal layer without pinholes was formed on the ABS/PEEA (95/5) blend substrate (Figure 4.12(d)).

Figure 4.13 shows digital camera and optical microscope images of the substrate surfaces of (a) Ni-P-plated neat SAN, (b) the Ni-P-plated SAN/PEEA (95/5) blend and (c) Ni-P-plated ABS. $Pd(hfa)_2$ was infused into all the substrates at a concentration of 9.52×10^{-4} g-$Pd(hfa)_2$/g-CO_2. Following Pd-infusion, the substrates were immersed in the plating solution, and the temperature was controlled at 65 ºC. The electroless plating reaction continued in the plating solution for over 120 min. Figure 4.13(a) shows that the Ni-P metal did not uniformly coat the surface of the neat

SAN substrate. The Ni-P metal layer partially covered the surface of the SAN/PEEA (95/5) blend substrate. This result was attributed to the presence of the PEEA copolymer. The dispersed butadiene domains in the SAN matrix enabled the neat ABS substrate to be completely coated by the Ni-P metal layer after 30 min. The difference in the time required to cover the substrate by electroless plating could be related to the amount of Pd that was infused into these polymeric substrates, as explained in section 4.3.4.

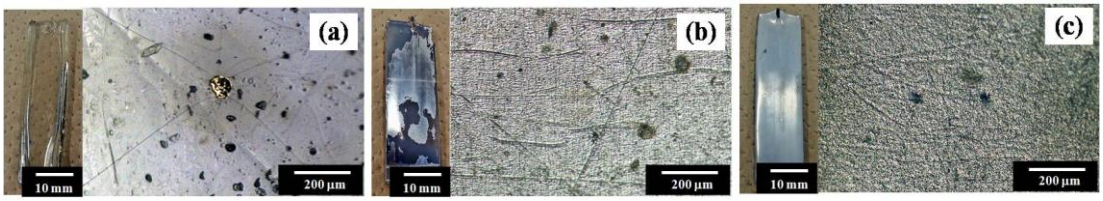

Figure 4.13. Digital camera (left) and optical microscope images (right) of surfaces for (a) Ni-P-plated neat SAN substrate, (b) Ni-P-plated SAN/PEEA blend (95/5) substrate and (c) Ni-P-plated ABS substrate; the polymeric substrates were impregnated with the Pd catalyst by $scCO_2$ infusion at a $Pd(hfa)_2$ concentration of 9.52×10^{-4} g-$Pd(hfa)_2$/g-CO_2.

4.3.6. Adhesive strength of the contact between the Ni-P metal and the polymer substrates

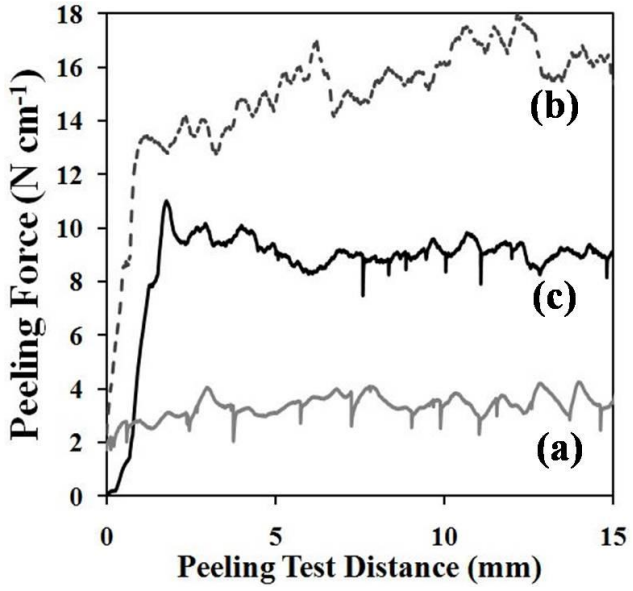

Figure 4.14. Peeling force of Ni-P-plated substrates: (a) neat ABS, (b) ABS/PEEA (95/5) blend and (c) PA6

The peeling force of the Ni-P metal layer from the three different types of polymer substrates was measured. The ABS and ABS/PEEA (95/5) blend substrates were electroless-plated after $scCO_2$ infusion of $Pd(hfa)_2$ at a loading concentration of 0.317×10^{-3} g-$Pd(hfa)_2$/g-CO_2, and the PA6 substrate was prepared by $scCO_2$ infusion of $Pd(hfa)_2$ at a loading concentration of 1.587×10^{-3} g-$Pd(hfa)_2$/g-CO_2. ABS/PEEA was prepared by blending ABS with 5% PEEA. The plating reaction occurred at 65 ºC for 60 min as in Ohshima group's report [11]. Figure 4.14 shows that the average peeling force for the neat ABS substrate was 3 $N\cdot cm^{-1}$, which was far lower than that for the PA6 substrate. The peeling force increased dramatically to 15 $N\cdot cm^{-1}$ when the substrate was modified by blending with 5 wt% PEEA copolymer. This result was attributed to the increased solubility of the plating solution in the ABS/PEEA (95/5) blend substrate by hydrophilic modification, which enabled the plating reaction to occur in the interior of the polymer substrate.

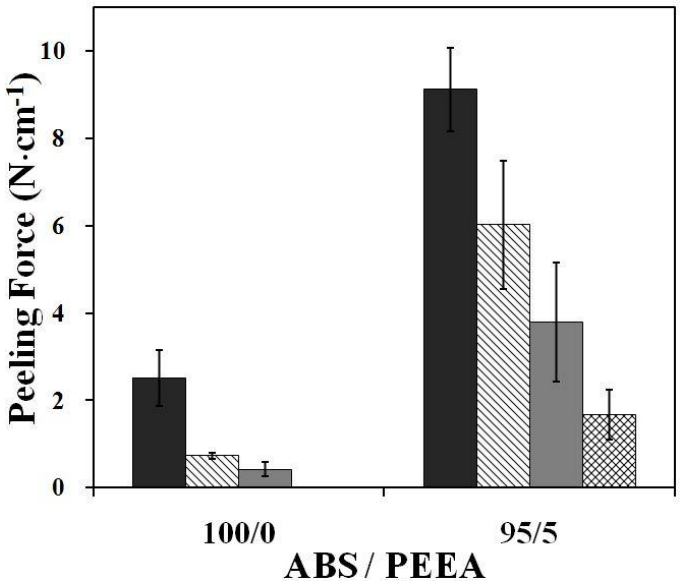

Figure 4.15. Peeling force of Ni-P-plated substrates, i.e., neat ABS and ABS/PEEA (95/5) blend, prepared using different loading concentrations of Pd in $scCO_2$ (each data point is an average of 4-10 samples for each case) (Amount of $Pd(hfa)_2$ in $scCO_2$ (g/g-CO_2) ($\times10^{-3}$): ■ = 0.063; ▨= 0.127; ▩ = 0.317; ▨ = 0.952)

The effect of the infused $Pd(hfa)_2$ concentration on the peeling force, i.e., the adhesive strength of the Ni-P layer, was investigated by varying the $Pd(hfa)_2$ loading

concentration in the $scCO_2$ infusion. Figure 4.15 shows the average peeling force for the Ni-P-plated neat ABS substrate and the ABS/PEEA (95/5) blend substrate, which were prepared using different $Pd(hfa)_2$ loading concentrations. The adhesion of the metal layer was dramatically improved by hydrophilic modification for all the $Pd(hfa)_2$ loading concentrations that ranged between 6.35×10^{-5} and 9.52×10^{-4} g-$Pd(hfa)_2$/g-CO_2. However, the Pd concentration apparently affected the peeling force of the Ni-P metal film from the substrate for both the ABS substrate and the ABS/PEEA (95/5) blend substrates. Note that increasing the Pd loading concentration beyond the aforementioned range did not increase the adhesive strength of the Ni-P metal layer. The metal-polymer composite layers formed at the interface between the electroless-plated metal layer and the polymer substrate. In Ohshima group's report, it showed that the adhesive strength of the Ni-P metal layer depended strongly on the thickness of the metal-polymer composite layer [11]. For high $Pd(hfa)_2$ loading concentrations, the plating reaction rate became faster than the mass transfer rate of the plating solution into the polymer substrate, and the plating reaction occurred only on the surface of the substrates. Thus, the metal layer rapidly formed on the surface. The layer reduced the amount of plating solution that diffused into the substrate, and the thickness of the composite layer decreased.

4.3.7. Metal-polymer composite layer

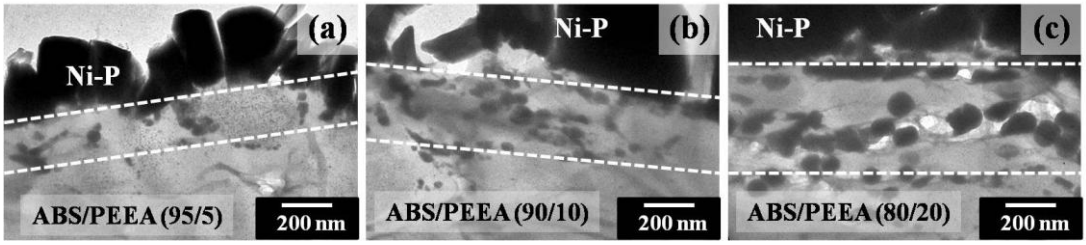

Figure 4.16. TEM micrographs of cross-sections of the interface between Ni-P film and stained ABS/PEEA blend substrates for different blend ratios: (a) 95/5, (b) 90/10 and (c) 80/20 ($Pd(hfa)_2$ loading concentration = 6.35×10^{-5} g-$Pd(hfa)_2$/g-CO_2)

Figure 4.16 shows TEM micrographs of cross-sections near the surface of the electroless Ni-P-plated ABS/PEEA blend substrates. The samples were prepared by blending different PEEA copolymer weight ratios of (a) 5, (b) 10 and (c) 20% for a $Pd(hfa)_2$ loading concentration of 6.35×10^{-5} g-$Pd(hfa)_2$/g-CO_2 and electroless-plating

at 65 ºC for 60 min. In Figure 4.16, the black regions correspond to the Ni–P metal layer and the Ni-P metal nanoparticles, the gray layers correspond to the dispersed PEEA domains, and the white region corresponds to the base ABS polymer. The thickness of the metal-polymer composite layer was determined from the TEM micrographs and is shown by white dotted lines. The thickness of the composite layer increased with the PEEA copolymer blend ratio in the blend samples.

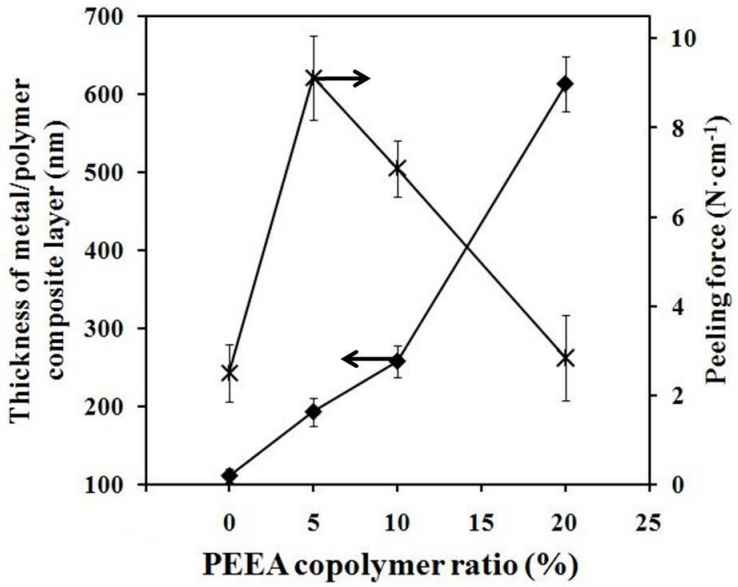

Figure 4.17. Relationship between weight percentage of PEEA copolymer in blend and thickness of metal-polymer composite layer and peeling force

Figure 4.17 shows the relationship between the weight percentage of the PEEA copolymer in the blend and the thickness of the metal-polymer composite layer and the peeling force. The thickness of the metal-polymer composite layer increased with the weight percentage of the PEEA copolymer. However, the peeling force decreased when the weight percentage of PEEA copolymer exceeded 10%. This result was obtained because the location of the peeling in the substrate varied with the PEEA weight percentage. In ABS/PEEA, peeling occurred in the metal-polymer composite layer (Figure 4.18(a)). Figure 4.18(a) shows a metal phase was present in both the peeled adherent and the substrate. When the weight percentage of PEEA was increased, the composite layer was too strong to be broken, and peeling occurred at the interface between the composite layer and the matrix polymer as shown in Figure 4.18(b), where there was no metal in the peeled substrate.

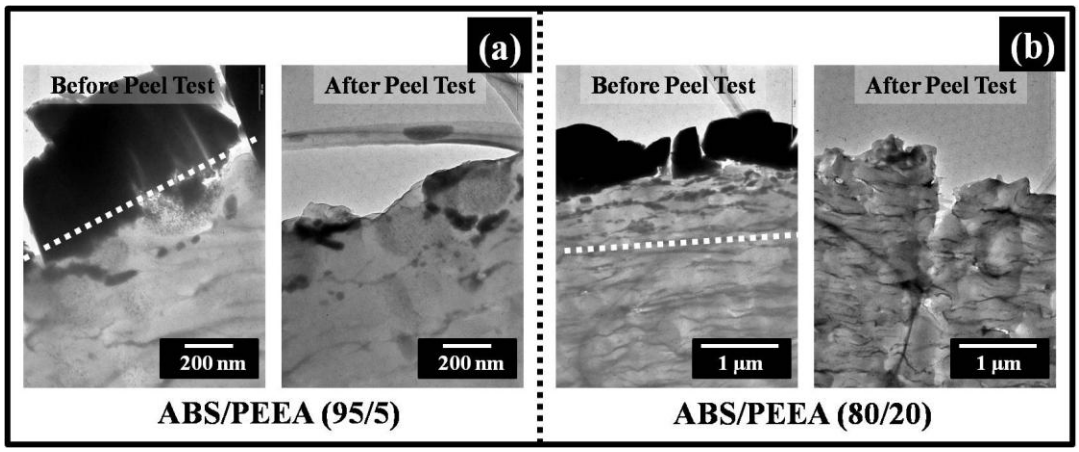

Figure 4.18. TEM micrographs of cross-sections of interface between Ni-P film and ABS/PEEA blend substrates for two different blend ratios: (a) 95/5 and (b) 80/20 (left: before peeling; right: after peeling)

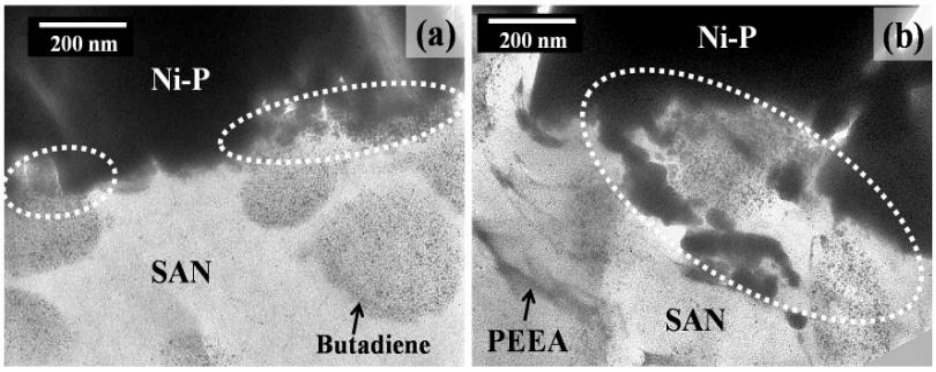

Figure 4.19. TEM micrographs of cross-section of interface between Ni-P film and substrates: (a) neat ABS and (b) ABS/PEEA (95/5) blend ($Pd(hfa)_2$ loading concentration = 6.35×10^{-5} g-$Pd(hfa)_2$/g-CO_2)

The effect of the butadiene domain on the electroless plating was also investigated. Figure 4.19 shows TEM micrographs of cross-sections near the surface of the electroless Ni-P plated substrates: (a) neat ABS and (b) the ABS/PEEA (95/5) blend. The samples were prepared by infusing $Pd(hfa)_2$ at a loading concentration of 6.35×10^{-5} g-$Pd(hfa)_2$/g-CO_2 and conducting electroless-plating at 65 ºC for 60 min. The black region corresponds to the Ni–P metal layer and the Ni-P metal nanoparticles, the white region corresponds to the SAN matrix, and the dark-grey spherical domains correspond to the butadiene domains. The small black dots

correspond to the Ni-P metal nanoparticles. The Ni-P metal nanoparticles were located in or at the periphery of the butadiene and PEEA domains. For the ABS/PEEA (95/5) blend substrate, the Ni-P metal nanoparticles were located in the PEEA dispersed domains, and the metal-polymer composite layer was formed such that the butadiene domains were connected with the Ni-P metal layer.

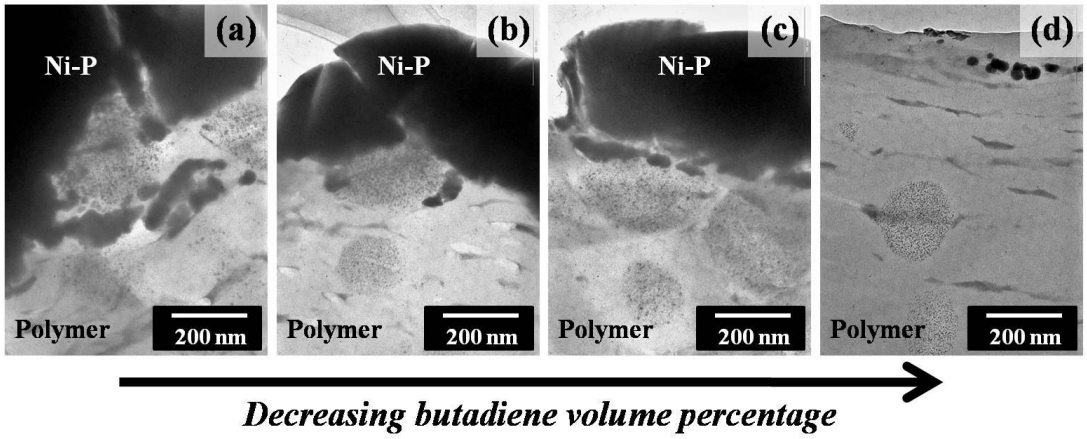

Figure 4.20. TEM micrographs of cross-sections of interface between Ni-P film and ABS/PEEA (95/5) blend substrate for different butadiene volumetric percentages: (a) 36%, (b) 28%, (c) 20% and (d) 10% ($Pd(hfa)_2$ loading concentration = 6.35×10^{-5} g-$Pd(hfa)_2$/g-CO_2)

The effect of the butadiene domains was further investigated by blending ABS with SAN at different weight percentages (25, 50 and 75%) and varying the butadiene volumetric percentage in the substrates. The blends were impregnated with $Pd(hfa)_2$ at a loading concentration of 6.35×10^{-5} g-$Pd(hfa)_2$/g-CO_2. Figure 4.20 shows TEM micrographs of cross-sections near the surface of the electroless Ni-P-plated ABS/PEEA (95/5) blend substrates for different butadiene volumetric percentages. Figure 4.20 obviously shows that the thickness of the metal-polymer composite layer could be found at the interface between the Ni-P film and the polymer matrix, however, the thickness of the composite layer and the connection between the metal nanoparticles in the ABS matrix and the Ni-P layer on the surface of substrates were decreased according to reducing of butadiene domain volume percentage near the interface.

Figure 4.21 shows the relationship between the thickness of the metal-polymer composite layer and the peeling force and the butadiene volume percentage near the

surface of the substrates. Figure 4.21 clearly shows that the thickness of the metal-polymer composite layer and the peeling force increased with the butadiene volume percentage near the substrate surface.

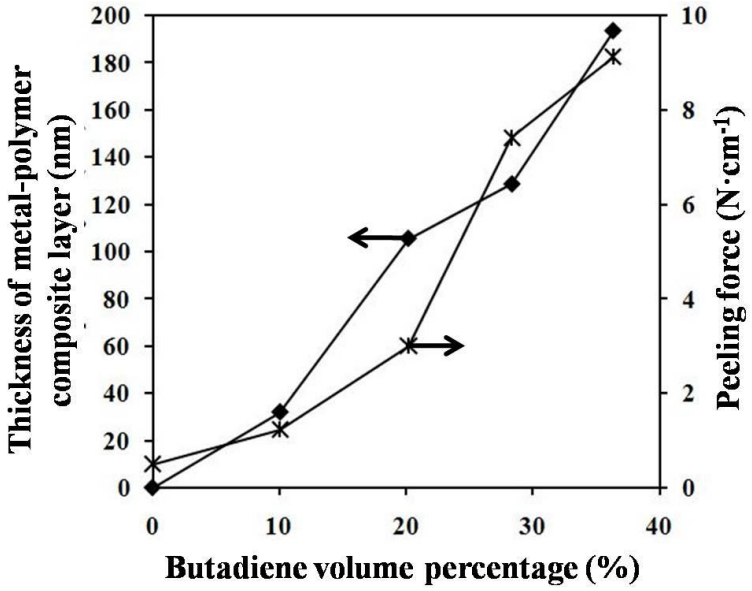

Figure 4.21. Relationship between butadiene volume percentage and thickness of metal-polymer composite layer and peeling force (all the blends were modified with 5 wt% PEEA copolymer)

4.4. Conclusion

The hydrophilicity of ABS was modified by blending with a PEEA copolymer, which facilitated the application of a supercritical carbon dioxide ($scCO_2$)-assisted electroless Ni-P alloy plating technique for ABS plastic products. This technique was used to produce a remarkably uniform Ni-P metal layer with a sufficiently strong adhesive strength on an ABS-based substrate. The adhesive strength of the contact between the Ni-P metal layer and the polymer substrate was controlled by the thickness of the metal-polymer composite layer. The thickness of the metal-polymer composite layer could be controlled by the degree of hydrophilic modification and the amount of catalyst infused into the polymeric substrate. The butadiene domain appeared to attract the Pd complex during $scCO_2$ infusion and affected the thickness and adhesive strength of the composite layer. Hydrophilic modification of polymer surfaces increases the application potential of the $scCO_2$-assisted electroless Ni-P

plating technique to a wide variety of polymers.

4.5. References

[1] G. Grundmeier, M. Stratmann, Annu Rev Mater Res, 35 (2005) 571-615.

[2] E. Sacher, Acs Sym Ser, 440 (1990) 1-7.

[3] S.M. Rossnagel, J Vac Sci Technol B, 16 (1998) 2585-2608.

[4] B.-H. Woo, M. Sone, A. Shibata, C. Ishiyama, S. Edo, M. Tokita, J. Watanabe, Y. Higo, Surface and Coatings Technology, 204 (2010) 1785-1792.

[5] G.O. Mallory, J.B. Hajdu, in, William Andrew Publishing/Noyes, 1990, pp. 1-3.

[6] J. Sudagar, J.S. Lian, W. Sha, J Alloy Compd, 571 (2013) 183-204.

[7] G.A. Krulik, J Chem Educ, 55 (1978) 361-365.

[8] M. Schlesinger, Electroless Deposition of Nickel, in: Modern Electroplating, John Wiley & Sons, Inc., 2010, pp. 447-458.

[9] X. Zhao, K. Hirogaki, I. Tabata, S. Okubayashi, T. Hori, Surface and Coatings Technology, 201 (2006) 628-636.

[10] N. Martinez, K. Hisada, I. Tabata, K. Hirogaki, S. Yonezawa, T. Hori, The Journal of Supercritical Fluids, 56 (2011) 322-329.

[11] H. Adachi, K. Taki, S. Nagamine, A. Yusa, M. Ohshima, The Journal of Supercritical Fluids, 49 (2009) 265-270.

[12] C. Erkey, J Supercrit Fluid, 47 (2009) 517-522.

[13] D.M. Kulich, S.K. Gaggar, V. Lowry, R. Stepien, Acrylonitrile–Butadiene–Styrene Polymers, in: Encyclopedia of Polymer Science and Technology, John Wiley & Sons, Inc., 2002.

[14] L.A.C. Teixeira, M.C. Santini, Journal of Materials Processing Technology, 170 (2005) 37-41.

[15] C.W. Extrand, Contact Angle, Wettability and Adhesion, Vol 2, (2002) 289-297.

[16] S. Kisin, F. Scaltro, P. Malanowski, P.G.T. van der Varst, G. de With, Polymer Degradation and Stability, 92 (2007) 605-610.

[17] H.Y. Nie, M.J. Walzak, B. Berno, N.S. McIntyre, Applied Surface Science, 144–145 (1999) 627-632.

[18] H. Kupfer, G. Hecht, R. Ostwald, Surface and Coatings Technology, 112 (1999) 379-383.

[19] M. Charbonnier, M. Romand, International Journal of Adhesion and Adhesives, 23 (2003) 277-285.

[20] M.D. Green, F.J. Guild, R.D. Adams, International Journal of Adhesion and Adhesives, 22 (2002) 81-90.

[21] W. Gui-xiang, L. Ning, H. Hui-li, Y. Yuan-chun, Applied Surface Science, 253 (2006) 480-484.

[22] G.G. Kim, J.A. Kang, J.H. Kim, K.-y. Lee, S.J. Kim, S.-J. Kim, Scripta Materialia, 56 (2007) 349-351.

[23] L. Magallón-Cacho, J.J. Pérez-Bueno, Y. Meas-Vong, G. Stremsdoerfer, F.J. Espinoza-Beltrán, Surface and Coatings Technology, 206 (2011) 1410-1415.

[24] A. Garcia, T. Berthelot, P. Viel, A. Mesnage, P. Jégou, F. Nekelson, S.b. Roussel, S. Palacin, ACS Applied Materials & Interfaces, 2 (2010) 1177-1183.

[25] T. Yabuta, Polymer Preprints, 58 (2009) 87.

[26] Y. Fu, J. Wang, G. Zhao, Y. Wang, S. Chen, Journal of Applied Polymer Science, 122 (2011) 12-18.

[27] R. Greco, A. Sorrentino, Advances in Polymer Technology, 13 (1994) 249-258.

[28] R. Greco, M.F. Astarita, L. Dong, A. Sorrentino, Advances in Polymer Technology, 13 (1994) 259-274.

[29] V.J. Triacca, S. Ziaee, J.W. Barlow, H. Keskkula, D.R. Paul, Polymer, 32 (1991) 1401-1413.

Chapter V

General Conclusion

In this research, the newly developed environmentally-friendly benign electroless nickel-phosphorus (Ni-P) alloy plating process was employed as a metallization for several thermoplastic polymer substrates including, polyamide6 (PA6), polypropylene (PP), and acrylonitrile-butadiene-styrene (ABS) polymers. The conventional chemical etching, catalyzing, and activation steps has been replaced by using the hydrophilic modification via polymer blending and the supercritical carbon dioxide ($scCO_2$)-assisted impregnation of Pd-catalyst, respectively.

In Chapter 2 and Chapter 3, the hydrophilicity of PP was modified by blending the base PP polymer with a polypropylene (PP)-polyethyleneoxide (PEO) (PP-b-PEO) copolymer, and then a $scCO_2$-assisted electroless Ni-P plating technique could be applied to the PP-made plastic products. In both chapters were mainly discussed and investigated about the effect of the PP-b-PEO copolymer, the processing conditions of polymeric substrate preparation, and the plating process variables and process conditions on the adhesive strength of the Ni-P metal film to the polymeric substrate

In Chapter 2, the novel electroless Ni-P technique successfully prepared a remarkably uniform Ni-P metal layer on a PP-based substrate with sufficiently strong adhesion. The hydrophilic modification by blending PP-b-PEO copolymer with PP is the key point for this study. Because the solubility of the plating solution in the polymer substrate could be enhanced with increasing PP-b-PEO copolymer content in polymer blend substrate, and the increase in solubility of plating solution directly indicates the improvement of mass transfer of the plating solution in polymer substrate. The enriching of penetration of the plating solution into polymer phase, the initiation of Ni-P metal nanoparticles from the electrolessly-plating reaction was increased in the area beneath the polymer surface. Also according to we speculated the metallic nanoparticles which were dispersed and their density was increased as the location was closer to the metal layer, as the “metal-polymer composite” layer and

this layer played as a role of anchoring. Thus, the thickness of metal-polymer composite layer at the interface between the Ni-P alloy coating layer and the hydrophilicity-modified PP substrate was thicken due to increasing of mass transfer of plating solution, and it consequently affected the enhancement of metal-polymer adhesion, as shown in Figure 5.1, and the metal-polymer adhesiveness could be dramatically shifted into high level by addition of PP-b-PEO, 25 %wt, in PP/PP-b-PEO blend substrate.

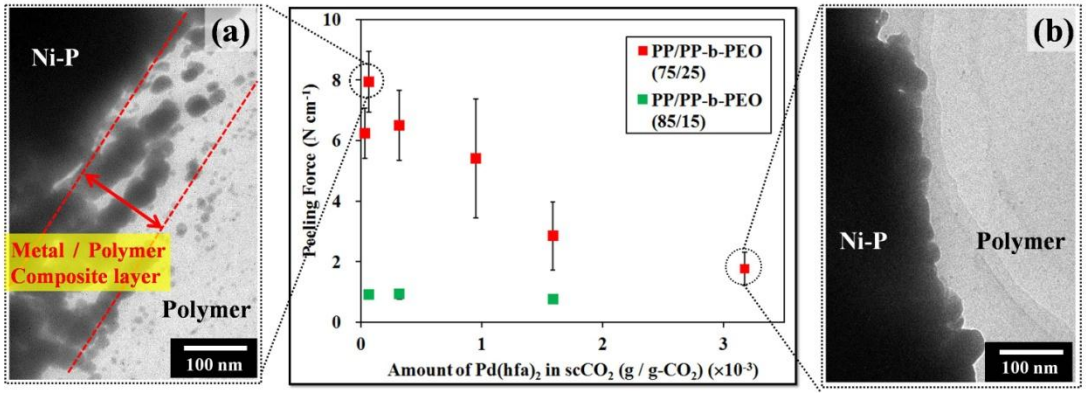

Figure 5.1. Relationship between the thickness of the metal-polymer composite layer and the metal-polymer adhesion, which was affected from the amount of infused-Pd in polymer substrate as well as the degree of hydrophilic modification of PP/PP-b-PEO blend substrates. In addition, TEM micrographs of the cross-section of the interface between the Ni-P film and the PP/PP-b-PEO (75/25) blend substrate using concentrations of the Pd catalyst precursor of (a) 3.17×10^{-3} and (b) 6.35×10^{-5} g-$Pd(hfa)_2$/g-CO_2

Moreover, as illustrated in Figure 5.1, the thickness of the metal-polymer composite layer also was determined by a competitive relationship between the mass transfer of the plating solution and the electroless plating reaction rate. When the plating reaction rate was faster than the mass transfer rate of the plating solution, the plating reaction occurred on the surface of the substrates, and the metal layer formed on the surface prevented the plating solution from diffusing into the interior of the substrate and the metal-polymer composite layer was thin. Thus, the amount of infused Pd catalyst, which can be controlled by adjusting the concentration of Pd-

complex during the $scCO_2$-assisted Pd infusion process, must be manipulated because when the infused Pd content increased in the polymer substrate, the electrolessly-plating reaction rate increased. The increase in reaction rate reduced the adhesiveness of metal layer to polymer. Thus, the concentration of the infused Pd metal catalyst in the polymer substrate as well as the hydrophilicity must be optimally controlled to increase the adhesive strength. In other word, the metal-polymer adhesion could be controlled by adjusting the PP-b-PEO copolymer weight percentage and the concentration of the infused Pd catalyst in the polymer substrate.

In Chapter 3, we still mainly focused on the $scCO_2$-assisted electroless Ni-P plating technique on PP via the hydrophilic modification followed the previous chapter. According to this research that the PP-b-PEO copolymer was blended with base polymer as the strategy to overcome the hydrophobic nature of the PP polymer, and the blend morphology of the PP/copolymer composite was strongly influenced by the PP and copolymer viscosities. This is because when PP and PP-b-PEO were blended and injected into the mold cavity, the difference between the viscosities of two polymers should sufficiently minimal for the polymers to be well blended but large enough to bring the lower viscosity polymer (PP-b-PEO) to the surface of injection-molded parts. Thus, from the results of this chapter, it clearly shows that the concentrations of the PP-b-PEO domains and their orientations near the surface regions of blend substrates could be controlled by adjusting the viscosity ratio of PP to PP-b-PEO, and there was an optimal viscosity difference between the PP-b-PEO and the PP that achieved the highest concentration and the highest degree of orientation of the copolymer domains in the PP matrix near the surface of substrate. In addition, the injection molding conditions such as the mold cavity temperature also affected the degree of orientation and the concentration of the PP-b-PEO domains in the PP matrix.

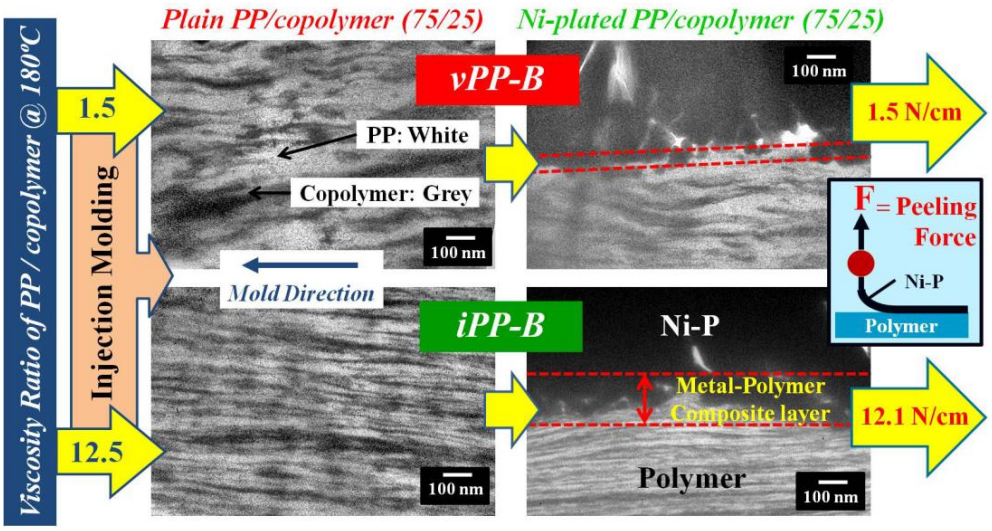

Figure 5.2. Relationship between the thicknesses of metal-polymer composite layer and the peeling forces of the Ni-P metal layer as well as the concentration of PP-b-PEO domains in PP matrix near the surface of the PP/PP-b-PEO (75/25) blend substrates which were prepared from different base PP grades (different viscosity ratio of PP to PP-b-PEO)

The different concentration and the degree of orientation of PP-b-PEO domains near the surface region of the PP blend samples also lead to change the sorption rates of electrolessly-plating solution as well as the infused-Pd catalyst in the PP/PP-b-PEO blend substrate. However, as concluded in Chapter 2, the adhesiveness of the Ni-P metal layer to the polymer substrate was dominated by the thickness of the metal-polymer composite layer, and the thickness of the metal-polymer composite layer could be controlled by the degree of the hydrophilic modification and the amount of infused catalyst in the polymeric substrate. Apart from the hydrophilicity and the amount of catalyst, the concentration and the degree of orientation of PP-b-PEO (hydrophilicity modifier) in the PP matrix beneath the surface were the most important factors for determining the thickness of the metal-polymer composite layer as illustrated in Figure 5.2. In addition, the relationship between the thickness and metal-polymer adhesion also re-confirmed from the results of this work.

In Chapter 4, the novel $scCO_2$-assisted electroless deposition with co-polymer-based hydrophilic modification was shifted into acrylonitrile-butadien-styrene (ABS) copolymer. In this work, the hydrophilicity of ABS was modified by blending the polymer with a poly(ether-ester-amide) (PEEA) copolymer, and then the $scCO_2$-assisted electroless Ni-P plating technique could be applied to the ABS-made plastic products. The technique successfully prepared a remarkably uniform Ni-P metal layer on a ABS-based substrate with sufficiently strong adhesion. In case of ABS substrate, the metal-polymer adhesion was dominated by the thickness of the metal-polymer composite layer likes in case of PP substrate. Thus, the thickness of the metal-polymer composite layer could be controlled by the degree of the hydrophilic modification and the amount of infused catalyst in the polymeric substrate. From the results, however, butadiene rubbery domain which dispersed in styrene-acrylonitrile copolymer (SAN) matrix shows important roles on the blend morphology (especially on the dispersion of PEEA copolymer domain in SAN matrix), the sorption rates of infused-Pd catalyst, and the characteristic and thickness of metal-polymer composite layer. In particular, as shown in Figure 5.3, the volume percentage of the butadiene domain at the skin region near surface of the ABS substrate has strongly influence on the characteristic and thickness of the composite layer, which is consequently affected the adhesive strength of Ni-P alloy film to ABS substrate.

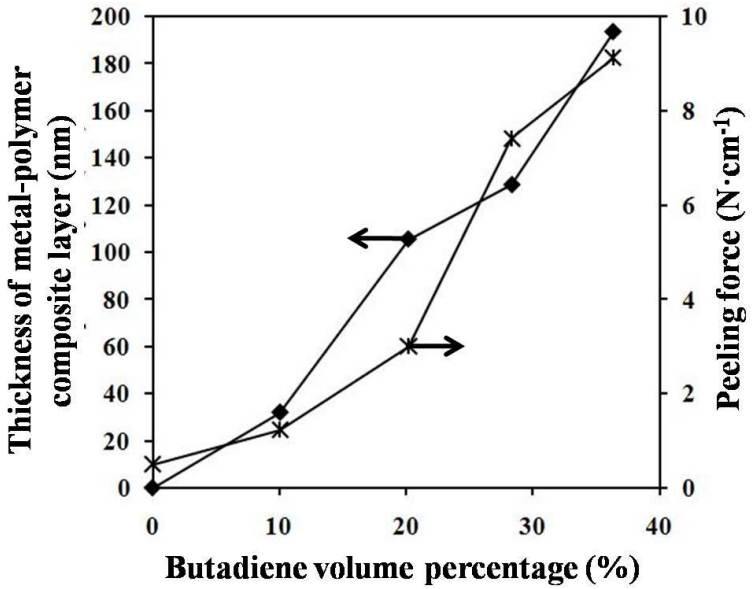

Figure 5.3. Relationship between the thicknesses of metal-polymer composite layer and the peeling forces of the Ni-P alloy layer as well as the concentration of butadiene domains in SAN matrix near the surface of the hydrophilicity-modified SAN and ABS substrates which were blended with PEEA copolymer, 5%.

Regarding to the results clarified from Chapter 2 to Chapter 4, the integration between the supercritical carbon dioxide-assisted Pd-complex infusion, the electroless nickel-phosphorus alloy plating, and the hydrophilic modification of polymer substrate by blending base-polymer with highly hydrophilic copolymer, can increase the potential for applying this metallization technique to other polymers.

Future work

According to the results presented in this thesis have demonstrated the effectiveness of the developed electroless plating on PP and ABS polymers process, however, it could be further developed in a number of ways. The way to introduce this environmentally friendly plating method into the industrial section is one of the most interesting developing ways. By the way, several points of the process must be replaced or eliminated because of the technical constraints such as usage of alcohol during the plating reaction, blending content ratio of hydrophilic modifier (copolymer) in polymer substrates, etc. As resulted in Chapters 2 and 3, the weight percentage of

copolymer in the PP/copolymer blend samples, which could provide a high degree of hydrophilic modification and strong metal-polymer adhesion, are needed more than 20 wt%. The higher blend ratio content of the copolymer means a rising of material cost and changing in mechanical properties of blend substrates. Thus, a question likes how to decrease amount of copolymer in PP/copolymer blend substrate must be considered as an improvement of this plating process before shifting it into the industries. Moreover, because the batch processing was occupied in this study especially during the $scCO_2$-assisted Pd catalyst infusion step, the different approaching ways for the $scCO_2$-assisted impregnation of the catalyst should be proposed to replace the batch processing. Furthermore, as shown in Chapter 4, which reported about the different amount of the infused Pd metal catalyst in SAN and ABS polymers, however, the reason for this result is not clearly explained in this study, thus, the study about the role of butadiene domain on the catalyst attraction and/or the electroless metal nucleation should be extended.

List of Figures

List of Tables

Acknowledgements

I would like to gratefully and sincerely thank to my PhD advisor, Professor Masahiro Ohshima, for his guidance, understanding, patience, and most importantly, his mentorship during my graduate studies at Kyoto University. During these three years, he always encouraged me to not only grow as an experimentalist and engineer but also as an instructor and an independent thinker. For everything you have done for me, Ohshima sensei, I thank you very much.

Moreover, I would like to thank to Dr. Shinsuke Nagamine, Associate Professor of Kyoto University and Dr. Kentaro Taki, Associate Professor of Yamagata University for their constructive advices and comments regarding on my experiments. Particularly, many technical supports provided by Dr. Taki was greatly appreciated, without his assistance this study would not have been successful.

In addition, I would like to thank Ms. Maki Yamamoto for her kind help which was highly appreciated for enabling me to survive in Japan. Additionally, I am very grateful for the friendship of all of the members of Material Processing Engineering (MPE) research group, especially Mr. Pengjian Gong, with whom I know as one of my best friends. I also would like to thank the Department of Chemical Engineering at Kyoto University, especially Professor Miyahara and Professor Kawase whose were members of my doctoral committee for their input, valuable discussions and accessibility.

Furthermore, I will forever be thankful to my former college research advisor, Dr. Surat Areerat. He has been helpful in providing advice many times during my graduate school career, and most particularly, his encouragement which pushed me to move on to PhD study.

Finally, and most importantly, I would like to thank my family for their support and encouragement throughout my study.

List of Publications

Chapter 2

Tengsuwan, S.; Ohshima, M. Electroless Nickel Plating on Polypropylene via Hydrophilic Modification and Supercritical Carbon Dioxide Pd-complex Infusion, *Journal of Supercritical Fluids*, **2012**, 69, 117-123.

Chapter 3

Tengsuwan, S.; Ohshima, M. Supercritical Carbon Dioxide-assisted Electroless Nickel Plating on Polypropylene −The effect of Copolymer Blend Morphology on Metal-Polymer Adhesion−, *Journal of Supercritical Fluids*, **2014**, 85, 123-134.

Chapter 4

Tengsuwan, S.; Ohshima, M. Environmentally Benign Electroless Nickel Plating using Supercritical Carbon-Dioxide on Hydrophilically Modified Acrylonitrile-Butadiene-Styrene, *Journal of Applied Surface Science*, **2014**, submitted.

International Conferences

Tengsuwan, S.; Ohshima, M. Supercritical Carbon Dioxide-assisted Electroless Nickel Plating on Polypropylene Substrate −Effect of Injection Molding on Hydrophilic Modification with Antistatic Agents−, *Polymer Processing Society 2013*, Pataya, Thailand, Oral Presentation.

Tengsuwan, S.; Ohshima, M. Supercritical Carbon Dioxide Assisted Electroless Plating on PP and ABS with Hydrophilic Modification, *Asian Workshop on Polymer Processing 2012*, Kyoto, Japan, Oral Presentation.

Tengsuwan, S.; Ohshima, M. Electroless Nickel Plating on Polypropylene via Hydrophilic Modification and Supercritical Carbon Dioxide Pd-complex Infusion, *10th International Symposium on Supercritical Fluids 2012*, San Francisco, USA, Poster Presentation.

Domestic Conferences

Tengsuwan, S.; Ohshima, M. Electroless Nickel Plating on Polypropylene via Hydrophilic Modification and Supercritical Carbon Dioxide Pd-complex Infusion, *SCEJ 45th Autumn Meeting 2013*, Okayama, Japan, Oral Presentation.

Tengsuwan, S.; Ohshima, M. Electroless Nickel Plating on Polypropylene via Hydrophilic Modification and Supercritical Carbon Dioxide Pd-complex Infusion, *Japan Society of Polymer Processing Annual Meeting(Sekei-Kako) 2012*, Tokyo, Japan, Oral Presentation.